EFFECT OF NEAR-FIELD GROUND MOTIONS ON DISPLACEMENT AMPLIFICATION SPECTRA IN INELASTIC SEISMIC PERFORMANCE EVALUATION

by

Yunus Emre Bülbül

B.S., Civil Engineering, Kocaeli University, 2008

Submitted to the Kandilli Observatory and
Earthquake Research Institute in partial fulfillment of
the requirements for the degree of
Master of Science

Graduate Program in Earthquake Engineering

Boğaziçi University

2011

EFFECT OF NEAR-FIELD GROUND MOTIONS ON DISPLACEMENT AMPLIFICATION SPECTRA IN INELASTIC SEISMIC PERFORMANCE EVALUATION

APPROVED BY:

Asst. Prof. Dr. Gülüm TANIRCAN (Thesis Supervisor)	. . . . .
Prof. Dr. M. Nuray AYDINOĞLU	. . . . .
Assoc. Prof. Dr. Yasin FAHJAN (Gebze Institute of Technology)	. . . . .

DATE OF APPROVAL: 31.10.2011

To my family

ACKNOWLEDGEMENTS

I am heartily thankful to my supervisor, Asst. Prof. Dr. Gülüm Tanırcan, whose encouragement, guidance and support helped me during the development of my thesis. I also would like to show my gratitude to Prof. Dr. M. Nuray Aydınoğlu for his advice on the subject and sharing his knowledge of the subject.

I would like to express my deepest gratitude to faculty members, Prof. Dr. Sami Arsoy, Assoc. Prof. Dr. Kemal Beyen, Assist. Prof. Dr. Fuad Okay and Assist. Prof. Dr. Aydın Kavak, in the civil engineering department in Kocaeli University for their support and encouragement to follow my masters after undergraduate.

I am greatly indebted to my family to support my decisions and to encourage me.

Lastly, I offer my regards and blessings to Engin Berker and Halit Demiral who supported me in any respect during my university and masters education.

ABSTRACT

EFFECT OF NEAR-FIELD GROUND MOTIONS ON DISPLACEMENT AMPLIFICATION SPECTRA IN INELASTIC SEISMIC PERFORMANCE EVALUATION

Behavior of the structures under near-field ground motions is different than behavior of the structures under far-field ground motions, in terms of strength demand or inelastic displacement demand, and therefore, design processes should reflect characteristic properties of near-field ground motions. Current applications on inelastic structural performance estimation under earthquake excitations are based on constant ductility approach. However this approach is inadequate to capture inelastic displacement demand of near field earthquakes, since ductility demands are limited to certain values. In this study, nonlinear analysis of single degree of freedom structures under near-field strong ground motion excitations were performed based on constant strength reduction approach. Strength-based displacement amplification spectra of near-field ground motions were developed by utilizing 105 near-field records of 25 worldwide earthquakes. Near-field ground motions were classified according to their pulse periods. Vibration period was normalized with respect to pulse periods to eliminate the distinct pulses observed at long period regions on the amplification spectra. Effects of the stiffness degradation and post-yield stiffness ratio on the strength-based displacement amplification spectra were investigated. It was found that stiffness degradation has significant influence on the spectral displacement amplification ratios. Systems with modified-Clough stiffness degradation hysteretic model exhibit larger spectral amplification ratio than those with elasto-plastic hysteretic model. Post-yield stiffness ratios affect the spectra especially at the short normalized period regions. Finally, mean strength-based displacement amplification ratios for each pulse period intervals were proposed as regression equations as a function of normalized period and strength reduction factor. Numerical examples have revealed that for SDOF whose period larger than 1 sec., displacement amplification spectra take values between 1.1-2.6, where this value (modification factor, C_1) is fixed to 1 in ASCE41-06.

ÖZET

ELASTİK OLMAYAN DEPREM PERFORMANS DEĞERLENDİLMESİNDE YAKIN-ALAN YER HAREKETLERİNİN YERDEĞİŞTİRME BÜYÜTME SPEKTRUMLARINA ETKİSİ

Yakın-alan depremlerine maruz kalan yapıların davranışları uzak-alan depremlerine maruz kalan yapıların davranışlarından farklıdır. Bu nedenle tasarım yöntemleri yakın-alan depremin özelliklerini yansıtmalıdır. Deprem etkisi altında mevcut yapısal performans tahmini için kullanılan yöntemler süneklik bazlı yaklaşıma dayanırlar. Fakat bu yaklaşım yakın-alan depremlerin elastik olmayan deplasman istemlerini yakalamada yetersizdir çünkü süneklik istemi belli değerlere sınırlandırılmıştır. Bu çalışmada yakın-alan depremlerin etkidiği tek serbestlik dereceli sistemlerin lineer olmayan analizleri dayanım bazlı yerdeğiştirme büyütme spektrumları kullanılarak gerçekleştirilmiştir. Yakın-alan depremlerinin dayanım bazlı yerdeğiştirme büyütme spektrumları dünyanın farklı yerlerinde olmuş 25 farklı depremin 105 adet kayıdı kullanılarak oluşturulmuştur. Yakın-alan depremleri vurum periyotlarına göre sınıflara ayrılmıştır. Titreşim periyotları büyütme spektrumlarının uzun periyot bölgelerinde gözlemlenen ani vurumları ortadan kaldırmak için vurum periyotlarına göre normalize edilmiştir. Sertlik azalmasının ve akma sonrası sertlik oranının dayanım bazlı yerdeğiştirme büyütme spektrumlarına etkisi araştırılmıştır. Sertlik azalmasının spektral yerdeğiştirme büyütme oranlarına önemli bir etkisinin olduğu bulunmuştur. Değiştirilmiş Clough sertlik azalması histeretik modeline sahip sistemler elasto-plastik sistemlere göre daha büyük spektral yerdeğiştirme oranına sahiptirler. Akma sonrası sertlik oranı özellikle kısa normalize edilmiş periyot değerlerinde spektrumu etkiler. Son olarak ortalama dayanım bazlı yerdeğiştirme büyütme oranı her bir vurum periyodu aralığı için normalize edilmiş periyot değerleri ve dayanım azaltma katsayısının fonksiyonu olarak regresyon denklemleriyle tanımlanmıştır. Sayısal örneklerden elde edilen sonuçlara göre, 1 sn den yüksek periyoda sahip tek serbestlik dereceli sistemlerde, yerdeğiştirme büyütme spektrumları 1.1-2.6 arasında değerler alırlar ki bu değer (modifikasyon katsayısı, C_1) ASCE 41-06' da 1 olarak sabitlenmiştir.

TABLE OF CONTENTS

LIST OF FIGURES

LIST OF TABLES

LIST OF SYMBOLS

C_1	Modification factor that represents the relation between the elastic s spectral displacement and inelastic spectral displacement of an equivalent SDOF system (FEMA 356 and ASCE 41-06)
R_y	Strength reduction factor
R	The ratio of elastic strength demand to yield strength coefficient (ASCE 41-06)
S_{ay}	Yield spectral pseudo-acceleration
S_{dy}	Yield spectral displacement
S_{ae}	Elastic spectral acceleration
S_{de}	Elastic spectral displacement
S_{di}	Inelastic spectral displacement
S_{daR}	Strength-based spectral displacement amplification ratio
$S_{da\mu}$	Ductility-based spectral displacement amplification ratio
T	The first natural vibration period of structural system
T_e	The effective fundamental period of the building in the direction of interest in sec. (FEMA 356)
T_s	Characteristic period of the response spectrum, defined as the period associated with the transition from the constant acceleration segment of the spectrum to the constant velocity segment of the spectrum (FEMA 356)
T_p	Pulse period of the near-field ground motions
Vy	The yield strength calculated using results of the NSP for the idealized nonlinear force-displacement curve developed for the building in accordance with Section 3.3.3.2.5 in ASCE 41-06
W	The effective seismic weight, as calculated in Section 3.3.1.3.1 in ASCE 41-06.
C_m	Effective mass factor from Table 3-1. Alternatively, C_m taken as the effective modal mass participation factor calculated for the fundamental mode using an Eigenvalue analysis shall be permitted.
μ	Ductility factor
α	Post-yield stiffness ratio

$\Phi(.)$	The mother wavelet function
$C_{s,l}$	The coefficient associated with the wavelet having scale s and position l

1. INTRODUCTION

1.1. Motivation for the Study

Inelastic response spectra were first studied by Veletsos (1969) who constructed the inelastic response spectra by using pulse-type excitations (half-cycle velocity pulses, half-cycle displacement pulses, full-cycle displacement pulses) and two recorded ground motions. Murakami and Penzien (1975) computed probabilistic nonlinear response spectra for Single Degree of Freedom (SDOF) systems with four types of hysteretic behavior. Their study was based on constant-strength nonlinear spectra of 100 artificially generated earthquakes divided into five groups, depending on intensity and duration.

During the development of the seismic design procedures, far-field strong ground motions have been utilized to develop design equations for buildings to resist earthquakes. Near-field seismic excitations have not been considered in design equations due to the lack of near-field ground motion records. After the destructive and high magnitude earthquakes, among others, Northridge (1994), Hyogo-Ken Nambu (Kobe) (1995), and Kocaeli (1999), devastating effects of the near-field ground motions led to comprehend the importance of these kinds of ground motions in the design of the structures.

Performance-based design is currently a sophisticated design procedure and employs the nonlinear static procedure (NSP). NSP (Pushover Analysis) is preferred due to the its simplicity as compared to nonlinear time history analysis. There are three types of nonlinear static procedures which are capacity spectrum method, displacement coefficient method, and the secant method. Seismic codes, for example FEMA-356 and ASCE 41-06, utilize the displacement coefficient method. This method comprises of the coefficients (C_0, C_1, C_2, C_3 (in FEMA-356), and C_m) take into consideration influences of the parameters on the overall seismic behavior of the structures. C_1 coefficient is the modification factor and defines the relation between the maximum inelastic displacement and displacement calculated for the linear elastic response. C_1 coefficient is developed for the constant-ductility factors and mainly using far-field strong ground motions. Yet, due to the

characteristic properties of the near-field motions the ratio of inelastic displacement to elastic displacement needs to be investigated and modified.

C_1 coefficient for different ductility levels does not correspond to the necessary lateral strength demand on a nonlinear constant-ductility spectrum due to the excessive displacement or lateral strength demand of the near-field ground motions. Several studies were carried out to develop C_1 modification factor, for instance Chopra (2004), Miranda (2000, 2004, and 2006). In those studies, importance of the frequency content of the ground motions was demonstrated to estimate seismic demand accurately. Chopra (2004) used transition period, T_c, it is one of the corner periods at the design spectrum and separates acceleration sensitive region to velocity sensitive regions, to eliminate differences between near-field and far-field ground motions. Miranda (2006) utilized predominant period of the ground motion, T_g, which is the period corresponding to the peak spectral velocity at the spectral velocity spectrum in order to determine peak displacement of the structures built on the soft soils. In addition to these studies, Shimazaki and Sozen (1984), Uang and Maarouf (1996), Tiwari and Gupta (2000), and Chakraborti and Gupta (2005) also used predominant period for better characterization of the seismic deformation demands.

1.2. The Objective and Scope of the Study

The objective of this study is to propose strength-based displacement amplification factors, S_{daR}, for the near-field strong ground motions. For this purpose, parameters which affect the S_{daR} coefficient are determined. During the analyses, following parameters are concerned,

- The effects of the hysteretic models
- The stiffness degradation
- The post-yield stiffness ratio (α) and
- The influence of the normalization of the elastic period through the pulse period of the near-field ground motions

In addition, deterministic examples are made to compare the differences between the proposed equation in this study and suggested C_1 coefficient equation in ASCE 41-06.

Chapter 2 covers the previous studies about ductility-based and strength-based displacement amplification factors and studies in which normalization of the elastic period are considered.

In Chapter 3, development of the NSP and evaluation of the inelastic seismic demand is summarized. In addition, evaluation of the inelastic seismic demand in performance based guidelines is presented.

Chapter 4 focuses on hysteretic models of the concrete utilized in this study to construct the strength-based spectral displacement amplification spectra. An explanation of the models with stiffness deterioration and non-degradation is provided.

In Chapter 5, reasons for choosing the strength-based spectral displacement amplification spectra instead of constant-ductility spectral displacement ratio are given.

Chapter 6 presents the properties of the near-field records considered in this study. Preferred pulse identification method to determine near-field records is also summarized. In tables, names of the eartquakes utilized in the study and names of the recorded stations with the ground motion properties, pulse periods obtained from velocity time histories and response spectra of near-field records, and those obtained from proposed equation by Baker (2007) are given.

Chapter 7 describes the results of the statistical study observed in this study. The results are explained in details and showed in figures. Nonlinear regression models are also provided for the mean strength-based spectral displacement amplification spectra for each pulse period interval. Numerical examples by using suggested regression formulae were given for different earthquake moment magnitudes, structural periods, post-yield stiffness ratios, and for several strength reduction factors. Outputs were commented and discussed.

Chapter 8 presents a summary of the whole study. Conclusions are drawn.

2. LITERATURE REVIEW

2.1. Past Studies on Inelastic Displacement Ratios and Constant-Ductility and Constant-Strength Spectral Displacement Amplification Ratios

Chopra and Chintanapakdee (2001) performed a study that aims to extend the concepts based on elastic and inelastic response spectra for far-field ground motions to near-field motions. First of all, the elastic response spectra of the two types of motions, in the context of the acceleration-sensitive, velocity-sensitive and displacement-sensitive regions of the response spectrum, are compared. Secondly, the response of inelastic systems, especially, the strength reduction factor, R_y, and the ratio of deformations of inelastic and elastic systems, u_m/u_o, in the context of spectral regions, is analyzed. Lastly, the validity of the previously proposed design equations for the R_y and u_m/u_o for the near field motions is investigated. 15 near-field ground motions of 6 earthquakes and 15 far-field records of 9 earthquakes are employed for the analysis. From this study following conclusions were drawn: for the same ductility factor, near field ground motions impose a larger strength demand in their acceleration-sensitive region compared to far-field motions. This difference is associated with the T_c values for the two types of excitations. However, provided that period axis is normalized with respect to T_c, differences between strength reduction factors of the two types of the records will be similar over all spectral regions. Another consequence related to T_c is that the peak deformation in the acceleration sensitive region of inelastic system as a result of the near-field ground motions will be underestimated if the u_m/u_o data obtained from far-field motions is applied. This difference can be eliminated in order to obtain similar u_m/u_o ratios over all spectral regions by normalization of the period axis with T_c like the same procedure applied to strength reduction factors. According to authors, as long as the appropriate values of T_a, T_b, T_c are used design equation for R_y and u_m/u_o can be applicable to many different classes of motions. Therefore, proposed equations by Veletsos and Newmark in the 1960s for R_y are used with T_a, T_b, T_c computed for 15 near-field ground motions. Calculated transition periods for near-field records determined as 0.04 sec., 0.35 sec., and 0.79 sec. for T_a, T_b, T_c, respectively.

Chopra and Chintanapakdee (2004) carried out a comprehensive study which presents the median and dispersion of the inelastic deformation ratio of SDOF systems for several groups of ground motions, including large and small earthquake magnitudes and small or large distances, NEHRP site classes, B, C, and D. Near-field ground motions were included as well as far-field ground motion records. 214 ground motion records were divided into well-organized 11 ensembles of ground motions. The earthquake response of bilinear systems was investigated, but stiffness and strength degradation, and pinching effect was not taken into consideration. In this study, regression equations are proposed for both ductility based design and strength based design procedures and limit cases were determined for these proposed equations. The proposed equations depend on the normalized period T_n/T_c in order to eliminate differences between C_R and C_μ spectra of the near-field and of the far-field records. According to the study, equations for the constant-strength and constant-ductility yield the similar results with those obtained from the median of the ensemble of ground motions. It is suggested that the equation presented for C_μ can be used for new or rehabilitated structures to estimate inelastic deformation and that presented for C_R can be useful for existing structures with known lateral strength.

Baez and Miranda (2000) conducted a work to study the effects of the rupture directivity at near-field sites on the inelastic displacement ratios. 82 earthquake ground motions (fault normal and fault parallel) correspond to 9 North America earthquakes were used. These ground motions recorded at a distance closer than 15 km from the surface projection of the rupture and horizontal components of these motions have peak ground accelerations (PGA) larger than 200 cm/s^2 and peak ground velocities (PGV) larger than 20 cm/s. Results of the study showed that inelastic displacement ratios computed from near-field records are larger than those computed from distant records. Similarly, inelastic displacement ratios corresponding to fault-normal components are larger than those of fault-parallel components. In addition, results showed that structures subjected to ground motions with large velocity pulses may experience maximum inelastic deformations larger than those subjected to ground motions that do not have these pulses, even if linear elastic ordinates in the short period spectral region are similar. Thus, it was concluded that modification of linear elastic design spectra alone, as done in the 1997 UBC, may not be enough to adequately control maximum inelastic deformations in structures located near active faults.

Miranda (2000) performed a comprehensive statistical study of the ratio of maximum inelastic displacement demand to maximum elastic displacement demand for firm sites. The effect of the earthquake magnitude, soil condition, and epicentral distance on these ratios was investigated. In this study, 264 acceleration time histories of earthquakes occurred in California recorded on firm sites were utilized. The following conclusions were drawn for the analysis: the effect of the earthquake magnitude on the inelastic displacement ratios can be neglected and the influence of the epicentral distance to rupture upon the inelastic displacement ratios can be relatively small. Soil conditions have also small effect on these ratios. The proposed equation derived from nonlinear regression analysis correlates closely with the mean inelastic displacement ratio of the ground motion records whose average shear-wave velocities is higher than 180 m/s. In addition, proposed equation can be used for all sites without the need for estimating a characteristic or corner period for the site.

Miranda and Ruiz-Garcia (2002) conducted a detailed statistical study of constant relative strength inelastic displacement ratios to estimate maximum lateral inelastic displacement demands on existing structures from maximum lateral elastic displacement demands. Different parameters, the period of vibration, level of lateral yielding strength, site conditions, earthquake magnitude, distance to the source, and strain-hardening ratio, were taken into account to investigate the effects of them on the inelastic displacement ratios. The results of the study demonstrated that distance to the source has a negligible effect on constant relative strength inelastic displacement ratios. However, influences of the earthquake magnitude and soil conditions have a moderate effect on these ratios as periods are smaller than 1 sec.. Strain hardening decreases maximum inelastic displacement at a fairly constant rate depending on the level of relative strength for periods of vibration longer than about 1 sec. whereas it decreases maximum inelastic displacement non-linearly as the period of vibration shortens and as the relative-strength ratio increases for periods of vibration shorter than 1 sec.. Proposed non-linear regression analysis results provided that a simplified expression to be used to approximate mean inelastic displacement ratios during the evaluation of existing structures built on firm sites.

A study was conducted by Ruiz-Garcia and Miranda (2004) to investigate inelastic displacement ratios of the structures built on the soft soil. The effect of the period of

vibration normalized by the predominant period of the ground motion, the level of inelastic deformation, epicentral distance and earthquake magnitude are evaluated. Two sets of the ground motion database, totally 116 earthquakes, recorded on bay-mud sites of the San Francisco and on the sites in the former lake-bed zone of Mexico City were employed for the study. The following conclusions were drawn from the results of the study. The inelastic displacement ratio is not affected by earthquake magnitude and epicentral distance. In order to show the stiffness degrading effect, modified-Clough nonlinear hysteresis model is compared to elasto-plastic model. The inelastic displacement demand of the stiffness degrading hysteresis model is larger than that of the elastoplastic hysteresis model as T/T_g is small. While for the rest of the spectral regions inelastic displacement ratio of the stiffness degrading hysteresis model is smaller than that of the elasto-plastic hysteresis model. The stiffness degradation has significant influence on the structure built on soft soil than those on firm soil. This observation was made in previous studies (*e.g.* Rahnama, M., and Krawinkler, H. (1993)). It was suggested that proposed nonlinear regression formula in order to estimate inelastic displacement of the Multi-Degree-of-Freedom (MDOF) systems should be used for structures whose first vibration period is dominant. However, proposed equation can estimate the inelastic displacement ratio of the SDOF system relatively good.

3. NONLINEAR STATIC PROCEDURE AND EVALUATION OF INELASTIC SEISMIC DEMAND

3.1. Nonlinear Static Procedure (NSP)

Nonlinear static procedure (Pushover Analysis) is a tool for the performance-based evaluation which has been developed to eliminate limitations and deficiencies of the conventional strength-based design. These limitations and deficiencies are as follows,

- Available strength and ductility capacity of an existing structure cannot be accurately predicted by a presumed strength reduction factor, R_y, given in seismic codes
- Inelastic deformation demands on the structural components beyond their elastic limits cannot be estimated quantitatively.
- Force and story drift distribution may change considerably due to the yielding of structural elements. This change cannot be estimated by a linear elastic analysis and a strength reduction factor.
- Excessive deformation demands in the critical regions of a structure that may cause a story mechanism in the first or the upper floors cannot be determined by an elastic analysis.

Therefore, performance-based design is provided in seismic evaluation and retrofit design guidelines such as Vision 2000 (SEAOC, 1995), ATC 40 (1996) and FEMA 273 (1997). In these guidelines, nonlinear analysis tools are utilized to evaluate the seismic performance of building expected to deform in the nonlinear range.

Nonlinear dynamic analysis is the best choice for the quantification of the inelastic behavior of the structural system. Yet, implementation of this analysis method requires carefully selected ground motions to account for the effects of the distance to fault, magnitude, ground motion duration, and the differences in the frequency characteristics on the structures. Complexity of the definition of damping and the computational effort

related to the numerical integration process are some of the major effects which make the method difficult to use in practice. Due to these drawbacks of the nonlinear dynamic analysis, NSP or pushover analysis is preferred due to its simplicity and its reliability.

Pushover analysis is particularly referred to as a nonlinear capacity estimation tool and generally called as “capacity analysis”, which is performed under an invariant load pattern consistent with the fundamental mode. Under this load pattern, the structure is pushed until a selected control point (generally located at the roof level of a building) reaches a predetermined displacement value, which may eventually correspond to a collapse state. Thus, available capacity of the structure in terms of both displacement and strength can be estimated. After the introduction of the Capacity Spectrum Method (CSM) developed by Freeman (1978, 1998) pushover analysis is also utilized as a demand estimation tool. In this method, seismic demand is represented by response spectra and capacity curve is obtained from the pushover analysis are plotted in the same graph. The inelastic displacement demand of the earthquake ground motion is determined by means of this figure by using initial period of the structure. Inelastic displacement demand can be obtained as follows from the elastic displacement demand,

$$S_{di}(T, R_y)=S_{daR}(T, R_y)S_{de}(T) \tag{3.1}$$

in which, S_{di} is inelastic spectral displacement for a given initial period (T) of the system and constant strength reduction factor R_y, S_{de} is elastic spectral displacement of the corresponding SDOF system with the same mass and initial period, and S_{daR} is spectral displacement amplification factor. Inelastic spectral displacement can be expressed as

$$S_{di}=(\mu/R_y)S_{de} \tag{3.2}$$

where, μ is ductility and R_y refers to strength reduction factors, and they are defined as

$$R_y=S_{ae}/S_{ay} \quad ; \quad \mu=S_{di}/S_{dy} \tag{3.3}$$

where, S_{ae} represents the elastic spectral acceleration demand of the corresponding linear SDOF system with a given initial natural frequency of period ($w=2\pi/T$), S_{ay} and S_{dy} denote

spectral acceleration and displacement at yield, respectively. Spectral displacement amplification can be expressed as the ratio of the main parameters of the inelastic response,

$$S_{daR}(T, R_y)=\mu(T, R_y)_{max}/R_y=S_{di}(T, R_y)/S_{de}(T) \quad (3.4)$$

3.2. Evaluation of Inelastic Seismic Demand in Performance-Based Design Guidelines

3.2.1. General

FEMA 356 and ASCE 41-06 provide Coefficient Method for calculating target displacement of structures. For other calculation methods of target displacement of structures, in these guidelines, FEMA 274 is referred to be utilized for other methods such as Capacity Spectrum Method to calculate target displacement demand.

3.2.2. Displacement Coefficient Method

Pushover analysis is performed until the displacement value, called target displacement, estimated by the Displacement Coefficient Method in FEMA 356. In this method, target displacement is defined through C_1 coefficient, which represents the relation between the elastic spectral displacement and inelastic spectral displacement of an equivalent SDOF system, depending on the initial period and the strength level of the SDOF system.

3.2.2.1. FEMA-356. Coefficient C_1 is given as follows for the different intervals of the period of the structures,

$$C_1 = 1.0 \quad T_e \geq T \quad (3.5)$$

$$C_1 = [1.0 + (R-1)T_s/T_e] / R \quad T_e < T_s \quad (3.6)$$

where, T_e shows the effective fundamental period of the building in the direction of interest in sec. T_s is characteristic period of the response spectrum, defined as the period associated

with the transition from the constant acceleration segment of the spectrum to the constant velocity segment of the spectrum.

In addition, C_1 should not be greater than the 1.5 for $T < 0.10$ second and 1.0 for $T \geq T_s$ and less than 1.0.

3.2.2.2. ASCE 41-06. The ASCE 41-06 (Seismic Rehabilitation of Existing Buildings, 2007) is the latest generation of a performance-based seismic rehabilitation standards, which was developed from the pre-standard FEMA 356. This new standard includes a simplified pushover procedure based on a single load pattern consistent with the fundamental mode shape instead of several different load patterns as recommended in FEMA 356. In addition, the improved procedure for displacement coefficient method based on the recommendation contained in FEMA 440 has been adopted by ASCE 41-06.

For periods less than 0.2 second, C_1 need not be taken greater than the value at the T=0.2 second. For periods greater than 1.0, $C_1=1.0$.

$$C_1=1+(R-1)/(aT_e^2) \tag{3.7}$$

in which, a is the site class factor and has values 130, 90, and 60 for site classes A and B, site class C, and site classes D, E, and F, respectively. T_e is the effective fundamental period of a building in the direction under consideration. R is the ratio of elastic strength demand to yield strength coefficient calculated in accordance with equation 3-15 in ASCE 41-06.

$$R=[S_a/(V_y/W)]C_m \tag{3.8}$$

S_a is the response spectrum acceleration, at the effective fundamental period and damping ratio of a building in the direction under consideration, as calculated in Sections 1.6.1.5 and 1.6.2.1 in ASCE 41-06. V_y is the yield strength calculated using results of the NSP for the idealized nonlinear force-displacement curve developed for the building in accordance with Section 3.3.3.2.5 in ASCE 41-06. W is the effective seismic weight, as calculated in Section 3.3.1.3.1. C_m is effective mass factor from Table 3-1. Alternatively,

C_m taken as the effective modal mass participation factor calculated for the fundamental mode using an Eigenvalue analysis shall be permitted. C_m shall be taken as 1.0 if the fundamental period, T, is greater than 1.0 second.

4. HYSTERETIC MODELS

4.1. Modified-Clough Bilinear Stiffness Degrading Model

During the analyses modified-Clough hysteresis model is used to represent flexural behavior of the SDOF concrete member.

A bilinear primary curve with ascending post-yielding branch is operated by the model. This model is developed to eliminate deficiency of Clough degrading model which is after the unloading from a part of the curve with reduced stiffness, reloading branch moves towards the previous largest point that is not always realistic, and thus the modification is made by Mahin and Bertero (in 1975 and 1976) so that during reloading the response point should move toward an immediately preceding unloading point (branches 7-8-9 and 10-11-12-13-14 in modified-Clough bilinear stiffness degrading model given in Figure 4.2, and corresponding modified branches 7-8-9 and 9-10-11-12 in Clough bilinear stiffness degrading model given in Figure 4.1).

Modified-Clough bilinear stiffness degrading model considers a system as elastic if load starts with small amplitude deformations below the yield point. When the load is reversed, the stiffness is reduced.

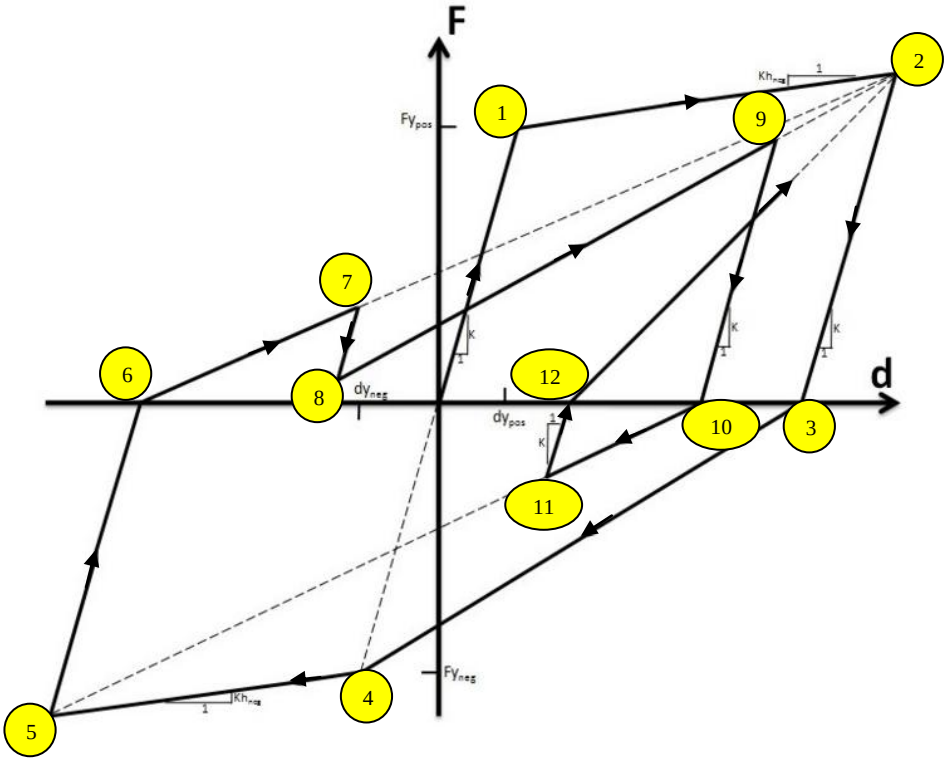

Figure 4.1. Hysteretic behavior of Clough bilinear stiffness degrading model

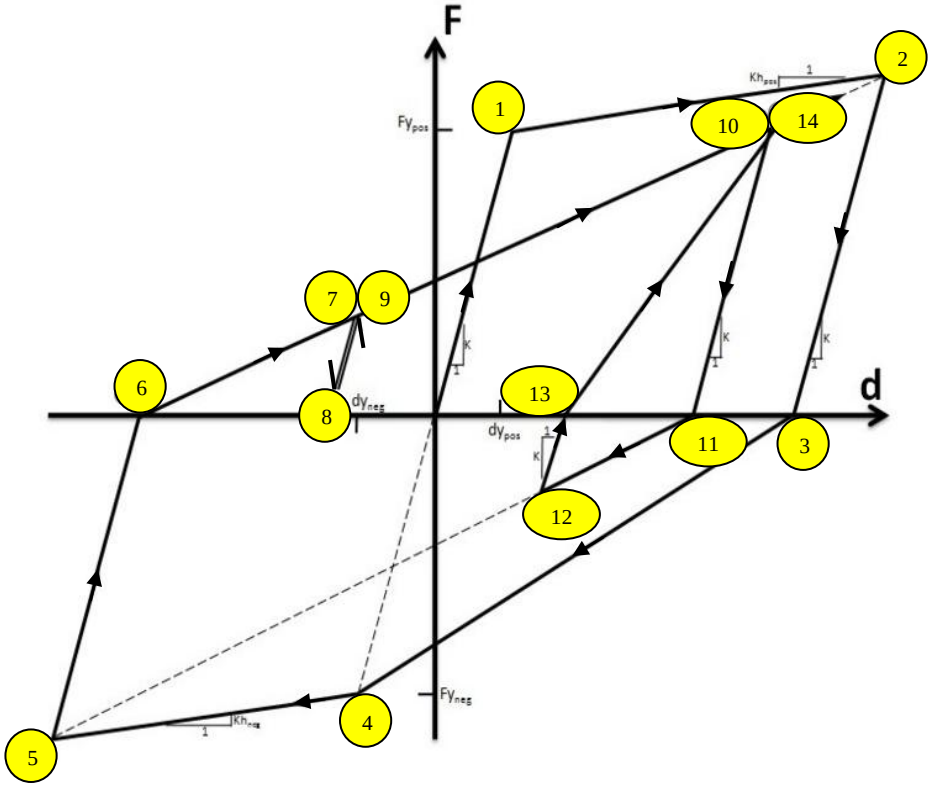

Figure 4.2. Hysteretic behavior of modified-Clough bilinear stiffness degrading model

4.2. Elasto-Plastic Model

Elastic portion which represents cracked section behavior represents the primary force-deformation curve. After reaching the yield load, stiffness increment is taken as zero. Unloading at this stage takes place with cracked-section properties. No reduction in slope is considered at the reversal stage. The model does not represent the cyclic response of the reinforced concrete. Yet, elastoplastic model represents the cyclic response of the steel.

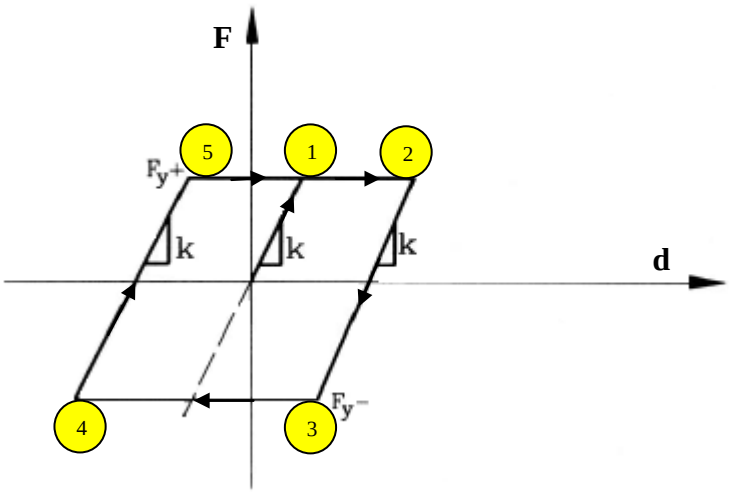

Figure 4.3. Hysteresis behavior of elasto-plastic model.

5. DUCTILITY-BASED VS. STRENGTH-BASED DISPLACEMENT AMPLIFICATION SPECTRA

5.1. Differences between Strength-Based Spectral Displacement Amplification and Ductility-Based Spectral Displacement Amplification Ratios Obtained for Near-Field Excitations

$$S_{da\mu}(T, \mu)=\mu/R_y(T, \mu)_{min}=S_{di}(T, \mu)/S_{de}(T) \quad (5.1)$$

Equation (5.1) assumes that a SDOF system with a given period possesses the required strength compatible with the specified fixed target ductility factor, which is deemed not being exceeded in any earthquake considered for the development of response spectrum. It means that if the system was not supplied with such a required strength for a given earthquake, Equation (5.1) would be meaningless. This shows the biased concept inherent in the constant ductility approach for the estimation of the inelastic displacement demand, which assumes that the ideal design conditions dictated by target ductility factors are always satisfied for all systems under all types of earthquake ground motions. Note that the strength that is actually supplied to the system can only be estimated by a nonlinear capacity analysis of the displacement-based evaluation procedure. On the other hand, when the required strength is assumed to be supplied, the maximum value of the ductility-based spectral displacement amplification can never exceed the specified target ductility factor, *i.e.*, $S_{daR}(T, \mu) \leq \mu$, because the strength reduction factor in the denominator of Equation (5.1) cannot be less than unity.

Note that the ideal design conditions inherently assumed in the constant ductility approach leads to a false impression especially for the effects of near-field records on the displacement demand. In fact in a statistical study based on near-field records conducted by Miranda (2000a), ductility-based spectral displacements obtained for an acceptable range of target ductility factors (with a maximum of = 6) are shown to exhibit relatively small mean amplifications in the order of not more than 20percent. In another recent study conducted by Miranda (2000b) with a total 264 records, 46 near-field records mixed with 218 far-field records are implicitly found to be ineffective in raising the ordinates of the

mean ductility-based displacement amplification spectra. These examples show that detrimental effects of near-field records on real (non-ideal) structures can only be evaluated with the strength-based displacement amplification spectra. In the following figures, constant-ductility and constant-strength spectra of the two records of the Imperial Valley (1979) earthquake were computed to demonstrate the differences between the ductility and strength demands of the same records. For example, in Figure 5.2, ductility demands of the near-field earthquake at the period around 0.5 sec. is higher than the strength reduction factors whereas in corresponding constant-ductility spectra given in Figure 5.1 strength demands are less than the prescribed target ductility values over the whole period range of the spectra. The same observation can also be made for the other given station of the Imperial Valley (1979) event.

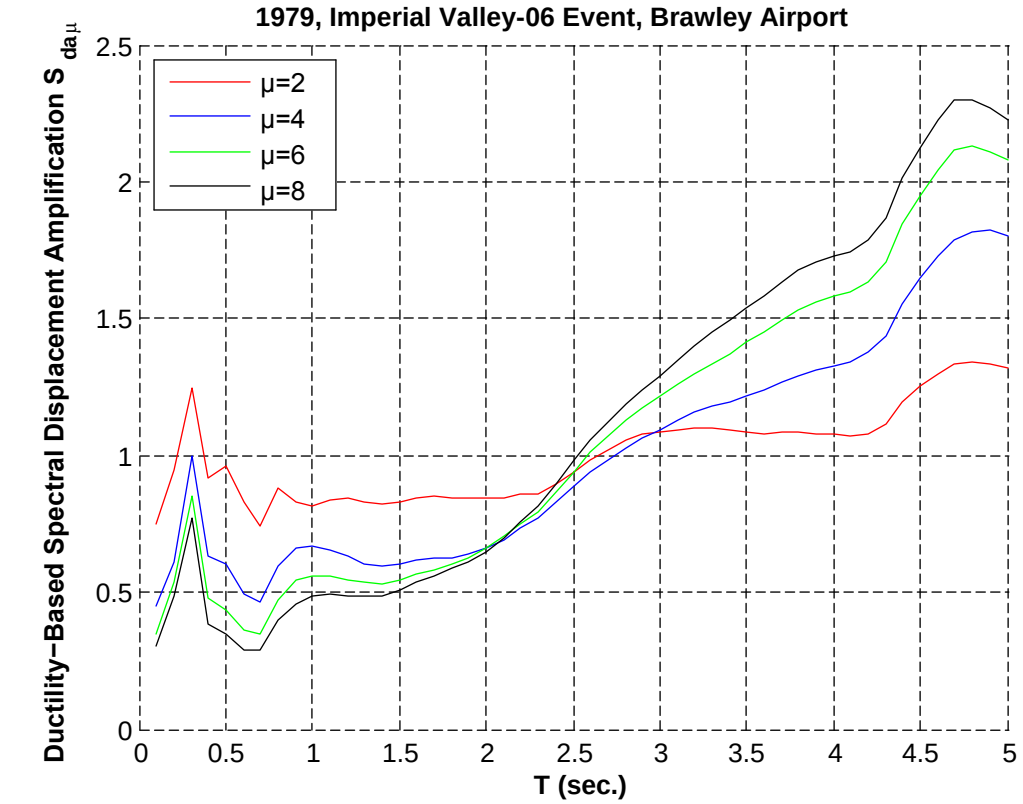

a)

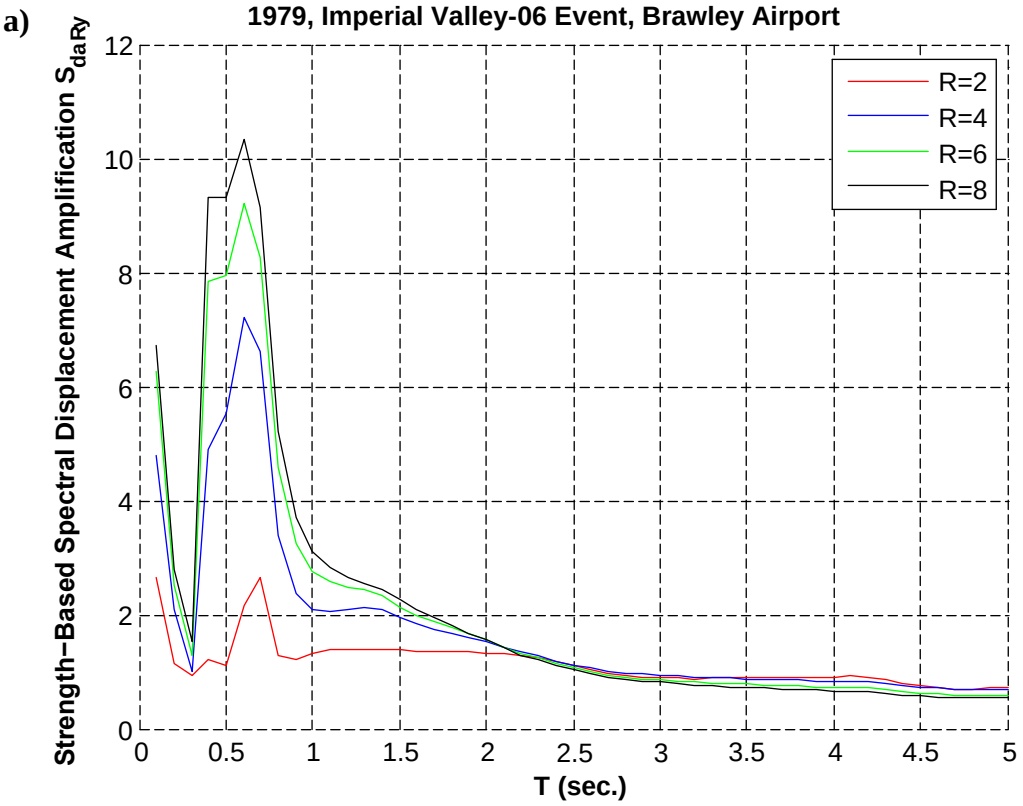

b)

Figure 5.1. **a)** Ductility-based displacement amplification spectra, and **b)** Strength-based displacement amplification spectra of the 1979, Imperial Valley-06 event recorded in Brawley Airport station

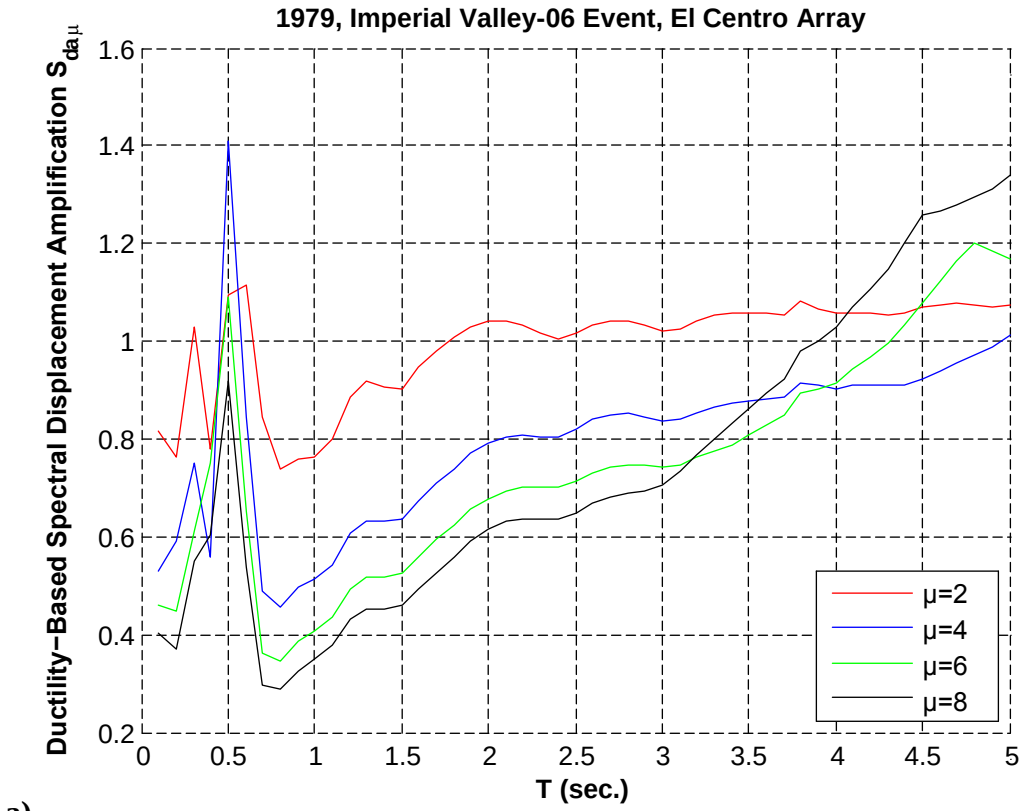

a)

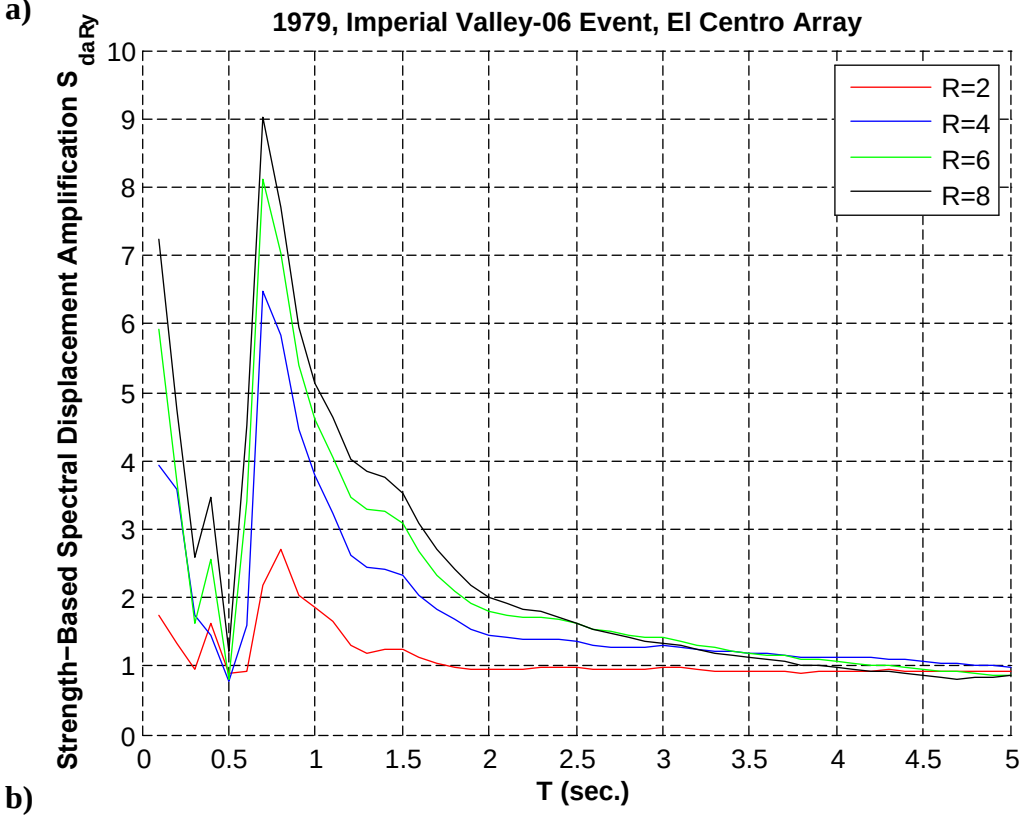

b)

Figure 5.2. **a)** Ductility-based displacement amplification spectra, and **b)** Strength-based displacement amplification spectra of the 1979, Imperial Valley-06 event recorded in El Centro Array #10

6. NEAR-FIELD GROUND MOTION RECORDS

6.1. General Properties of the Near-Field Ground Motions

A total of 105 near-field earthquake strong ground motions recorded in worldwide earthquakes with magnitude ranging from 5.0 to 7.6 were used herein. Dataset consists of both fault normal (FN) and fault parallel FP components of the near-field ground motion records whose station distance to fault is in the limit of 20 km. Except 3 rock site stations, all of the recording stations are located on NEHRP C and D sites. In order to identify pulse-like near-field ground motions pulse identification criteria suggested by Baker (2007) was followed. Details of the Baker (2007) study is given in the following subchapter.

Selected near-field earthquakes and complete list of all ground motions including the day of occurrence, earthquake magnitude, fault mechanism, strike, dip, and rake angles are given in Table 6.1 and component of the near-field ground motion, name of the recorded station, distance to fault (Joyner and Boore distance), shear wave velocity in upper 30 m of the soil deposit (in cm/s), earthquake magnitude, and fault mechanism are listed in Table 6.2. Figure 6.1 shows the distribution of magnitudes and distances to the horizontal projection of the rupture of the earthquake ground motions selected in this study. Number of the earthquakes plotted against their pulse periods in Figure 6.2.

Table 6.1. Near-field earthquakes included in the study

Event #	Earthquake	Date (m/d/y)	Moment magnitude (M_w)	Fault Mechanism	Strike (deg)	Dip (deg)	Rake Angle(deg)
1	San Fernando	2/9/71	6.6	Reverse	287	50	83
2	Coyote Lake	8/6/79	5.7	Strike-Slip	154	90	180
3	Imperial Valley-06	10/15/79	6.5	Strike-Slip	323	80	180
4	Mammoth Lakes-06	5/27/80	5.9	Strike-Slip	12	50	-35
5	Westmorland	4/26/81	5.9	Strike-Slip	249	45	-8
6	Coalinga-05	7/22/83	5.8	Reverse	247	31	44
7	Coalinga-07	7/25/83	5.2	Reverse	172	45	90
8	Morgan Hill	4/24/84	6.2	Strike-Slip	148	90	180
9	Nahanni, Canada	12/23/85	6.8	Reverse	160	25	90
10	N.Palm Spring	7/8/86	6.1	Reverse-Oblique	287	46	150
11	San Salvador	10/10/86	5.8	Strike-Slip	272	79	180
12	Whittier Narrows-01	10/1/87	6.0	Reverse-Oblique	280	30	100
13	Superstition Hills-02	11/24/87	6.5	Strike-Slip	127	90	180
14	Loma Prieta	10/17/89	6.9	Reverse-Oblique	128	70	140
15	Erzincan, Turkey	3/13/92	6.7	Strike-Slip	122	63	-164
16	Cape Mendocino	4/25/92	7.0	Reverse	350	14	68
17	Landers	6/28/92	7.3	Strike-Slip	336	90	180
18	Northridge-01	1/17/94	6.7	Reverse	122	40	103
19	Kobe, Japan	1/17/95	6.9	Strike-Slip	230	85	80
20	Kocaeli, Turkey	8/17/99	7.5	Strike-Slip	272	90	180
21	Chi-Chi, Taiwan	9/21/99	7.6	Strike-Slip	5	30	55
22	Duzce, Turkey	11/12/99	7.1	Reverse-Oblique	265	65	-178
23	Chi-Chi, Taiwan-03	9/20/99	6.2	Reverse	0	10	80
24	Chi-Chi, Taiwan-06	9/25/99	6.3	Reverse	5	30	100
25	Yountville	9/03/00	5.0	Strike-Slip	162	14	-128

Table 6.2. Near-field earthquake ground motions used in the study

Year	NGA#	Event	Comp.	Station	Rjb (km)	Vs30 (m/s)	Site Class	Moment Mag. (M_w)	Fault Mechanism
1971	77	San Fernando	FN	Pacoima Dam (upper left abut)	0.0	2016	A	6.6	Reverse
1979	150	Coyote Lake	FN	Gilroy Array #6	0.4	663	C	5.7	Strike-Slip
1979	158	Imperial Valley-06	FN	Aeropuerto Mexicali	0.0	275	D	6.5	Strike-Slip
1979	159	Imperial Valley-06	FN	Agrarias	0.0	275	D	6.5	Strike-Slip
1979	161	Imperial Valley-06	FN	Brawley Airport	8.5	209	D	6.5	Strike-Slip
1979	170	Imperial Valley-06	FN	EC County Center FF	7.3	192	D	6.5	Strike-Slip
1979	171	Imperial Valley-06	FN	EC Meloland Overpass FF	0.1	186	D	6.5	Strike-Slip
1979	173	Imperial Valley-06	FN	El Centro Array #10	6.2	203	D	6.5	Strike-Slip
1979	173	Imperial Valley-06	FP	El Centro Array #10	6.2	203	D	6.5	Strike-Slip
1979	174	Imperial Valley-06	FN	El Centro Array #11	12.5	196	D	6.5	Strike-Slip
1979	178	Imperial Valley-06	FN	El Centro Array #3	10.8	163	E	6.5	Strike-Slip
1979	178	Imperial Valley-06	FP	El Centro Array #3	10.8	163	E	6.5	Strike-Slip
1979	179	Imperial Valley-06	FN	El Centro Array #4	4.9	209	D	6.5	Strike-Slip
1979	180	Imperial Valley-06	FN	El Centro Array #5	1.8	206	D	6.5	Strike-Slip
1979	181	Imperial Valley-06	FN	El Centro Array #6	0.0	203	D	6.5	Strike-Slip
1979	181	Imperial Valley-06	FP	El Centro Array #6	0.0	203	D	6.5	Strike-Slip
1979	182	Imperial Valley-06	FN	El Centro Array #7	0.6	211	D	6.5	Strike-Slip
1979	182	Imperial Valley-06	FP	El Centro Array #7	0.6	211	D	6.5	Strike-Slip
1979	183	Imperial Valley-06	FN	El Centro Array #8	3.9	206	D	6.5	Strike-Slip
1979	184	Imperial Valley-06	FN	El Centro Differential Array	5.1	202	D	6.5	Strike-Slip
1979	184	Imperial Valley-06	FP	El Centro Differential Array	5.1	202	D	6.5	Strike-Slip
1979	185	Imperial Valley-06	FN	Holtville Post Office	5.5	203	D	6.5	Strike-Slip
1979	185	Imperial Valley-06	FP	Holtville Post Office	5.5	203	D	6.5	Strike-Slip
1980	250	Mammoth Lakes-06	FN	Long Valley Dam (Upr L Abut)	9.3	345	D	5.9	Strike-Slip
1981	316	Westmorland	FN	Parachute Test Site	16.5	349	D	5.9	Strike-Slip
1981	316	Westmorland	FP	Parachute Test Site	16.5	349	D	5.9	Strike-Slip
1981	319	Westmorland	FP	Westmorland Fire Sta	6.2	184	D	5.9	Strike-Slip
1983	407	Coalinga-05	FN	Oil City	2.4	376	D	5.8	Reverse
1983	415	Coalinga-05	FN	Transmitter Hill	4.1	376	D	5.8	Reverse
1983	418	Coalinga-07	FN	Coalinga-14th & Elm (Old CHP)	7.6	339	D	5.2	Reverse
1984	451	Morgan Hill	FN	Coyote Lake Dam (SW Abut)	0.2	597	C	6.2	Strike-Slip
1984	451	Morgan Hill	FP	Coyote Lake Dam (SW Abut)	0.2	597	C	6.2	Strike-Slip
1984	459	Morgan Hill	FN	Gilroy Array #6	9.9	663	C	6.2	Strike-Slip

Table 6.2. (continued)

Year	NGA#	Event	Comp.	Station	Rjb (km)	Vs30 (m/s)	Site Class	Moment Mag.(M_w)	Fault Mechanism
1985	496	Nahanni, Canada	FP	Site 2	0.0	660	C	6.8	Reverse
1986	529	N. Palm Springs	FN	North Palm Springs	0.0	345	D	6.1	Reverse-Oblique
1986	568	San Salvador	FP	Geotech Investig Center	2.1	545	C	5.8	Strike-Slip
1986	569	San Salvador	FP	National Geografical Inst	3.7	350	D	5.8	Strike-Slip
1987	615	Whittier Narrows-01	FN	Downey - Co Maint Bldg	15.0	272	D	6.0	Reverse-Oblique
1987	645	Whittier Narrows-01	FN	LB - Orange Ave	19.8	270	D	6.0	Reverse-Oblique
1987	722	Superstition Hills-02	FP	Kornbloom Road (temp)	18.5	207	D	6.5	Strike-Slip
1987	723	Superstition Hills-02	FN	Parachute Test Site	18.2	349	D	6.5	Strike-Slip
1989	763	Loma Prieta	FN	Gilroy - Gavilan Coll.	9.2	730	C	6.9	Reverse-Oblique
1989	764	Loma Prieta	FP	Gilroy - Historic Bldg.	10.3	339	D	6.9	Reverse-Oblique
1989	765	Loma Prieta	FN	Gilroy Array #1	8.8	1428	B	6.9	Reverse-Oblique
1989	766	Loma Prieta	FN	Gilroy Array #2	10.4	271	D	6.9	Reverse-Oblique
1989	767	Loma Prieta	FN	Gilroy Array #3	12.2	350	D	6.9	Reverse-Oblique
1989	767	Loma Prieta	FP	Gilroy Array #3	12.2	350	D	6.9	Reverse-Oblique
1989	779	Loma Prieta	FP	LGPC	0.0	478	C	6.9	Reverse-Oblique
1989	802	Loma Prieta	FN	Saratoga - Aloha Ave	7.6	371	C	6.9	Reverse-Oblique
1989	803	Loma Prieta	FN	Saratoga - W Valley Coll.	8.5	371	C	6.9	Reverse-Oblique
1989	803	Loma Prieta	FP	Saratoga - W Valley Coll.	8.5	371	C	6.9	Reverse-Oblique
1992	821	Erzincan, Turkey	FN	Erzincan	0.0	375	D	6.7	Strike-Slip
1992	821	Erzincan, Turkey	FP	Erzincan	0.0	275	D	6.7	Strike-Slip
1992	825	Cape Mendocino	FP	Cape Mendocino	0.0	514	C	7.0	Reverse
1992	828	Cape Mendocino	FN	Petrolia	0.0	713	C	7.0	Reverse
1992	828	Cape Mendocino	FP	Petrolia	0.0	713	C	7.0	Reverse
1992	879	Landers	FN	Lucerne	2.2	685	C	7.3	Strike-Slip
1994	1013	Northridge-01	FN	LA Dam	0.0	629	C	6.7	Reverse
1994	1013	Northridge-01	FP	LA Dam	0.0	629	C	6.7	Reverse
1994	1044	Northridge-01	FN	Newhall - Fire Sta	3.2	269	D	6.7	Reverse
1994	1045	Northridge-01	FN	Newhall - W Pico Canyon Rd.	2.1	286	D	6.7	Reverse
1994	1045	Northridge-01	FP	Newhall - W Pico Canyon Rd.	2.1	286	D	6.7	Reverse
1994	1050	Northridge-01	FN	Pacoima Dam (downstr)	4.9	2016	A	6.7	Reverse
1994	1063	Northridge-01	FP	Rinaldi Receiving Sta	0.0	282	D	6.7	Reverse
1994	1084	Northridge-01	FN	Sylmar - Converter Sta	0.0	251	D	6.7	Reverse
1994	1086	Northridge-01	FN	Sylmar - Olive View Med FF	1.7	441	C	6.7	Reverse

Table 6.2. (continued)

Year	NGA#	Event	Comp.	Station	Rjb (km)	Vs30 (m/s)	Site Class	Moment Mag. (M_w)	Fault Mechanism
1995	1119	Kobe, Japan	FN	Takarazuka	0.0	312	D	6.9	Strike-Slip
1995	1120	Kobe, Japan	FN	Takatori	1.5	256	D	6.9	Strike-Slip
1999	1176	Kocaeli, Turkey	FN	Yarimca	1.4	297	D	7.5	Strike-Slip
1999	1176	Kocaeli, Turkey	FP	Yarimca	1.4	297	D	7.5	Strike-Slip
1999	1193	Chi-Chi, Taiwan	FP	CHY024	9.6	428	C	7.6	Reverse-Oblique
1999	1202	Chi-Chi, Taiwan	FN	CHY035	12.6	555	C	7.6	Reverse-Oblique
1999	1244	Chi-Chi, Taiwan	FN	CHY101	10.0	259	D	7.6	Reverse-Oblique
1999	1480	Chi-Chi, Taiwan	FN	TCU036	19.8	495	C	7.6	Reverse-Oblique
1999	1480	Chi-Chi, Taiwan	FP	TCU036	19.8	495	C	7.6	Reverse-Oblique
1999	1482	Chi-Chi, Taiwan	FP	TCU039	19.9	541	C	7.6	Reverse-Oblique
1999	1486	Chi-Chi, Taiwan	FN	TCU046	16.7	466	C	7.6	Reverse-Oblique
1999	1492	Chi-Chi, Taiwan	FN	TCU052	0.0	579	C	7.6	Reverse-Oblique
1999	1493	Chi-Chi, Taiwan	FN	TCU053	6.0	455	C	7.6	Reverse-Oblique
1999	1494	Chi-Chi, Taiwan	FN	TCU054	5.3	461	C	7.6	Reverse-Oblique
1999	1496	Chi-Chi, Taiwan	FN	TCU056	10.5	440	D	7.6	Reverse-Oblique
1999	1498	Chi-Chi, Taiwan	FP	TCU059	17.1	230	D	7.6	Reverse-Oblique
1999	1499	Chi-Chi, Taiwan	FN	TCU060	8.5	496	D	7.6	Reverse-Oblique
1999	1501	Chi-Chi, Taiwan	FP	TCU063	9.8	476	C	7.6	Reverse-Oblique
1999	1502	Chi-Chi, Taiwan	FP	TCU064	16.6	358	D	7.6	Reverse-Oblique
1999	1503	Chi-Chi, Taiwan	FN	TCU065	0.6	306	D	7.6	Reverse-Oblique
1999	1505	Chi-Chi, Taiwan	FN	TCU068	0.0	487	C	7.6	Reverse-Oblique
1999	1505	Chi-Chi, Taiwan	FP	TCU068	0.0	487	C	7.6	Reverse-Oblique
1999	1510	Chi-Chi, Taiwan	FN	TCU075	0.9	573	C	7.6	Reverse-Oblique
1999	1511	Chi-Chi, Taiwan	FN	TCU076	2.8	615	C	7.6	Reverse-Oblique
1999	1515	Chi-Chi, Taiwan	FN	TCU082	5.2	473	C	7.6	Reverse-Oblique
1999	1519	Chi-Chi, Taiwan	FN	TCU087	7.0	562	C	7.6	Reverse-Oblique
1999	1529	Chi-Chi, Taiwan	FN	TCU102	1.5	714	C	7.6	Reverse-Oblique
1999	1529	Chi-Chi, Taiwan	FP	TCU102	1.5	714	C	7.6	Reverse-Oblique
1999	1530	Chi-Chi, Taiwan	FN	TCU103	6.1	494	C	7.6	Reverse-Oblique
1999	1531	Chi-Chi, Taiwan	FP	TCU104	12.9	544	C	7.6	Reverse-Oblique
1999	1548	Chi-Chi, Taiwan	FN	TCU128	13.2	600	C	7.6	Reverse-Oblique
1999	1548	Chi-Chi, Taiwan	FP	TCU128	10.0	600	C	7.6	Reverse-Oblique
1999	1550	Chi-Chi, Taiwan	FN	TCU136	8.3	538	C	7.6	Reverse-Oblique

Table 6.2. (continued)

Year	NGA#	Event	Comp.	Station	Rjb (km)	Vs30 (m/s)	Site Class	Moment Mag. (M_w)	Fault Mechanism
1999	1550	Chi-Chi, Taiwan	FP	TCU136	8.3	538	C	7.6	Reverse-Oblique
1999	1605	Duzce, Turkey	FP	Duzce	0.0	276	D	7.1	Strike-Slip
1999	1853	Yountville	FN	Napa Fire Station #3	8.4	271	D	5.0	Strike-Slip
1999	2457	Chi-Chi, Taiwan-03	FN	CHY024	18.5	428	C	6.2	Reverse
1999	2627	Chi-Chi, Taiwan-03	FN	TCU076	13.0	615	C	6.2	Reverse
1999	3475	Chi-Chi, Taiwan-06	FP	TCU080	0.0	509	C	6.3	Reverse

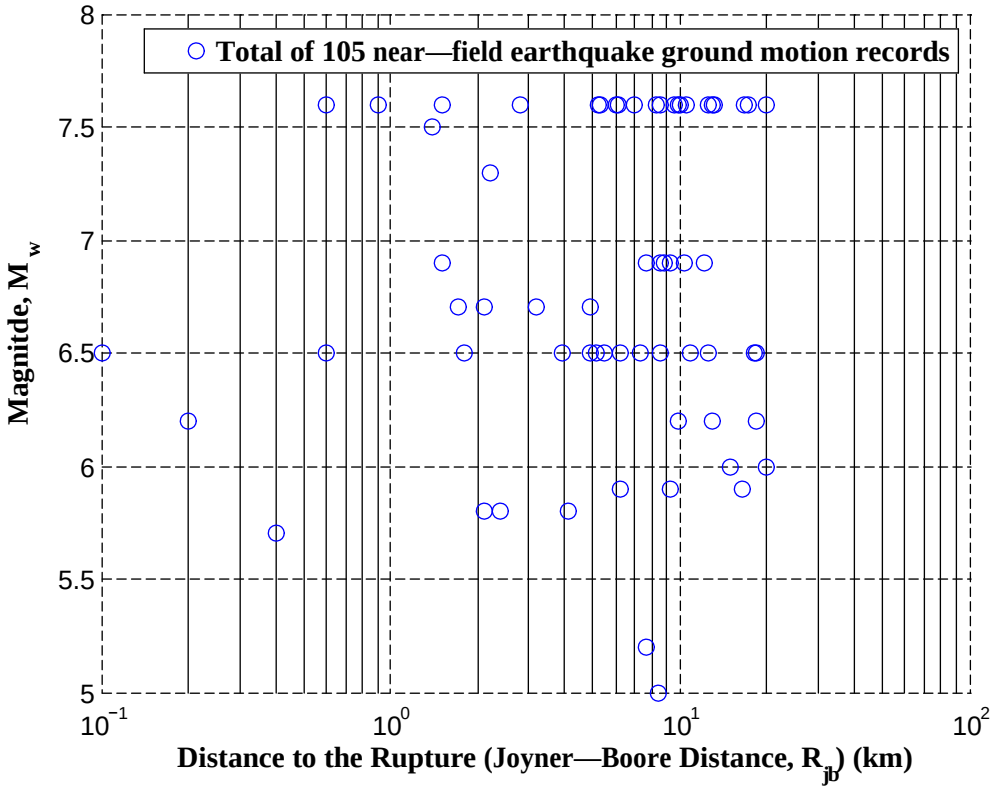

Figure 6.1. Magnitude versus distance (Joyner - Boore) to fault for earthquakes ground motions considered

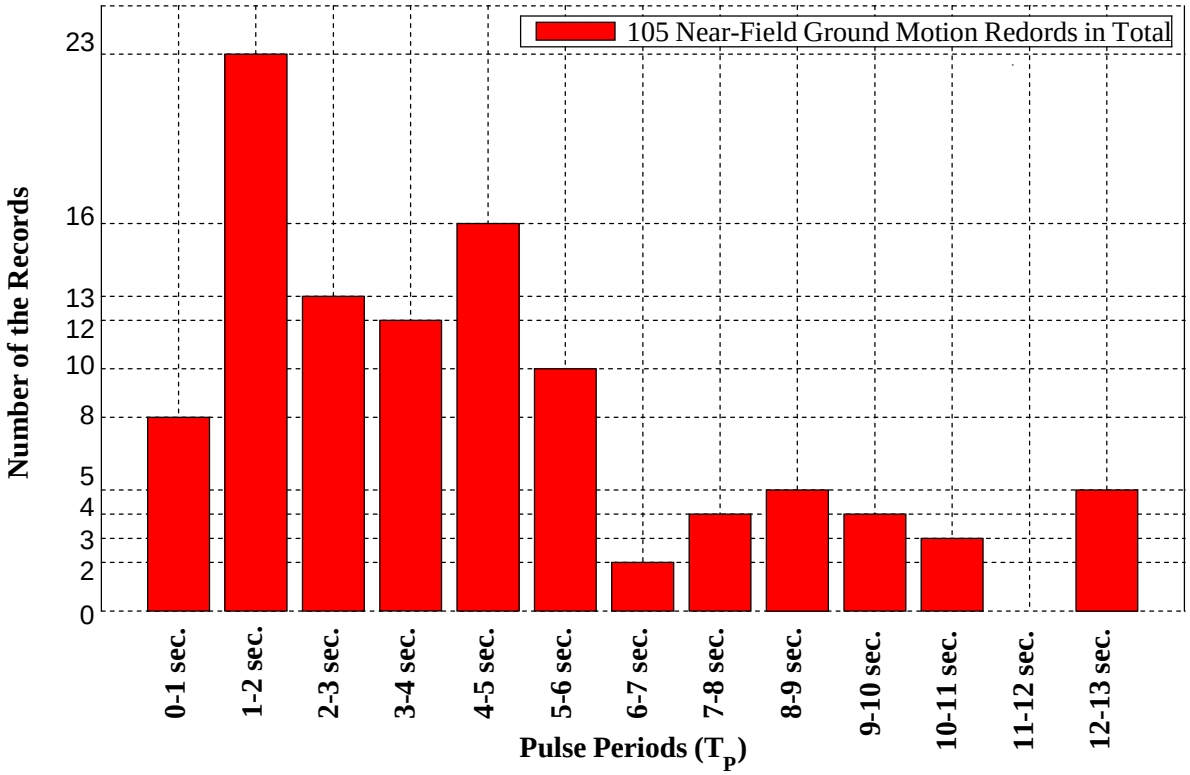

Figure 6.2. The number of the near-field ground motions for each classified pulse period intervals

6.2. Pulse Identification Method by Baker (2007)

In order to identify pulse-like ground motions by extracting the largest velocity pulse from a given ground motions is based on wavelet analysis proposed by Baker (2007). The Daubechies wavelet of order 4 is used as a mother wavelet because it can approximate the shape of many velocity pulses. The shape of the Daubechies wavelet is given in Figure 6.3.

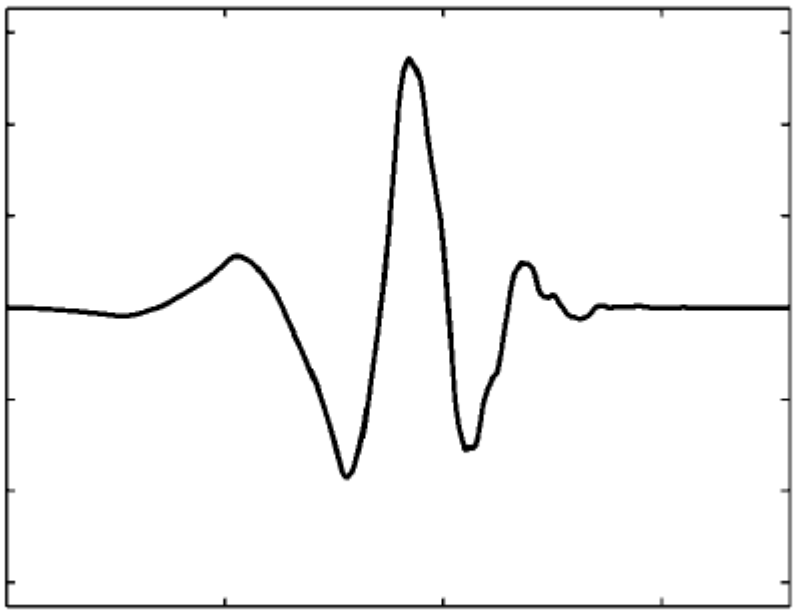

Figure 6.3. Daubechies wavelet of order 4

Mother wavelet basis function is defined as

$$\Phi_{s,l}(t) = \frac{1}{\sqrt{s}}\Phi\left(\frac{t-l}{s}\right) \tag{6.1}$$

In which $\Phi(.)$ is the mother wavelet function, s is the scale parameter that dilates the wavelet, and l is the location parameter that translates the wavelet in time. The ground motion of interest is transformed into coefficients for wavelet functions with varying scale and location. The coefficient associated with the wavelet having scale s and position l is given by

$$C_{s,l} = \int_{-\infty}^{\infty} f(t)\Phi_{s,l}(t)dt = \int_{-\infty}^{\infty} f(t)\frac{1}{s}\Phi\left(\frac{t-l}{s}\right)dt \quad (6.2)$$

In this procedure, first the continuous wavelet transform of the velocity time history is computed and the coefficient with the largest absolute value is identified. This coefficient, related to the largest wavelet, helps to establish the period and the location of the pulse. Moreover, energy of wavelet coefficient equals to that of the associated wavelet; therefore, the chosen pulse is the one with the largest energy. Selected wavelet is subtracted from the ground motion, and for the rest of the ground motion named as residual ground motion, the continuous wavelet transform is calculated. Calculation is done for the residual ground motion because wavelets having the same location and period at nearby extracted pulse would like to obtain. This step can be repeated several times until obtaining detailed extracted pulse.

After extraction of the pulse, original ground motion and residual ground motion is utilized to predict whether the inspected ground motion is pulselike. In order to achieve that pulse indicator is defined. Pulse indicator is defined in terms of the 'PGV ratio' and 'energy ratio'. The 'PGV ratio' is the ratio of the peak ground velocity of the residual record to the original record 's PGV and the 'energy ratio' energy of the residual record divided by the original record 's energy. Energy can be computed as the cumulative squared velocity of the signal, or, as the sum of the squared discrete wavelet coefficients. Pulse indicator can be calculated as follows,

$$1/1 + e^{-23.3+14.6(\text{PGV ratio})+20.5(\text{energy ratio})} \quad (6.3)$$

Pulse period takes values between 0 and 1. High values are the indication of the pulse like motion. In order to determine whether the extracted pulse is pulse-like motion or not, pulse indicator is utilized.

Finally Baker (2007) proposed following 3 conditions to choose pulse-like ground motions.

1) The original ground motion has a PGV of greater than 30 cm/sec.
2) Pulse indicator value is greater than 0.85.
3) The pulse arrives early in the time history

6.3. Pulse Period Estimation

6.3.1. General

The pulse period is associated with dominant amplitude in velocity response spectrum. The period of the velocity pulse is an important parameter for structural engineers, as the ratio of the fundamental period of the structure to the pulse period can greatly affect the structure's response (Anderson and Bertero, 1987; Alavi and Krawinkler, 2001; Mavroeidis *et al.*, 2004). T_p is calculated since it is related to an important physical parameter of the faulting process known as rise time (Mavroeidis *et al.*, 2004). Determination of the T_p is important in terms of eliminating the distinct pulses can be observed on the inelastic displacement spectra of the near-field ground motion records. In order to disregard the effect of these kinds of pulses, the pulse period is used to normalize the abscissa (period axis) of the strength-based spectral displacement amplification spectra to minimize the distinct pulse effects of the near-field records at the long period range (Mavroeidis *et al.*, 2004; Akkar *et al.*, 2004). In this study, normalization is done with respect to pulse periods proposed by Baker (2007).

Many researchers related to T_p with earthquake magnitude and in Table 6.3, proposed relations by several researchers between magnitude and T_p are given. Moreover, in Figure 6.4, pulse periods (obtained from the equation proposed by Baker (2007)) of the near-field ground motions is plotted versus earthquake magnitude M_w.

In addition to the empirical equations, pulse periods are obtained from velocity time histories and the pseudo spectral velocity response spectra of ground motion records. In case of difference between spectral-velocity-based T_p and wavelet-based T_p, the period with maximum spectral velocity is associated with high-frequency oscillatory portion of the ground motion, while the wavelet pulse period is associated with the visible velocity pulse.

Table 6.3. Predictive relationships between directivity pulse period and earthquake magnitude (M_w) (Tang *et al.*, 2011)

Source	General	Rock site	Soil site
Somerville (2003)	$\log_{10} T_P = -3.0 + 0.5M_w$	$\log_{10} T_P = -3.17 + 0.5M_w$	$\log_{10} T_P = -2.02 + 0.5M_w$
Mavroeidis and Papageorgiou (2003)	$\log_{10} T_P = -2.2 + 0.4M_w$ $\log_{10} T_P = -2.9 + 0.5M_w$ (self-similar)	-	-
Alavi and Krawinkler (2004)	$\log_{10} T_P = -1.76 + 0.31M_w$	-	-
Bray and Rodriguez-Marek (2004)	$ln\, T_P = -6.37 + 1.03M_w$ ($\log_{10} T_P = -2.77 + 0.45M_w$)	$ln\, T_P = -8.6 + 1.32M_w$ ($\log_{10} T_P = -3.73 + 0.57M_w$)	$ln\, T_P = -5.6 + 0.93M_w$ ($\log_{10} T_P = -2.43 + 0.40M_w$)
Baker (2007)	$ln\, T_P = -5.78 + 1.02M_w$ ($\log_{10} T_P = -2.51 + 0.44M_w$)	-	-
Tang and Zhang (2010)	$\log_{10} T_P = -2.18 + 0.38M_w$ $\log_{10} T_P = -3.02 + 0.50M_w$ (self-similar)	$\log_{10} T_P = -2.50 + 0.41M_w$ $\log_{10} T_P = -3.10 + 0.50M_w$ (self-similar)	$\log_{10} T_P = -2.18 + 0.38M_w$

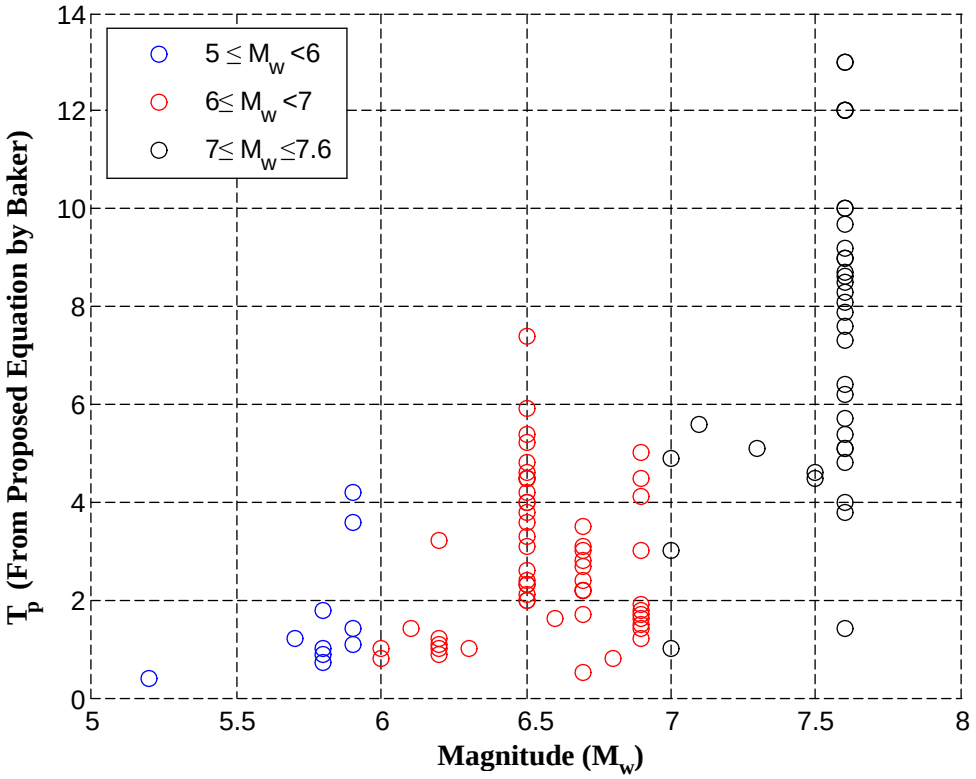

Figure 6.4. Pulse periods versus earthquake magnitude for 105 near-field pulselike ground motions

6.3.2. Estimation of the Pulse Period Defined by Baker (2007)

The period associated with the maximum Fourier amplitude of a wavelet can be used to define a pseudoperiod. To illustrate, an example wavelet and the sine wave with period equal to the wavelet's maximum Fourier amplitude are shown in Figure 6.5. The pseudoperiod of the largest wavelet coefficient is used as the ground motion's pulse period.

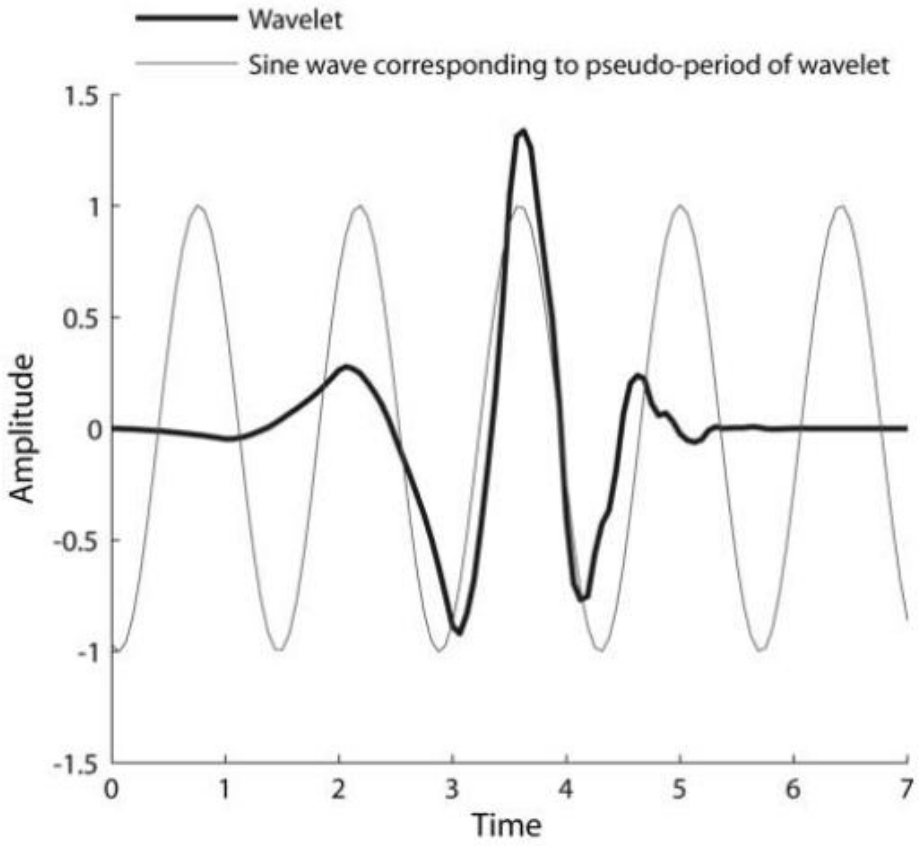

Figure 6.5. A Daubechies wavelet and a sine wave with peirod equal to the maximum of the wavelet's Fourier spectrum

6.3.3. Estimation of the Pulse Period from Velocity Time History and Velocity Response Spectrum

In this these, pulse periods were identified both from velocity time history and velocity response spectrum of each near-field records. In Figure 6.6, an example of pulse period obtained using two approaches are given. Here, the record has pulse periods of 3.4 sec. and 4.8 sec. when it is read from velocity time history and velocity response spectrum, respectively. Pulse periods obtained from all approaches utilized in this study are tabulated in Table 6.4, and are plotted against each other given in Figure, 6.7 and 6.8. When all catalog data were used, it has been observed that pulse periods estimated from velocity time histories and that of Baker's (2007) approach have similar trend, however pulse periods read from velocity response spectrum are generally smaller than that of Baker's

(2007) approach. In this study, pulse periods proposed by Baker (2007) was taken as a basis and used at period normalization.

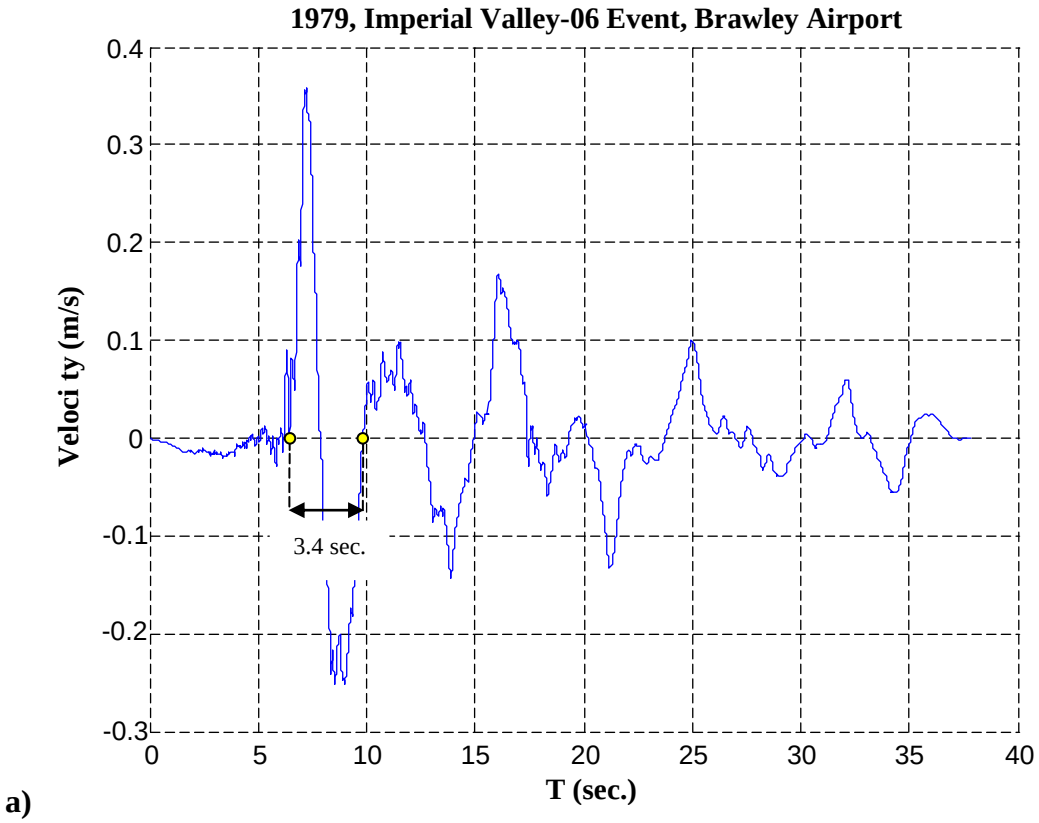

a)

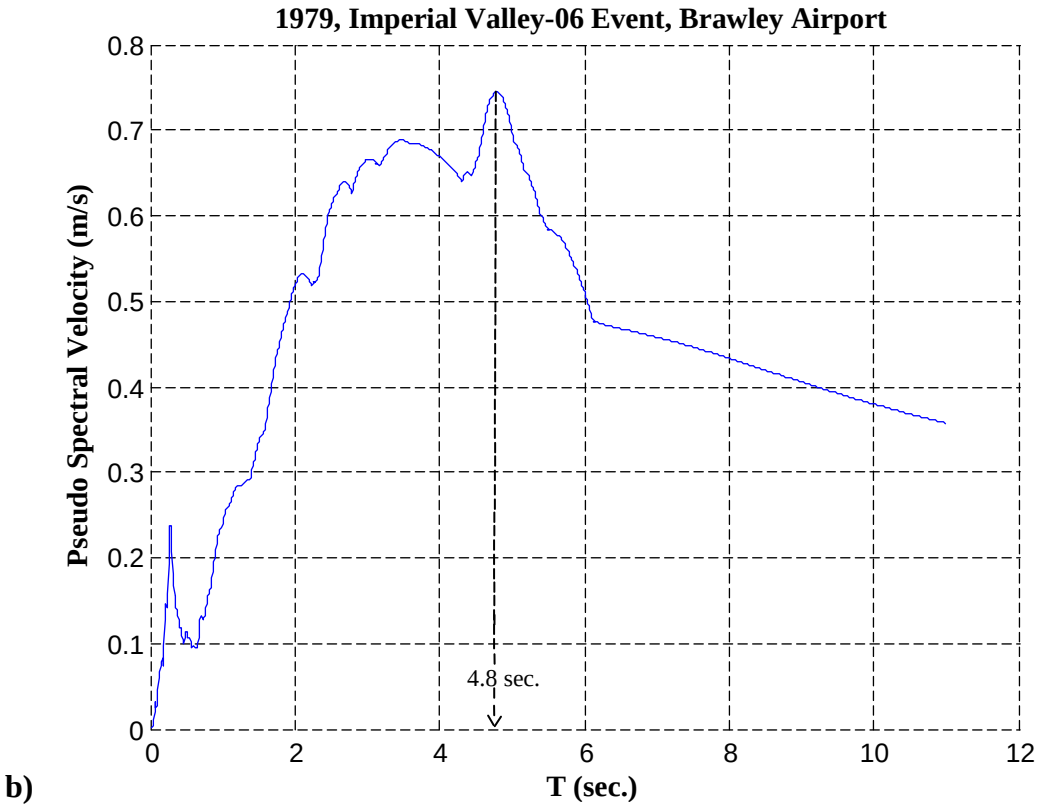

b)

Figure 6.6. **a)** Velocity time history, and **b)** Pseudo spectral velocity of the Imperial Valley-06 event recorded at Brawley Airport near-field station, and selection of the pulse period (T_p) from velocity time history and pseudo spectral velocity of the event

Table 6.4. Pulse periods of the near-field ground motions obtained from 3 approaches used in the study

NGA#	Comp.	Event	Station	Tp (Baker (sec.))	Tp (Velocity Time History (sec.))	Tp (Spectral Velocity (sec.))
77	FN	San Fernando	Pacoima Dam (upper left abut)	1.6	2.93	1.28
150	FN	Coyote Lake	Gilroy Array #6	1.2	0.92	0.91
158	FN	Imperial Valley-06	Aeropuerto Mexicali	2.4	1.84	1.63
159	FN	Imperial Valley-06	Agrarias	2.3	1.85	1.73
161	FN	Imperial Valley-06	Brawley Airport	4	3.4	4.79
170	FN	Imperial Valley-06	EC County Center FF	4.5	4.87	3.73
171	FN	Imperial Valley-06	EC Meloland Overpass FF	3.3	3.18	3.06
173	FN	Imperial Valley-06	El Centro Array #10	4.5	4.71	6.11
173	FP	Imperial Valley-06	El Centro Array #10	2	1.96	1.50
174	FN	Imperial Valley-06	El Centro Array #11	7.4	1.11	0.74
178	FN	Imperial Valley-06	El Centro Array #3	5.2	5.97	4.60
178	FP	Imperial Valley-06	El Centro Array #3	3.1	2.51	2.27
179	FN	Imperial Valley-06	El Centro Array #4	4.6	4.33	4.20
180	FN	Imperial Valley-06	El Centro Array #5	4	3.75	3.48
181	FN	Imperial Valley-06	El Centro Array #6	3.8	3.78	3.33
181	FP	Imperial Valley-06	El Centro Array #6	2.6	2.82	2.89
182	FN	Imperial Valley-06	El Centro Array #7	4.2	3.78	3.31
182	FP	Imperial Valley-06	El Centro Array #7	4.5	3.31	1.48
183	FN	Imperial Valley-06	El Centro Array #8	5.4	4.02	4.20
184	FN	Imperial Valley-06	El Centro Differential Array	5.9	5.56	2.67
184	FP	Imperial Valley-06	El Centro Differential Array	2	1.53	1.41
185	FN	Imperial Valley-06	Holtville Post Office	4.8	5.04	4.08
185	FP	Imperial Valley-06	Holtville Post Office	3.6	3.69	3.83
250	FN	Mammoth Lakes-06	Long Valley Dam (Upr L Abut)	1.1	1.27	0.83
316	FN	Westmorland	Parachute Test Site	3.6	3.10	0.88
316	FP	Westmorland	Parachute Test Site	4.2	5.10	3.26
319	FP	Westmorland	Westmorland Fire Sta	1.4	1.29	1.25
407	FN	Coalinga-05	Oil City	0.7	0.58	0.53
415	FN	Coalinga-05	Transmitter Hill	0.9	0.66	0.73
418	FN	Coalinga-07	Coalinga-14th & Elm (Old CHP)	0.4	0.52	0.36
451	FN	Morgan Hill	Coyote Lake Dam (SW Abut)	1	0.86	0.80

Table 6.4. (continued)

NGA	Comp.	Event	Station	Tp (Baker (sec.))	Tp (Velocity Time History (sec.))	Tp (Spectral Velocity (sec.))
451	FP	Morgan Hill	Coyote Lake Dam (SW Abut)	1.1	0.90	0.69
459	FN	Morgan Hill	Gilroy Array #6	1.2	1.04	1.14
496	FP	Nahanni, Canada	Site 2	0.8	0.61	0.61
529	FN	N. Palm Springs	North Palm Springs	1.4	1.35	0.90
568	FP	San Salvador	Geotech Investig Center	1.8	1.25	0.71
569	FP	San Salvador	National Geografical Inst	1	0.86	0.81
615	FN	Whittier Narrows-01	Downey - Co Maint Bldg	0.8	0.79	0.81
645	FN	Whittier Narrows-01	LB - Orange Ave	1	0.95	0.75
722	FP	Superstition Hills-02	Kornbloom Road (temp)	2.1	1.98	1.14
723	FN	Superstition Hills-02	Parachute Test Site	2.3	2.23	2.38
763	FN	Loma Prieta	Gilroy - Gavilan Coll.	1.8	1.43	0.41
764	FP	Loma Prieta	Gilroy - Historic Bldg.	1.8	1.37	1.33
765	FN	Loma Prieta	Gilroy Array #1	1.2	0.40	0.37
766	FN	Loma Prieta	Gilroy Array #2	1.7	1.41	1.45
767	FN	Loma Prieta	Gilroy Array #3	1.5	2.28	2.17
767	FP	Loma Prieta	Gilroy Array #3	3	3.26	0.47
779	FP	Loma Prieta	LGPC	4.1	1.86	0.82
802	FN	Loma Prieta	Saratoga - Aloha Ave	4.5	3.08	5.26
803	FN	Loma Prieta	Saratoga - W Valley Coll.	1.9	3.95	1.12
803	FP	Loma Prieta	Saratoga - W Valley Coll.	5	1.74	4.20
821	FN	Erzincan, Turkey	Erzincan	2.7	2.36	1.81
821	FP	Erzican, Turkey	Erzincan	2.2	2.84	2.06
825	FP	Cape Mendocino	Cape Mendocino	4.9	3.73	0.91
828	FN	Cape Mendocino	Petrolia	3	1.92	0.77
828	FP	Cape Mendocino	Petrolia	1	0.74	0.74
879	FN	Landers	Lucerne	5.1	7.04	4.63
1013	FN	Northridge-01	LA Dam	1.7	1.35	1.30
1013	FP	Northridge-01	LA Dam	2.8	1.38	2.65
1044	FN	Northridge-01	Newhall - Fire Sta	2.2	1.00	1.28
1045	FN	Northridge-01	Newhall - W Pico Canyon Rd.	2.4	3.20	2.18
1045	FP	Northridge-01	Newhall - W Pico Canyon Rd.	2.2	1.98	2.08
1050	FN	Northridge-01	Pacoima Dam (downstr)	0.5	0.47	0.46
1063	FP	Northridge-01	Rinaldi Receiving Sta	3	2.09	2.34

Table 6.4. (continued)

NGA	Comp.	Event	Station	Tp (Baker (sec.))	Tp (Velocity Time History (sec.))	Tp (Spectral Velocity (sec.))
1084	FN	Northridge-01	Sylmar - Converter Sta	3.5	2.53	2.97
1086	FN	Northridge-01	Sylmar – Olive View Med FF	3.1	1.91	2.58
1119	FN	Kobe, Japan	Takarazuka	1.4	1.41	1.33
1120	FN	Kobe, Japan	Takatori	1.6	2.30	1.25
1176	FN	Kocaeli, Turkey	Yarimca	4.5	4.14	3.47
1176	FP	Kocaeli, Turkey	Yarimca	4.6	4.67	4.53
1193	FP	Chi-Chi, Taiwan	CHY024	6.2	4.61	5.25
1202	FN	Chi-Chi, Taiwan	CHY035	1.4	1.43	1.39
1244	FN	Chi-Chi, Taiwan	CHY101	4.8	5.35	3.43
1480	FN	Chi-Chi, Taiwan	TCU036	5.4	5.82	5.04
1480	FP	Chi-Chi, Taiwan	TCU036	6.4	6.03	5.34
1482	FP	Chi-Chi, Taiwan	TCU039	8.1	5.16	5.40
1486	FN	Chi-Chi, Taiwan	TCU046	8.6	6.64	8.55
1492	FN	Chi-Chi, Taiwan	TCU052	8.5	5.96	6.51
1493	FN	Chi-Chi, Taiwan	TCU053	13	9.84	9.45
1494	FN	Chi-Chi, Taiwan	TCU054	10	6.93	8.89
1496	FN	Chi-Chi, Taiwan	TCU056	13	8.93	9.21
1498	FP	Chi-Chi, Taiwan	TCU059	7.6	7.42	5.63
1499	FN	Chi-Chi, Taiwan	TCU060	12	11.78	10.62
1501	FP	Chi-Chi, Taiwan	TCU063	5.1	5.20	3.65
1502	FP	Chi-Chi, Taiwan	TCU064	8.7	7.17	6.92
1503	FN	Chi-Chi, Taiwan	TCU065	5.7	4.86	4.53
1505	FN	Chi-Chi, Taiwan	TCU068	12	9.14	8.86
1510	FN	Chi-Chi, Taiwan	TCU075	5.1	5.30	4.47
1511	FN	Chi-Chi, Taiwan	TCU076	4	5.07	3.14
1515	FN	Chi-Chi, Taiwan	TCU082	9.2	6.48	8.43
1519	FN	Chi-Chi, Taiwan	TCU087	9	9.49	8.87
1529	FN	Chi-Chi, Taiwan	TCU102	9.7	5.88	2.61
1529	FP	Chi-Chi, Taiwan	TCU102	3.8	2.79	2.42
1530	FN	Chi-Chi, Taiwan	TCU103	8.3	8.06	8.34
1531	FN	Chi-Chi, Taiwan	TCU104	12	8.98	5.35
1531	FP	Chi-Chi, Taiwan	TCU104	7.3	6.51	5.42
1548	FN	Chi-Chi, Taiwan	TCU128	9	9.11	7.72

Table 6.4. (continued)

NGA	Comp.	Event	Station	Tp (Baker (sec.))	Tp (Velocity Time History (sec.))	Tp (Spectral Velocity (sec.))
1548	FP	Chi-Chi, Taiwan	TCU128	10	5.36	4.76
1550	FN	Chi-Chi, Taiwan	TCU136	10	7.60	8.50
1550	FP	Chi-Chi, Taiwan	TCU136	7.9	6.09	8.73
1605	FP	Duzce, Turkey	Duzce	5.6	4.11	5.13
1853	FN	Yountville	Napa Fire Station #3	0.7	0.60	0.66
2457	FN	Chi-Chi, Taiwan-03	CHY024	3.2	2.72	2.83
2627	FN	Chi-Chi, Taiwan-03	TCU076	0.9	1.05	0.88
3475	FP	Chi-Chi, Taiwan-06	TCU080	1	0.78	0.79

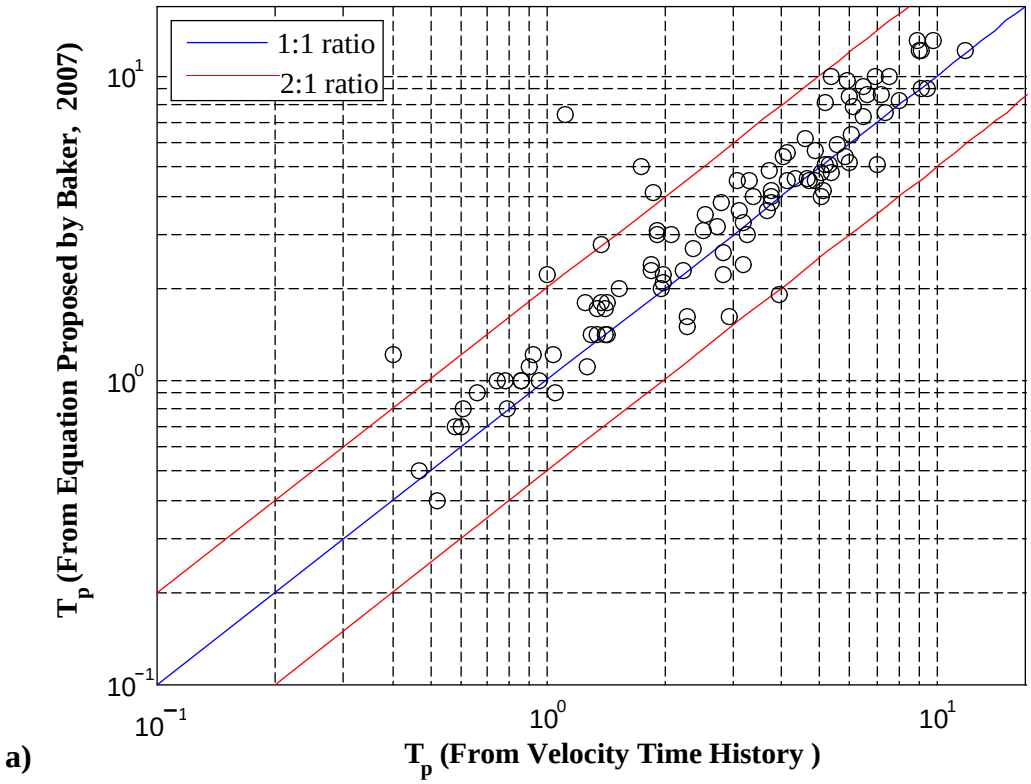

a)

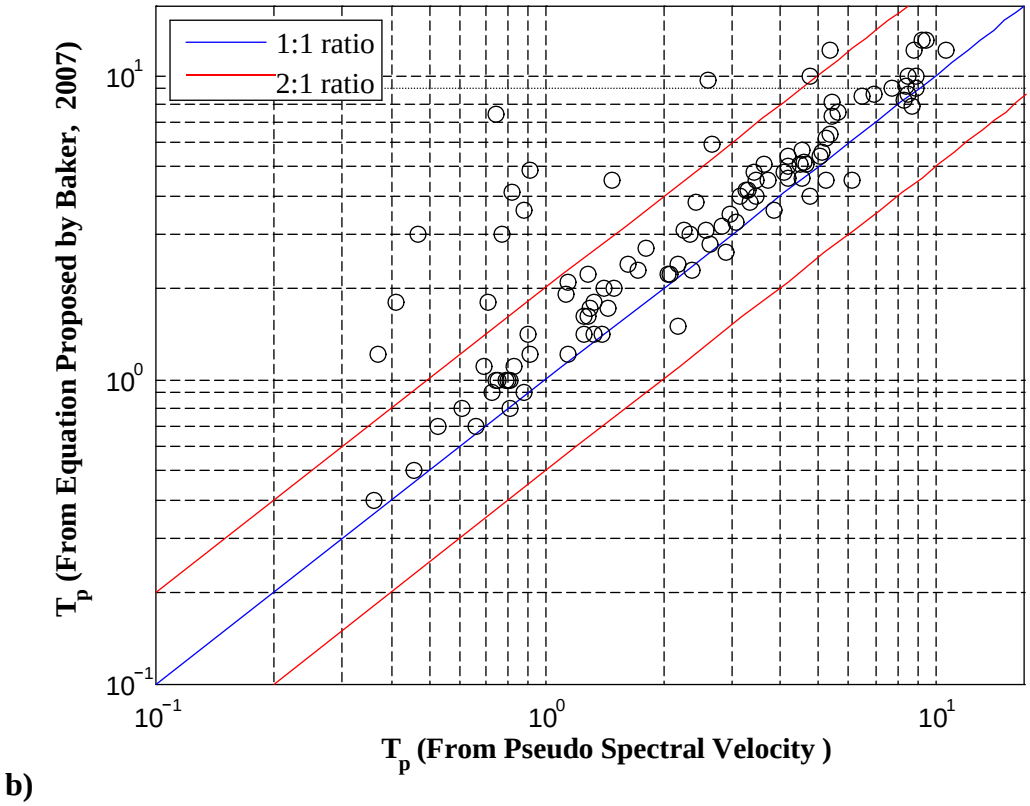

b)

Figure 6.7. T_p (pulse period) of the near-field ground motions (105 in total) obtained from **a)** empirical equation proposed by Baker (2007), and velocity time histories of the records **b)** emphirical equation proposed by Baker (2007), and pseudo-velocity response spectra of the records

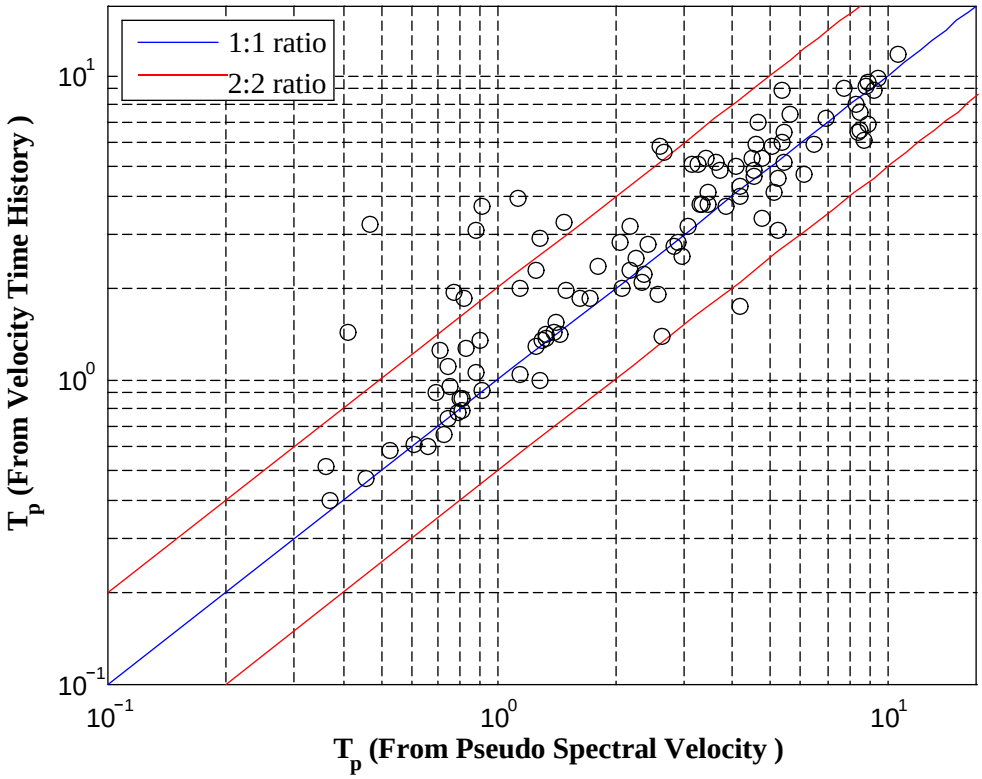

Figure 6.8. T_p (pulse period) of the near-field ground motions (105 in total) obtained from velocity time histories, and pseudo-velocity response spectra of the records

7. STRENGTH-BASED DISPLACEMENT AMPLIFICATION SPECTRA FOR NEAR-FIELD GROUND MOTIONS

7.1. Classification of the Near-Field Records With Respect to Their Pulse Periods

Pulse periods of 105 near-field records are divided into 8 groups. The intervals of the groups vary due to the lack of the near-field records for different periods. The interval of the groups whose period is smaller than 6 sec. changes in every 1 sec. . The other 2 groups have pulse periods which change between 6 and 8 sec., and the last group includes the pulse periods change between 8 and 13 sec.. The number of pulse periods in the groups is 8, 23, 13, 12, 16, 10, 6, and 17 for the groups from 1 to 8, respectively. Different soil types and earthquake magnitudes fall into these groups.

The mean strength-based displacement amplification spectra of each group were computed for each T/T_p ratios and different strength reduction factors. From Figure 7.1 to 7.12, the mean strength-based amplification ratios corresponding to the groups of the pulse periods were illustrated. During the analysis modified-Clough stiffness degrading hysteretic model was employed. The post-yield stiffness ratio (α) of the hysteretic model was changed to investigate the effect of it on the mean spectra of each T_p interval. For this purpose, post-yield stiffness ratio of the modified-Clough hysteretic model is taken as 2 percent and 5 percent and obtained strength-based displacement amplification spectra from these values were compared with that spectrum obtained by taking α equals to 0. In addition, to observe the effect of the stiffness degradation on the mean spectra, ratio of the strength-based displacement amplification spectra obtained from non-degrading, elasto-plastic, system to those obtained from stiffness degrading system, modified-Clough, with α equal to 0 is computed. In order to develop the strength-based displacement amplification spectra, constant-R_y response spectra computed with Bispec v.2.03, and calculated ductility values divided by the assigned different R_y levels in MATLAB.

7.2. Effect of the Post-Yield Stiffness Ratio

In order to study of effect of the post-yield stiffness on the strength-based spectral displacement amplification ratios, maximum displacement of the modified-Clough bilinear stiffness degrading systems (Figure 4.2) with post-yield stiffness ratios (post-yield stiffness normalized with initial stiffness) of α=0, 2 percent, and 5 percent when subjected to 105 near-field ground motions which were divided into 8 groups according to pulse periods of the near-field ground motions was computed. Then, ratios of the spectral displacement amplification of the modified-Clough bilinear stiffness degrading systems with α=2 percent and 5 percent to spectral displacement amplification of the modified-Clough bilinear stiffness degrading system with α=0 was obtained for each group and for lateral strength ratio, R_y =6. Figures from 7.13 to 7.16 show the mean ratios of the spectral displacement amplification of the modified-Clough bilinear stiffness degrading system having post-yield stiffness ratios of 2 percent and 5 percent to spectral displacement amplification ratio of the modified-Clough bilinear stiffness degrading system having post-yield stiffness ratio of 0.

For short mean T/T_p ranges, spectral displacement amplification ratio of systems with positive post-yield stiffness is smaller than that of systems have zero post-yield stiffness. It can be observed that when initial period, T, almost equals to mean of the pulse periods, T_p, of the records differences between systems with and without post-yield stiffness ratios is almost equal to 1. Moreover, for the very short T/T_p ratios, such as smaller than 0.2, the difference between systems with post-yield stiffness ratio and without post-yield stiffness ratio increases as the post-yield stiffness rises.

7.3. Effect of the Stiffness Degradation

The effect of the stiffness degradation on the strength-based displacement amplification spectra is studied by considering the modified-Clough model. In order to study the effect of stiffness degradation on the strength-based spectral displacement amplification ratios or on the inelastic displacement demands (relation between these two was given in Chapter 5), the ratio of S_{daR} for non-degrading, elastoplastic, systems to S_{daR} for stiffness degrading systems with zero post-yield stiffness ratio was computed. This

ratio also represents a measure of how larger or smaller the inelastic displacement demands are in the systems with stiffness-degradation compared to those in non-degrading systems. This ratio was obtained for each normalized period of vibration interval by using different levels of strength reduction factors. From Figure 7.17 to Figure 7.20, the ratio of $S_{daR,EP}$ to $S_{daR,MC\ (\alpha=0)}$ was illisturated for each pulse period group.

Systems have stiffness degradation exhibit significantly greater strength demand or inelastic displacement demand than those non-degrading for short T/T_p ratios. For R_y=1.5, ratio of $S_{daR,\ EP}$ / $S_{daR,\ MC\ (\alpha=0)}$ is equal to 1 with the exception of very short T/T_p range and records have pulse periods between 6 sec. and 8 sec., and 8 sec. and 13 sec.. Structures with high ductility levels and designed by using modified-Clough stiffness degrading hysteretic model experience higher inelastic displacement than systems having non-degrading hysteretic behaviour. Therefore, when strength reduction factors obtained for the far-field ground motions are chosen for the structures that are in risk from the near-field ground motions should be utilized with care. In addition, there are significant differences between the results of the hysteretic models,and thus they should also be used with care.

7.4. Dispersion of the Mean Values

To know the scatter that exists in the results about the mean, it is important to quantify the level of dispersion. To quantify the dispersion, coefficient of variation (COV), which defined as the ratio of the standard deviation to the mean is utilized. This statistical parameter was computed for each T_p group and different lateral strength levels with 5 percent post-yield stiffness ratio.

Dispersion of the spectral displacement amplification ratios of structures does not always increase as the lateral strength ratio increases. The primary reason is that ground motion ensembles were not categorised according to site class and earthquake magnitude; therefore, standard deviation of the mean of the ground motion records can be higher or almost equal to eachother for different lateral strength ratios. For T/T_p ratios smaller than 0.2, standard deviation of the ground motion ensembles ranges from 70 percent to 90 percent. From Figure 7.21 to Figure 7.24, the scatter of the mean of the records for each

pulse period interval are showed. Larger dispersion is not related to increase in the pulse period.

7.5. Nonlinear Regression Models for the Each Pulse Period Interval

7.5.1. Nonlinear Least Squares

Nonlinear regression curve of the data calculated for different strength reduction factors, post-yield stiffness ratios, and different T/T_p ratios were obtained by means of the 'Surface Fitting Toolbox' of the Matlab software. The process and steps of the obtaining these curves were given below.

Surface Fitting Toolbox software uses the nonlinear least-squares formulation to fit a nonlinear model to data. A nonlinear model is defined as an equation that is nonlinear in the coefficients or a combination of linear and nonlinear in the coefficients. For example, Gaussians, ratios of polynomials, and power functions are all nonlinear.

In matrix form, nonlinear models are given by the formula

$$y = f(x, \beta) + \varepsilon \tag{7.1}$$

where,

- y is an n-by-1 vector of responses.
- f is a function of β and X.
- β is a m-by-1 vector of coefficients.
- X is the n-by-m design matrix for the model.
- ε is an n-by-1 vector of errors.

Nonlinear models are more difficult to fit than linear models because the coefficients cannot be estimated using simple matrix techniques. Instead, an iterative approach is required that follows these steps:

1. Start with an initial estimate for each coefficient. For some nonlinear models, a heuristic approach is provided that produces reasonable starting values. For other models, random values on the interval [0,1] are provided.
2. Produce the fitted curve for the current set of coefficients. The fitted response value $\hat{y}$ is given by

$$\hat{y} = f(x, b) \tag{7.2}$$

and involves the calculation of the Jacobian of f(x,b), which is defined as a matrix of partial derivatives taken with respect to the coefficients.

3. Adjust the coefficients and determine whether the fit improves. The direction and magnitude of the adjustment depend on the fitting algorithm. The toolbox provides these algorithms:

- Trust-region — This is the default algorithm and must be used if you specify coefficient constraints. It can solve difficult nonlinear problems more efficiently than the other algorithms and it represents an improvement over the popular Levenberg-Marquardt algorithm.

- Levenberg-Marquardt — This algorithm has been used for many years and has proved to work most of the time for a wide range of nonlinear models and starting values. If the trust-region algorithm does not produce a reasonable fit, and coefficient constraints are not avaible, the Levenberg-Marquardt algorithm should be tried.

- Gauss-Newton — This algorithm is potentially faster than the other algorithms, but it assumes that the residuals are close to zero. It is included with the toolbox for pedagogical reasons and should be the last choice for most models and data sets.

Iterate the process by returning to step 2 until the fit reaches the specified convergence criteria.

Proposed equations are provided and coefficients in these equations are in Table 7.1 and 7.2. When post-yield stiffness ratio is 2 percent, for pulse periods between 1-2 sec. and 2-3 sec., same equation are proposed for these two intervals and for pulse periods between 6-8 sec. and 8-13 sec. same equation is proposed. In addition, as post-yield stiffness ratio is 5 percent, for pulse periods between 0-1 sec., 1-2 sec., and 2-3 sec., same equation are suggested for these three intervals and for pulse periods between 6-8 sec. and 8-13 sec. same eqution is proposed.

7.5.1.1. Equations Proposed for Each Pulse Period Interval and Post-Yield Stiffness Ratio, α=2 percent.

$0 < T_p < 1$ sec.

$$S_{daR} = a * \left(\frac{1}{(T/T_p)^b}\right) * e^{\left(-\frac{T}{T_p}/R_y\right)^c} + d * e^{(R_y)^e} + f * \ln\left(1/\left(\frac{T}{T_p}\right)\right) \quad (7.3)$$

$1 \text{ sec.} \leq T_p < 2$ sec. and $2 \text{ sec.} \leq T_p < 3$ sec.

$$S_{daR} = a * \left(\frac{1}{(T/T_p)^b}\right) * e^{\left(\frac{T}{T_p}/R_y\right)^c} + d * e^{(R_y)^e} * e^{\ln(\frac{T}{T_p})} + f \quad (7.4)$$

$3 \text{ sec.} \leq T_p < 4$ sec.

$$S_{daR} = a * \left(\frac{1}{(T/T_p)^b}\right) * e^{\left(\frac{T}{T_p}/R_y\right)^c} + d * e^{(R_y)^e} + f * \ln\left(\frac{1}{T/T_p}\right) + \frac{T/T_p}{R_y} \quad (7.5)$$

$4 \text{ sec.} \leq T_p < 5$ sec.

$$S_{daR} = a * \left(\frac{1}{(T/T_p)^b}\right) * e^{\left(\frac{T}{T_p}/R_y\right)^c} + d * \ln(R_y) + \frac{{R_y}^e}{T/T_p} \quad (7.6)$$

6 sec. ≤ T_p < 8 sec. and 8 sec. ≤ T_p ≤ 13 sec.

$$S_{daR} = a * \left(\frac{1}{(T/T_p)^b}\right) * e^{\left(\frac{T}{T_p}/R_y\right)^c} + d * e^{(R_y)^e} + f * \ln\left(\frac{T/T_p}{R_y}\right) + g * e^{\left(R_y/(T/T_p)\right)} \quad (7.7)$$

Table 7.1. Coefficients of the regression formulae of the T_p intervals for α=2 percent

Post-yield stiffness ratio, α=2 percent							
Coefficients	**0-1 sec.**	**1-2 sec.**	**2-3 sec.**	**3-4 sec.**	**4-5 sec.**	**6-8 sec.**	**8-13 sec.**
a	13.4	4.8	15.4	6.0	-1.36	0.56	3.9
b	0.34	0.7	0.25	0.5	0.93	1.0	0.49
c	27.8	-46	-67.6	-116.5	-2.29	-153.9	-254.5
d	0.39	-0.017	-0.1	0.1	0.37	0.25	0.286
e	-0.04	0.22	0.1	0.49	0.2	0.44	0.40
f	0.074	1	1.4	0.59	-	0.195	0.10
g	-	-	-	-	-	-0.026	-0.053

7.5.1.2. Equations Proposed for Each Pulse Period Interval and Post-Yield Stiffness Ratio, α=5 percent.

0 < T_p < 1 sec., 1 sec. ≤ T_p < 2 sec., and 2 sec. ≤ T_p < 3 sec.

$$S_{daR} = a * \left(\frac{1}{(T/T_p)^b}\right) * e^{\left(\frac{T}{T_p}/R_y\right)^c} + d * e^{(R_y)^e} * e^{\ln(\frac{T}{T_p})} + f \quad (7.8)$$

3 sec. ≤ T_p < 4 sec.

$$S_{daR} = a * \left(\frac{1}{(T/T_p)^b}\right) * e^{\left(\frac{T}{T_p}/R_y\right)^c} + d * e^{(R_y)^e} + \left(\frac{T}{T_p}\right)^f \quad (7.9)$$

4 sec. ≤ T_p < 5 sec.

$$S_{daR} = a * \left(\frac{1}{(T/T_p)^b}\right) * e^{\left(\frac{T}{T_p}/R_y\right)^c} + d * e^{(R_y)^e} + f * e^{\ln\left(\frac{T}{T_p}\right)} + g * \left(\frac{T}{T_p}/R_y\right) \quad (7.10)$$

6 sec. ≤ T_p < 8 sec. and 8 sec. ≤ T_p ≤ 13 sec.

$$S_{daR} = a * \left(\frac{1}{(T/T_p)^b}\right) * e^{\left(\frac{T}{T_p}/R_y\right)^c} + d * e^{(R_y)^e} + f * \ln\left(\frac{T/T_p}{R_y}\right) + g * e^{\left(R_y/(T/T_p)\right)} \quad (7.11)$$

Table 7.2. Coefficients of the regression formulae of the T_p intervals for α=5 percent

Post-yield stiffness ratio, α=5 percent							
Coefficients	**0-1 sec.**	**1-2 sec.**	**2-3 sec.**	**3-4 sec.**	**4-5 sec.**	**6-8 sec.**	**8-13 sec.**
a	12.6	5.9	12.7	9.6	0.49	1.08	2.37
b	0.164	0.415	0.07	0.184	0.9	0.7	0.45
c	-26.0	-43.0	-56.2	-114	-146	-159	-240
d	-0.004	-0.046	-0.26	0.0002	0.42	0.24	0.27
e	0.365	-33.4	-38.4	0.97	0.3	0.37	0.36
f	1.0	1.0	1.3	-0.2	-1.8	-0.13	-0.09
g	-	-	-	-	2.23	-0.019	-0.034

7.5.2. Numerical Examples

In order to better describe the displacement amplification factor quantitative results obtained from proposed regression formulae equations as a function of normalized period and strength reduction factor range from 1.5 to 6. T_p can be computed from the proposed

empirical equations mainly depend upon earthquake moment magnitude. Some equations were developed for different soil types and all suggested equations can be found in Table 6.3.

Calculation of the pulse period with respect to equation proposed by Baker (2007),

$$\ln T_p = -5.78 + 1.02 M_w \quad (7.12)$$

for an earthquake with moment magnitude of M_w=6.5, T_p equals to 2.34 sec.

Regression formula to be utilized depends on post-yield stiffness ratio is considered for the design and calculated T_p; therefore, both value have to be decided and known beforehand to compute spectral displacement amplification ratio S_{daR}. Then, the other two necessary parameters fundamental period of the structure is normalized by obtained T_P and chosen R_y will be put into formula.

For different moment magnitude values, initial structural periods and strength reduction factors calculated spectral displacement ratios, S_{daR}, were given in Appendix by tables. Initial period was chosen between 1 sec. and 2 sec. since in ASCE 41-06, for systems initial structural periods greater than 1 sec., inelastic displacement ratio (C_1 coefficient) was taken as 1. Thus, comparison can be made between calculated S_{daR} and C_1 coefficient as defined in ASCE 41-06.

It can be observed from the tables given in Appendix an increase in moment magnitude results in increase in spectral displacement amplification ratio, S_{daR}. Especially, as magnitude equals to 7.5 and R_y is taken 6, S_{daR} obtained from regression formulae is twice as large as the C_1 coefficient defined in ASCE 41-06. Numerical examples have revealed that for structures whose period larger than 1sec., displacement amplification spectra take values between 1.1-2.6, where this value (modification factor, C_1, equation 3.14) is fixed to 1 in ASCE 41-06. S_{daR} values also rise with the increase in R_y values. For magnitude 6.5 and systems with post-yield stiffness ratio equals to 5 percent, S_{daR} computed by suggested regression formulae are close to 1 with the increase in initial

structural periods. These findings imply that C_1 value used in ASCE 41-06 standard results in underestimation of target displacement in pushover analysis, when structure is subjected to near field strong ground motion.

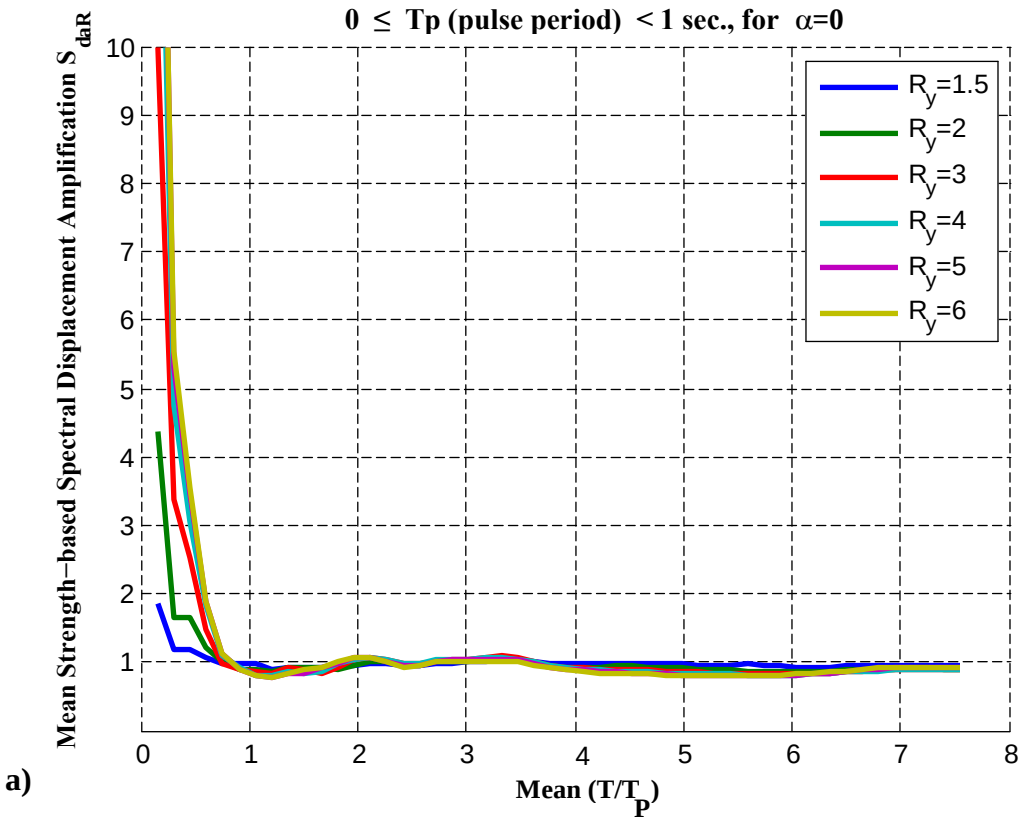

a)

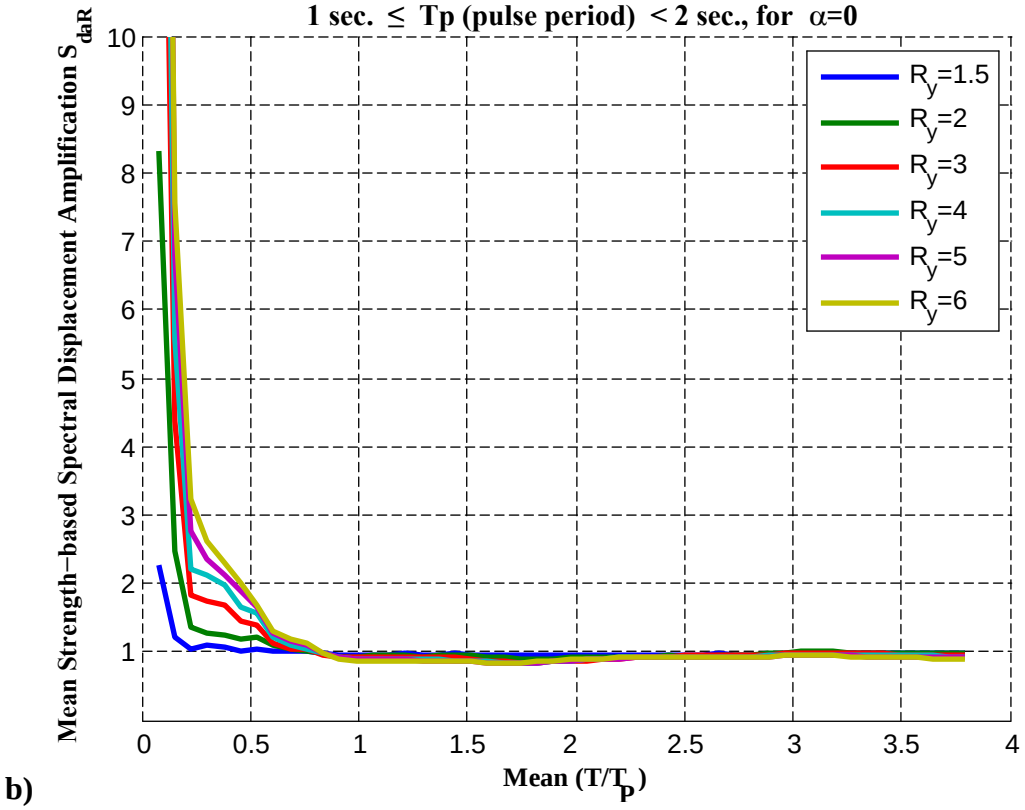

b)

Figure 7.1. Mean strength-based spectral displacement amplification vs. mean T/T_p spectra of the near-field records have pulse periods range from **a)** 0 to 1 sec. **b)** 1 sec. to 2 sec., and designed for post-yield stiffness ratio, α=0, and R_y =1.5, 2, 3, 4, 5, and 6

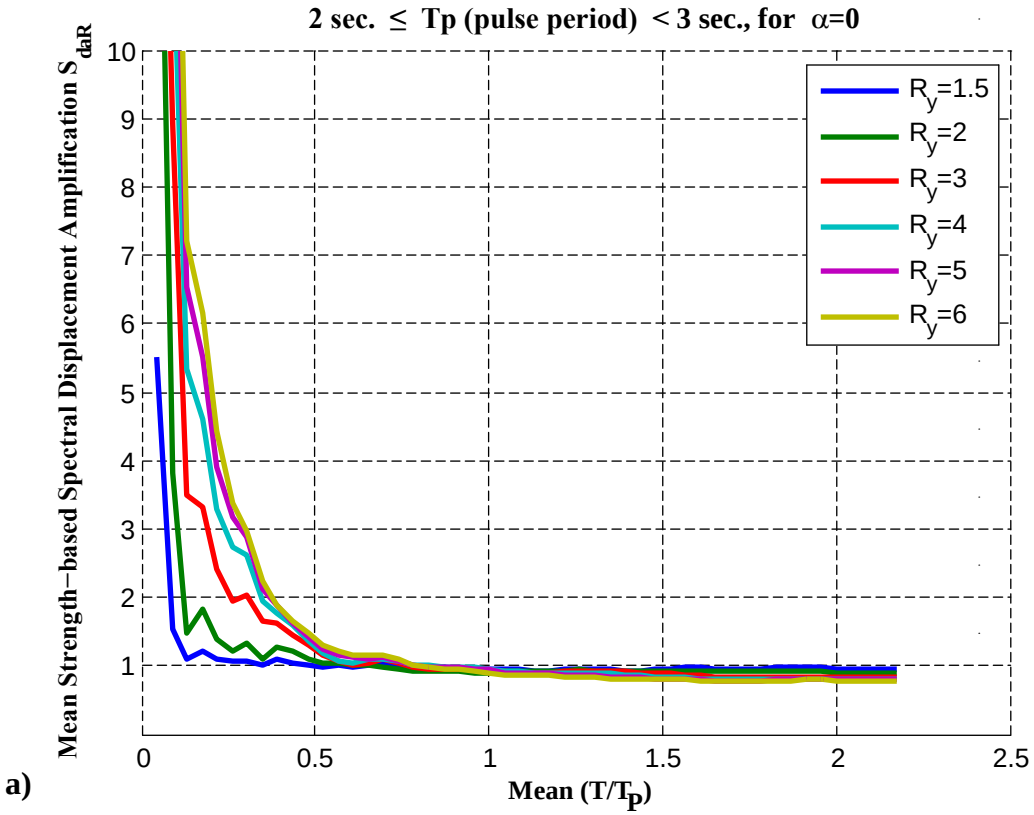

a)

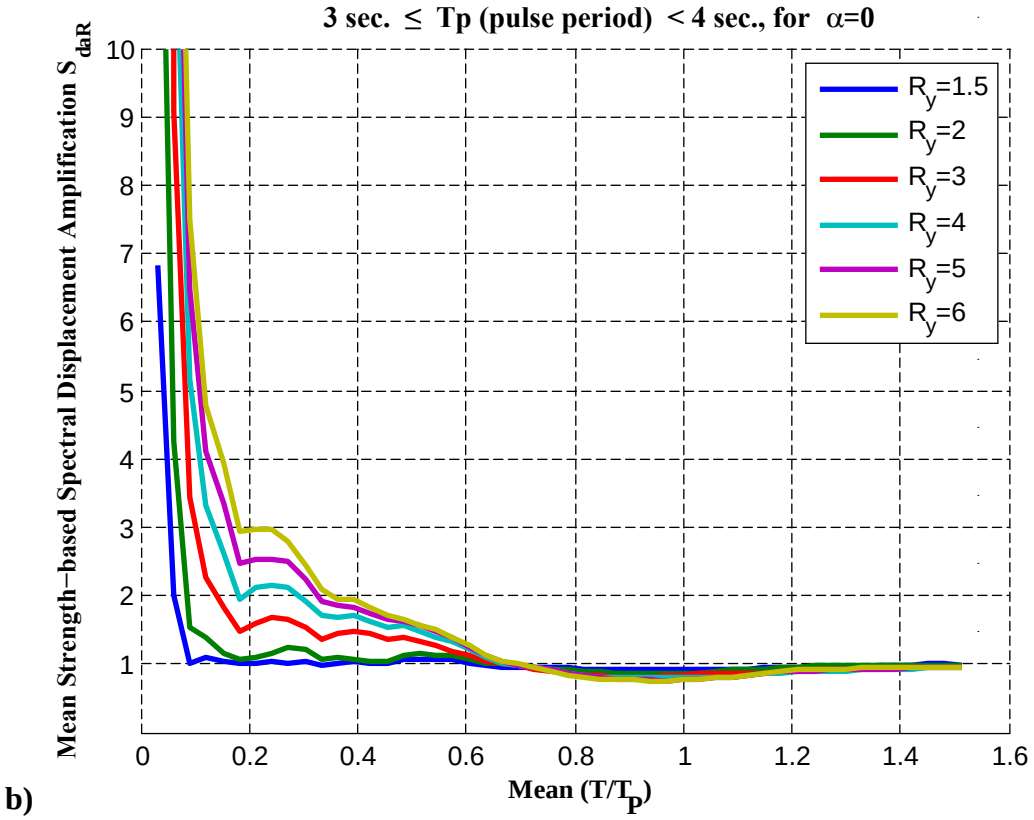

b)

Figure 7.2. Mean strength-based spectral displacement amplification vs. mean T/T_p spectra of the near-field records have pulse periods range from **a)** 2 sec. to 3 sec. **b)** 3 sec. to 4 sec., and designed for post-yield stiffness ratio, α=0, and R_y =1.5, 2, 3, 4, 5, and 6

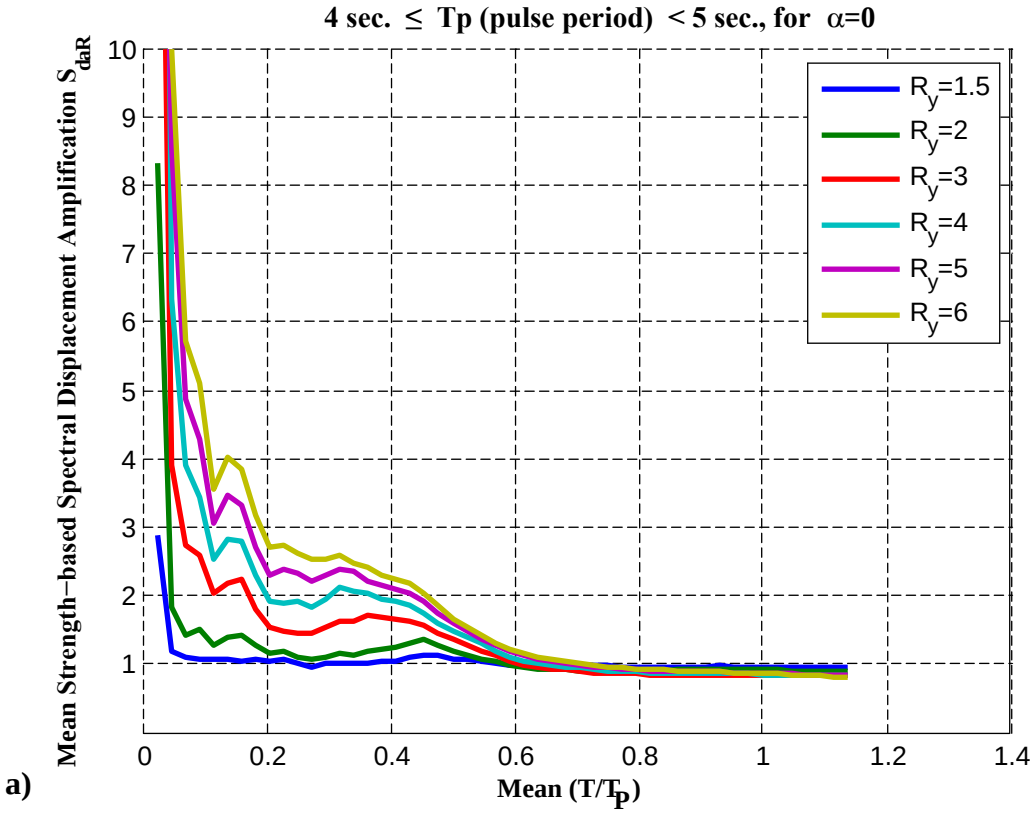

a)

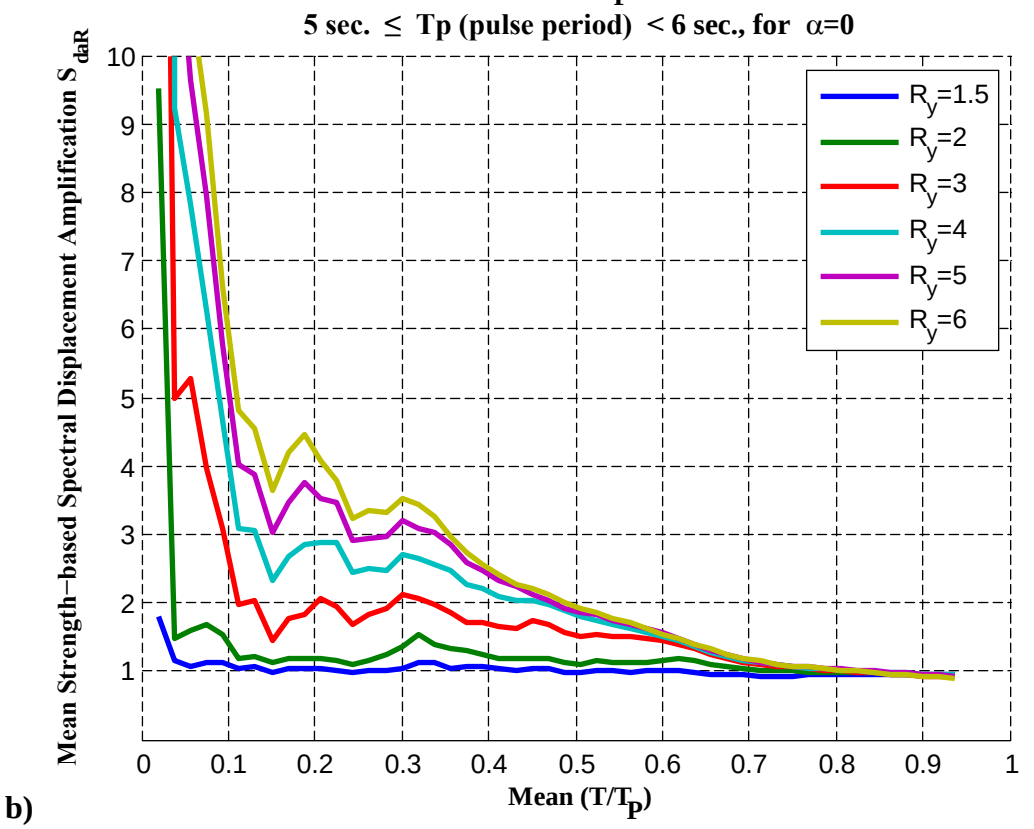

b)

Figure 7.3. Mean strength-based spectral displacement amplification vs. mean T/T_p spectra of the near-field records have pulse periods range from **a)** 4 sec. to 5 sec. **b)** 5 sec. to 6 sec., and designed for post-yield stiffness ratio, α=0, and R_y =1.5, 2, 3, 4, 5, and 6

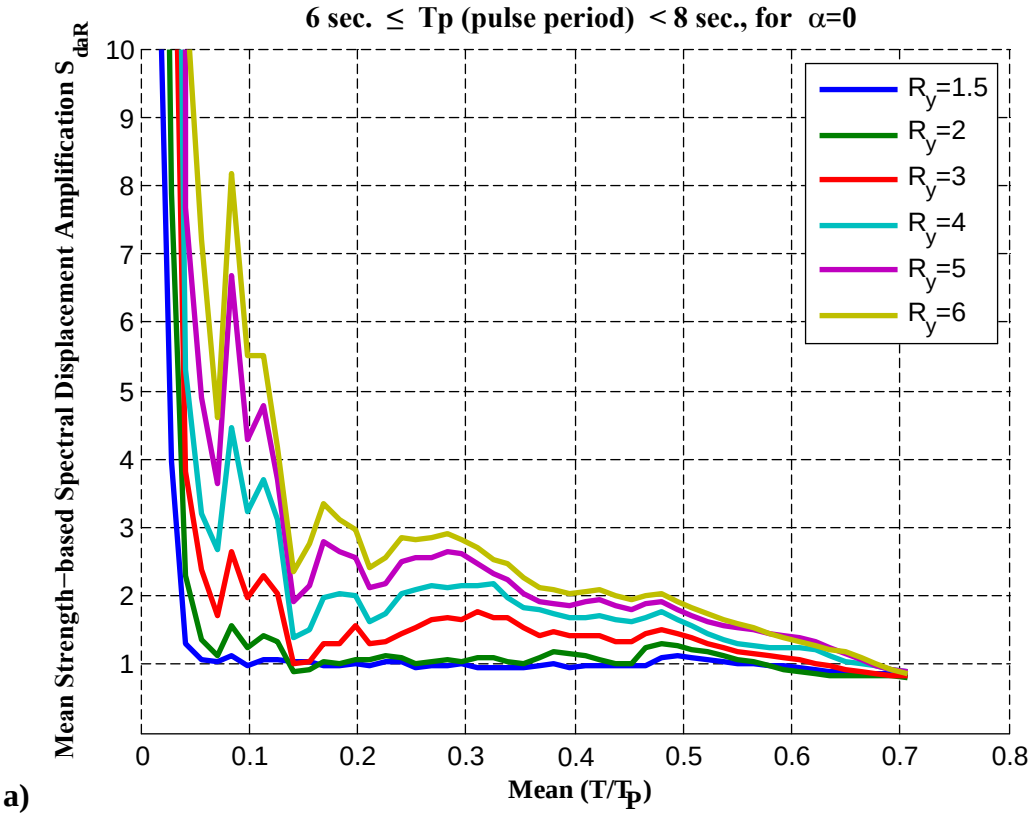

a)

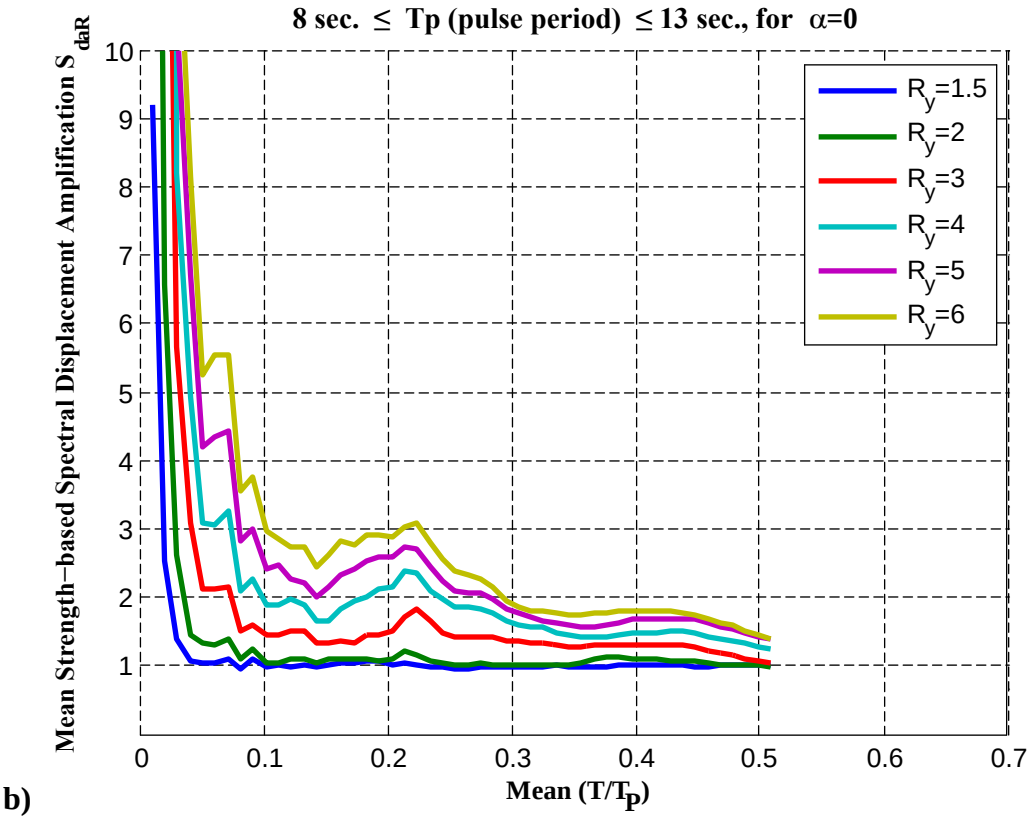

b)

Figure 7.4. Mean strength-based spectral displacement amplification vs. mean T/T_p spectra of the near-field records have pulse periods range from **a)** 6 sec. to 8 sec. **b)** 8 sec. to 13 sec., and designed for post-yield stiffness ratio, α=0, and R_y =1.5, 2, 3, 4, 5, and 6

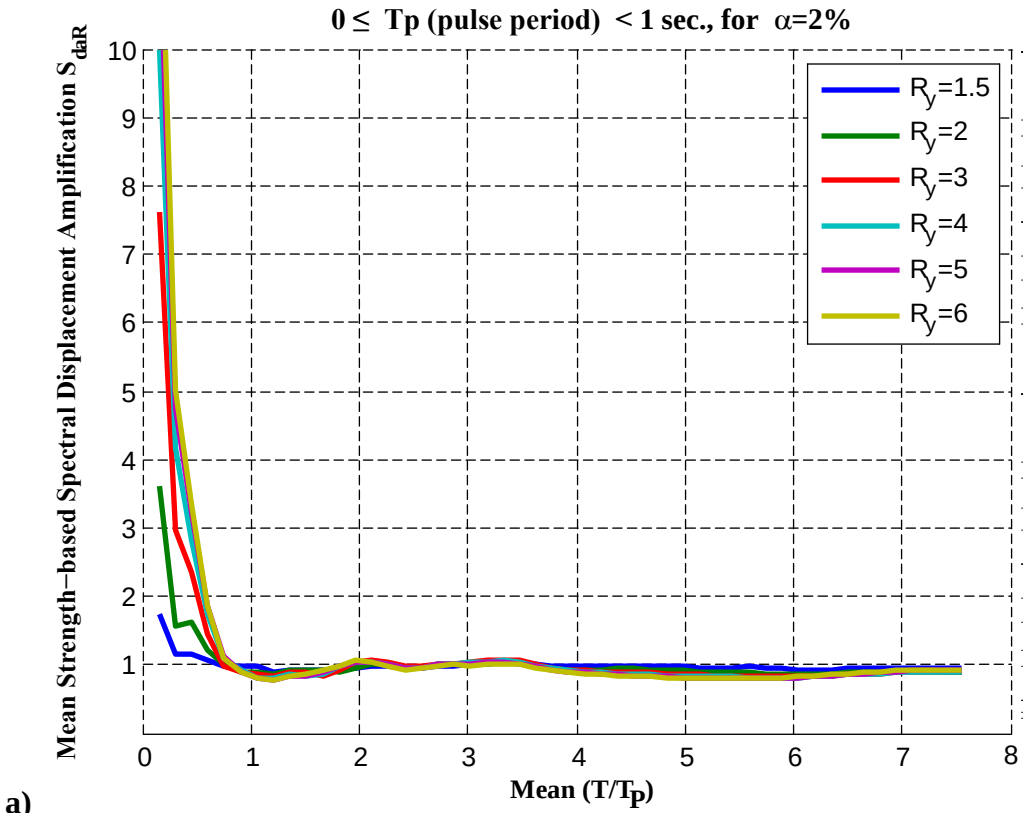

a)

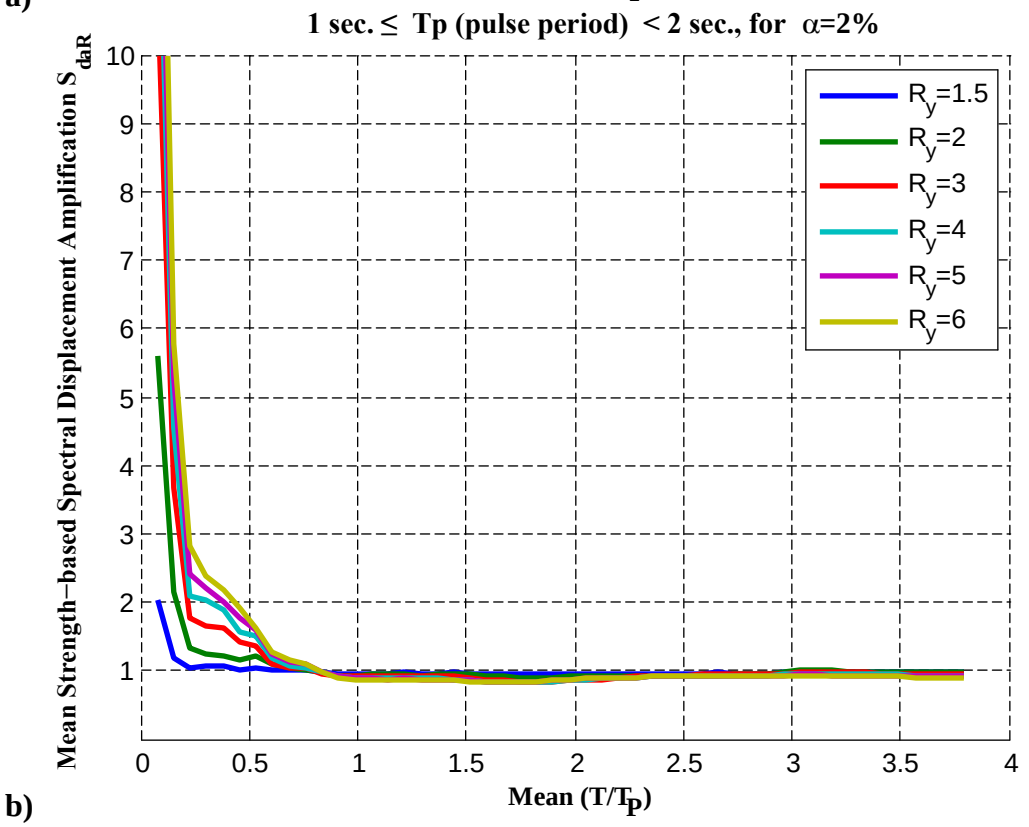

b)

Figure 7.5. Mean strength-based spectral displacement amplification vs. mean T/T_p spectra of the near-field records have pulse periods range from **a)** 0 to 1 sec. **b)** 1 sec. to 2 sec., and designed for post-yield stiffness ratio, α=2 percent, and R_y =1.5, 2, 3, 4, 5, and 6

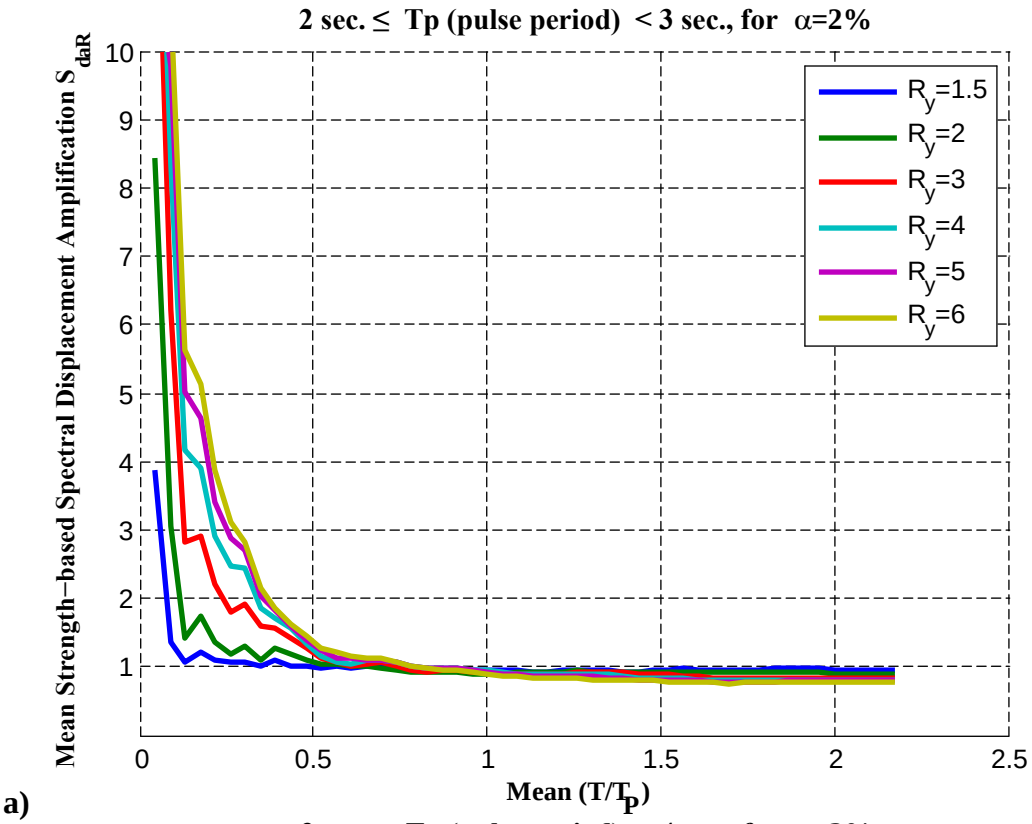

a)

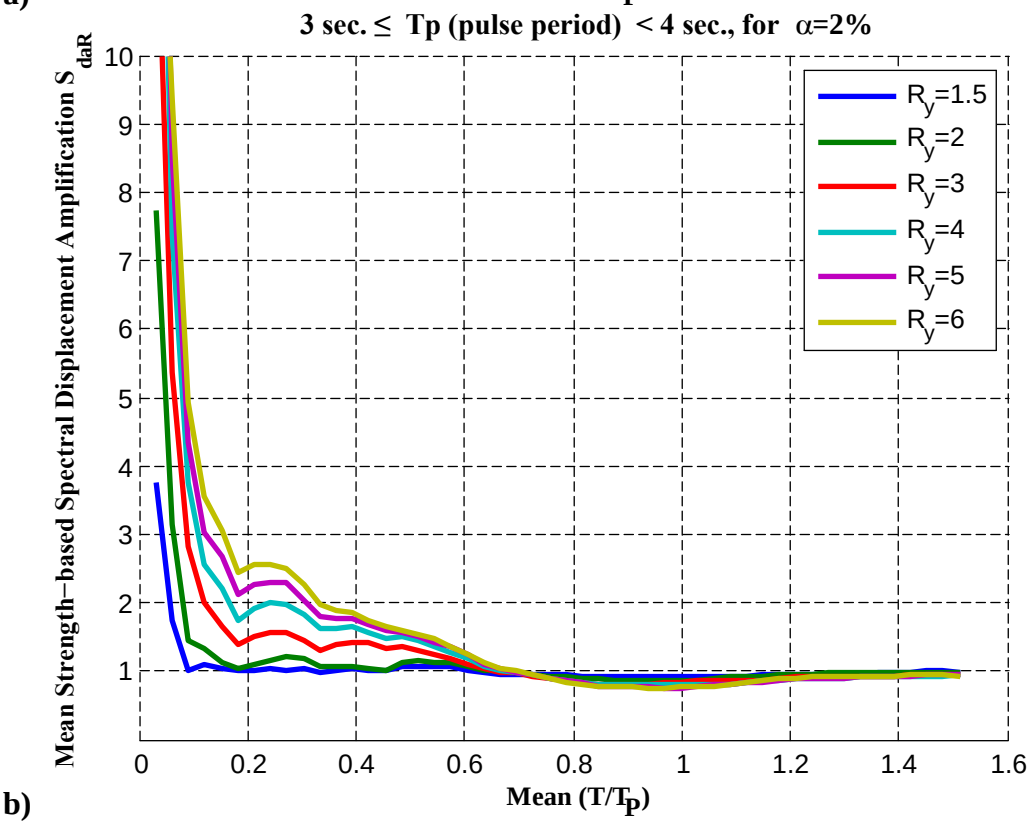

b)

Figure 7.6. Mean strength-based spectral displacement amplification vs. mean T/T_p spectra of the near-field records have pulse periods range from **a)** 2 sec. to 3 sec. **b)** 3 sec. to 4 sec., and designed for post-yield stiffness ratio, α=2 percent, and R_y =1.5, 2, 3, 4, 5, and 6

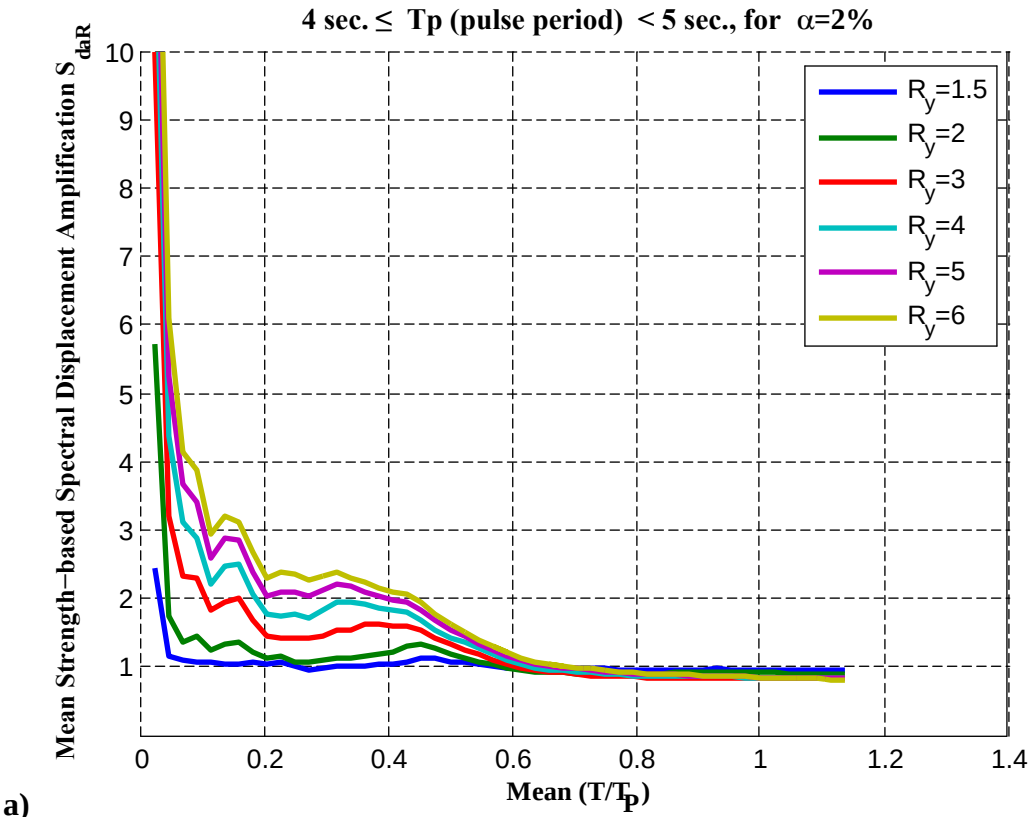

a)

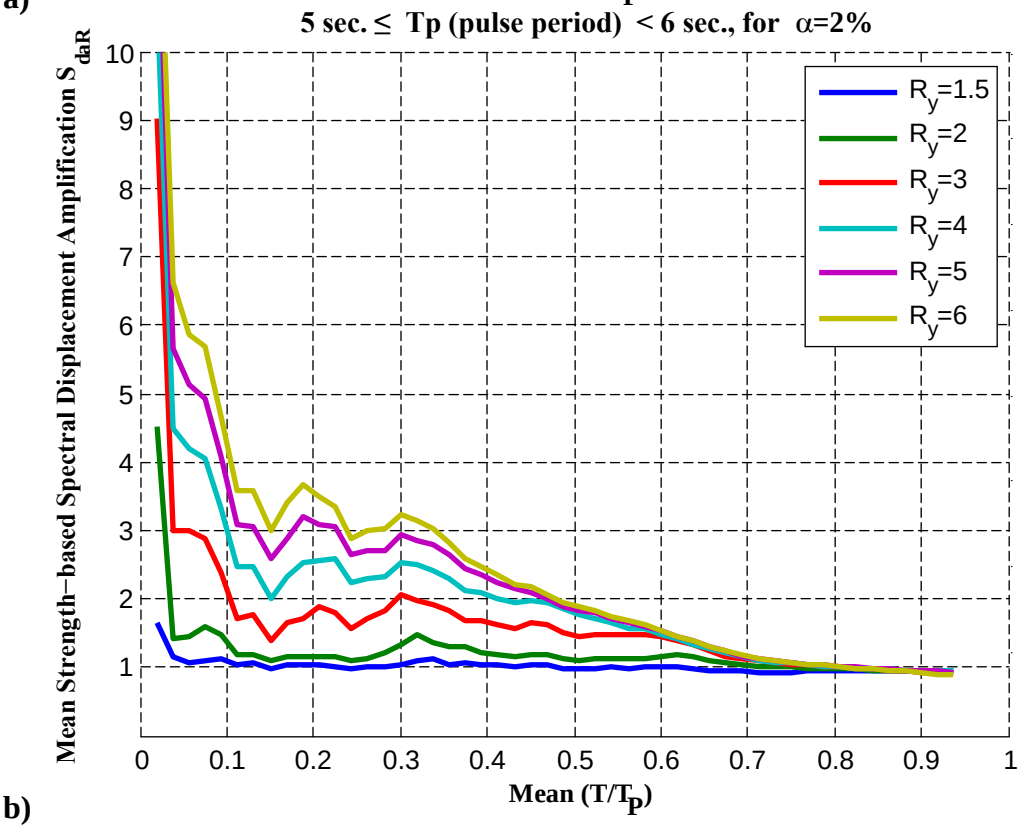

b)

Figure 7.7. Mean strength-based spectral displacement amplification vs. mean T/T_p spectra of the near-field records have pulse periods range from **a)** 4 sec. to 5 sec. **b)** 5 sec. to 6 sec., and designed for post-yield stiffness ratio, α=2 percent, and R_y =1.5, 2, 3, 4, 5, and 6

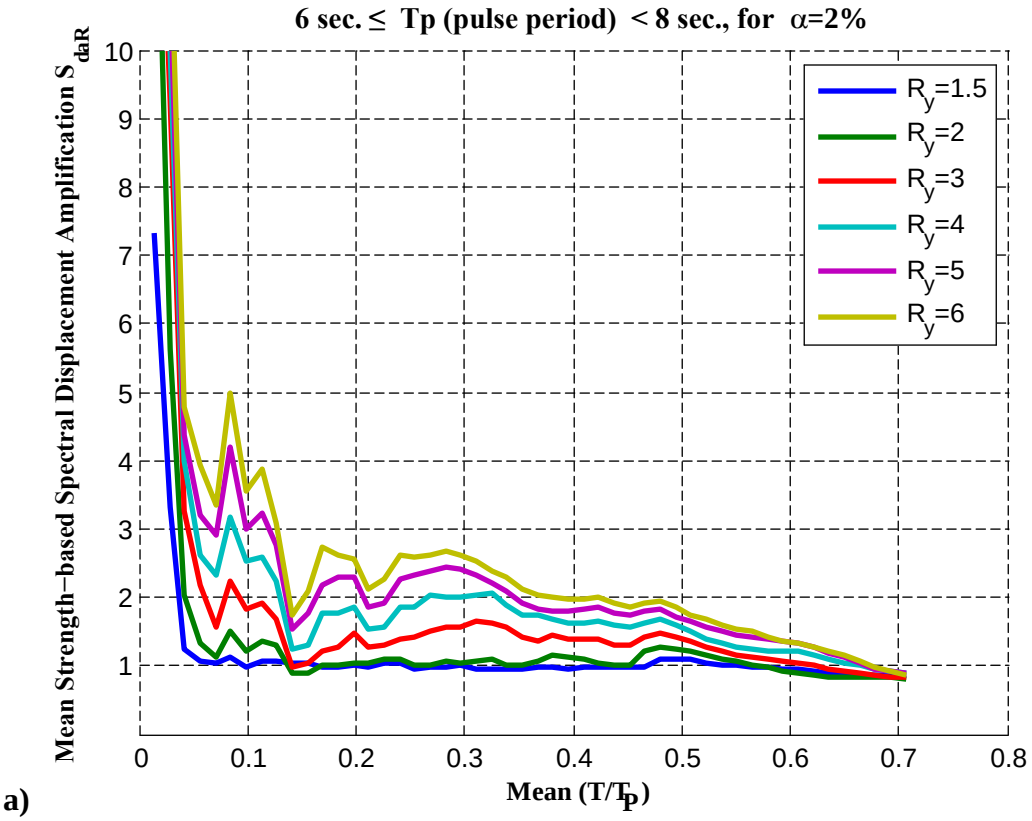

a)

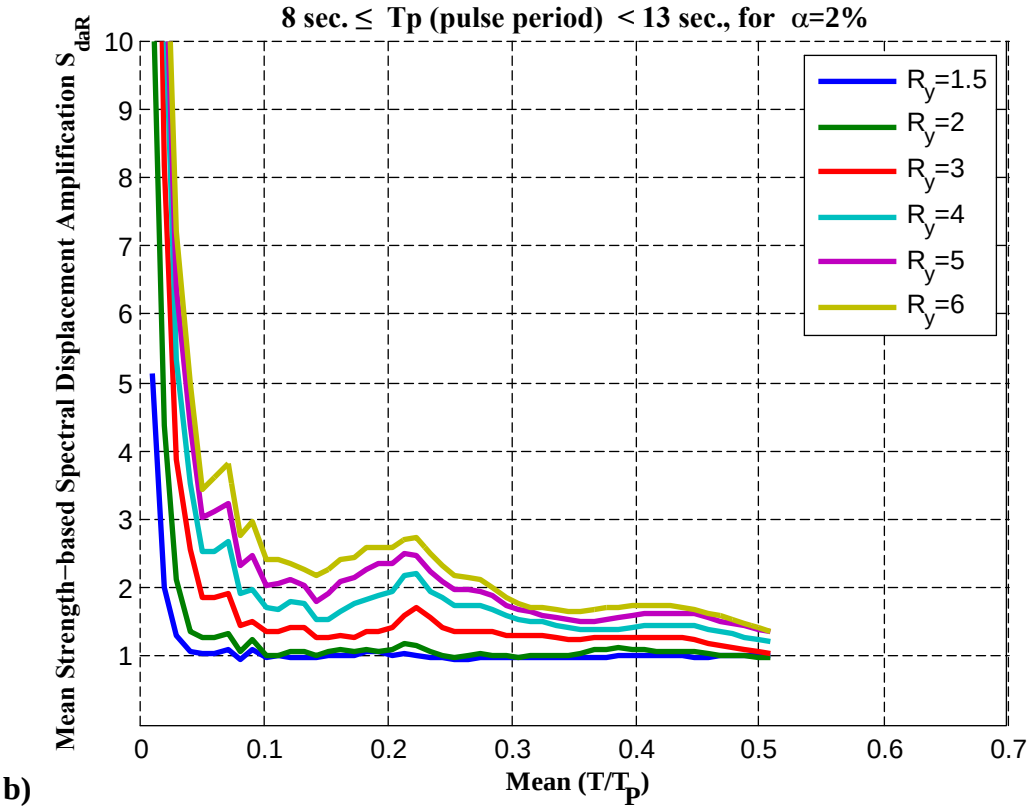

b)

Figure 7.8. Mean strength-based spectral displacement amplification vs. mean T/T_p spectra of the near-field records have pulse periods range from **a)** 6 sec. to 8 sec. **b)** 8 sec. to 13 sec., and designed for post-yield stiffness ratio, α=2 percent, and R_y =1.5, 2, 3, 4, 5, and 6

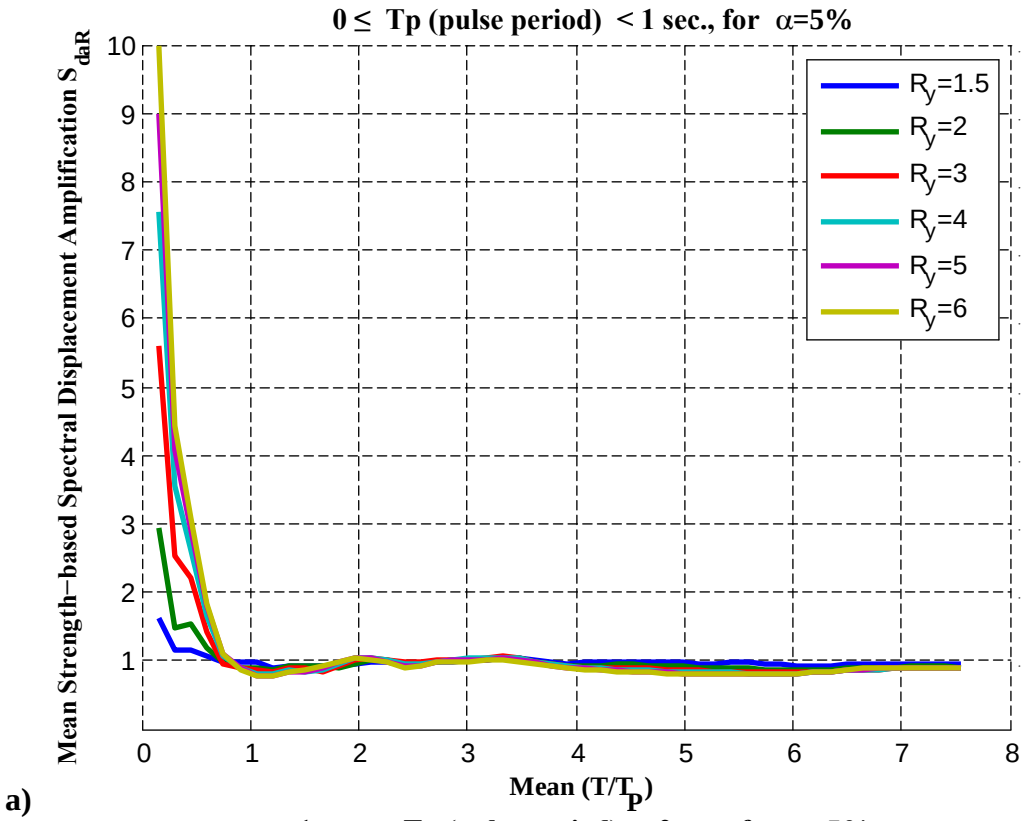

a)

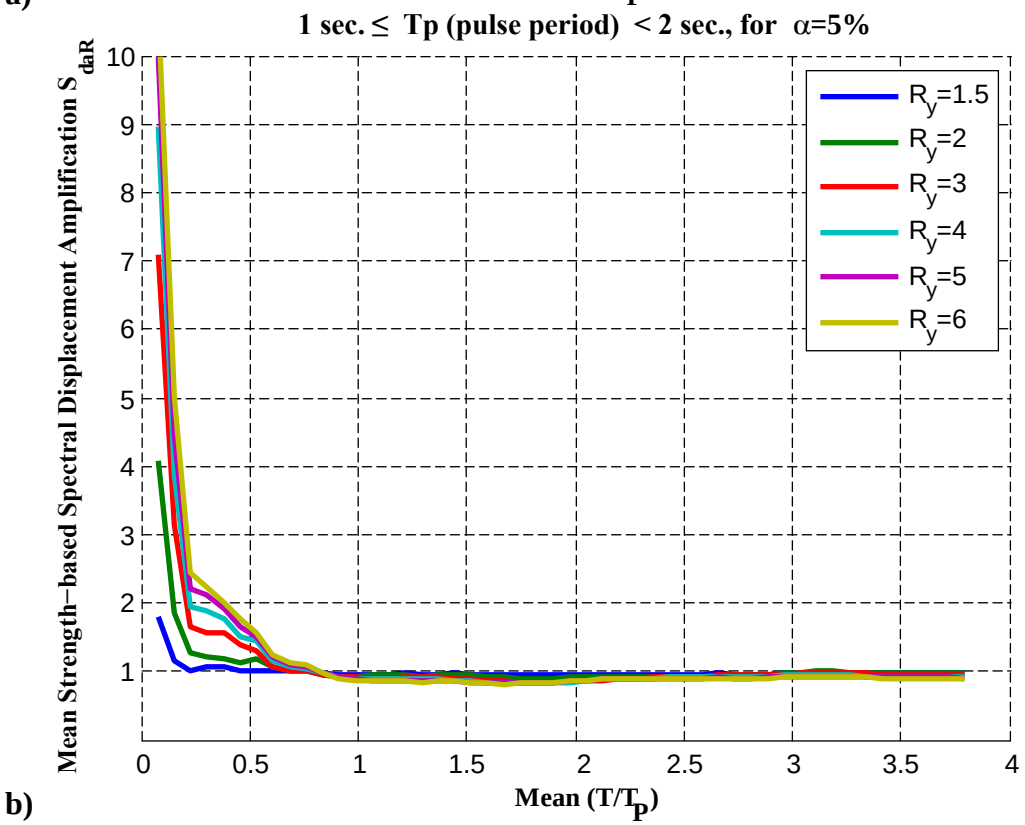

b)

Figure 7.9. Mean strength-based spectral displacement amplification vs. mean T/T_p spectra of the near-field records have pulse periods range from **a)** 0 sec. to 1 sec. **b)** 1 sec. to 2 sec., and designed for post-yield stiffness ratio, α=5 percent, and R_y =1.5, 2, 3, 4, 5, and 6

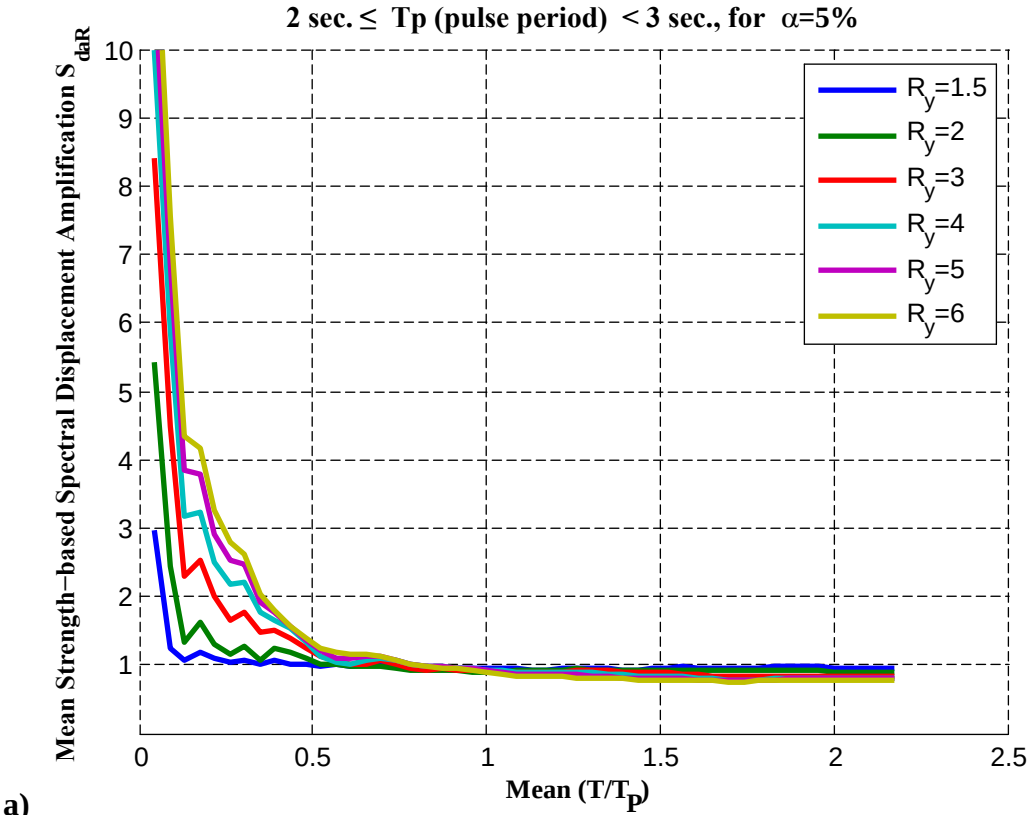

a)

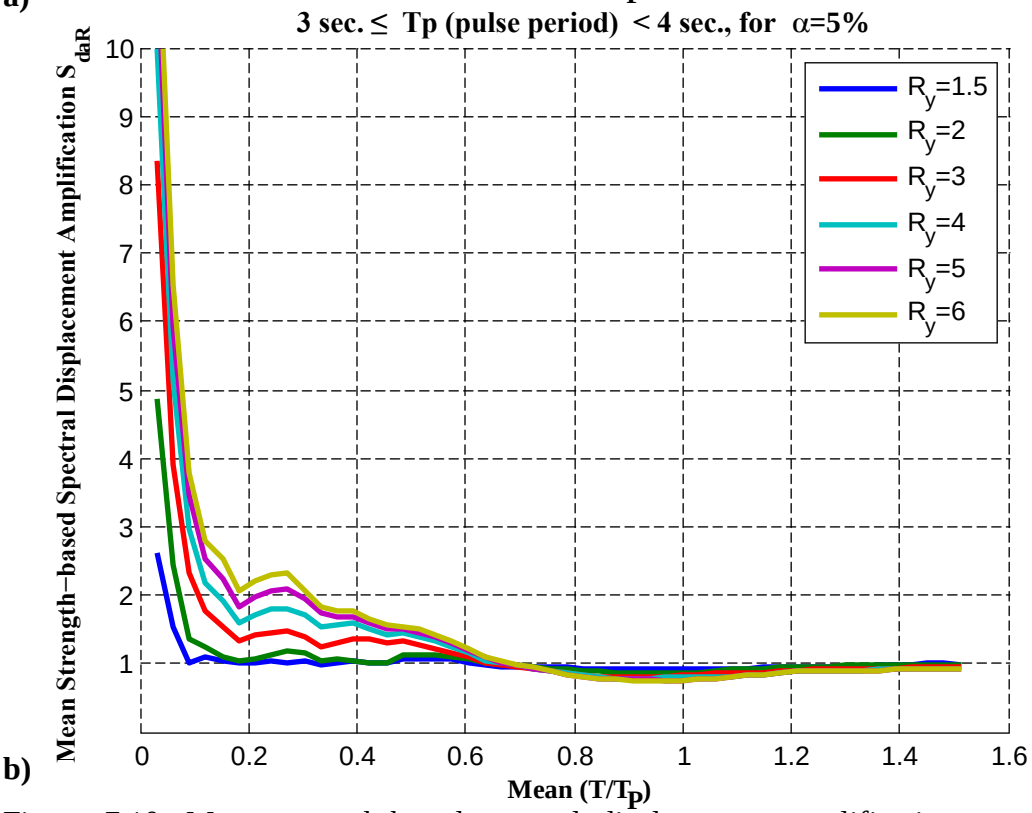

b)

Figure 7.10. Mean strength-based spectral displacement amplification vs. mean T/T_p spectra of the near-field records have pulse periods range from **a)** 2 sec. to 3 sec. **b)** 3 sec. to 4 sec., and designed for post-yield stiffness ratio, α=5 percent, and R_y =1.5, 2, 3, 4, 5, and 6

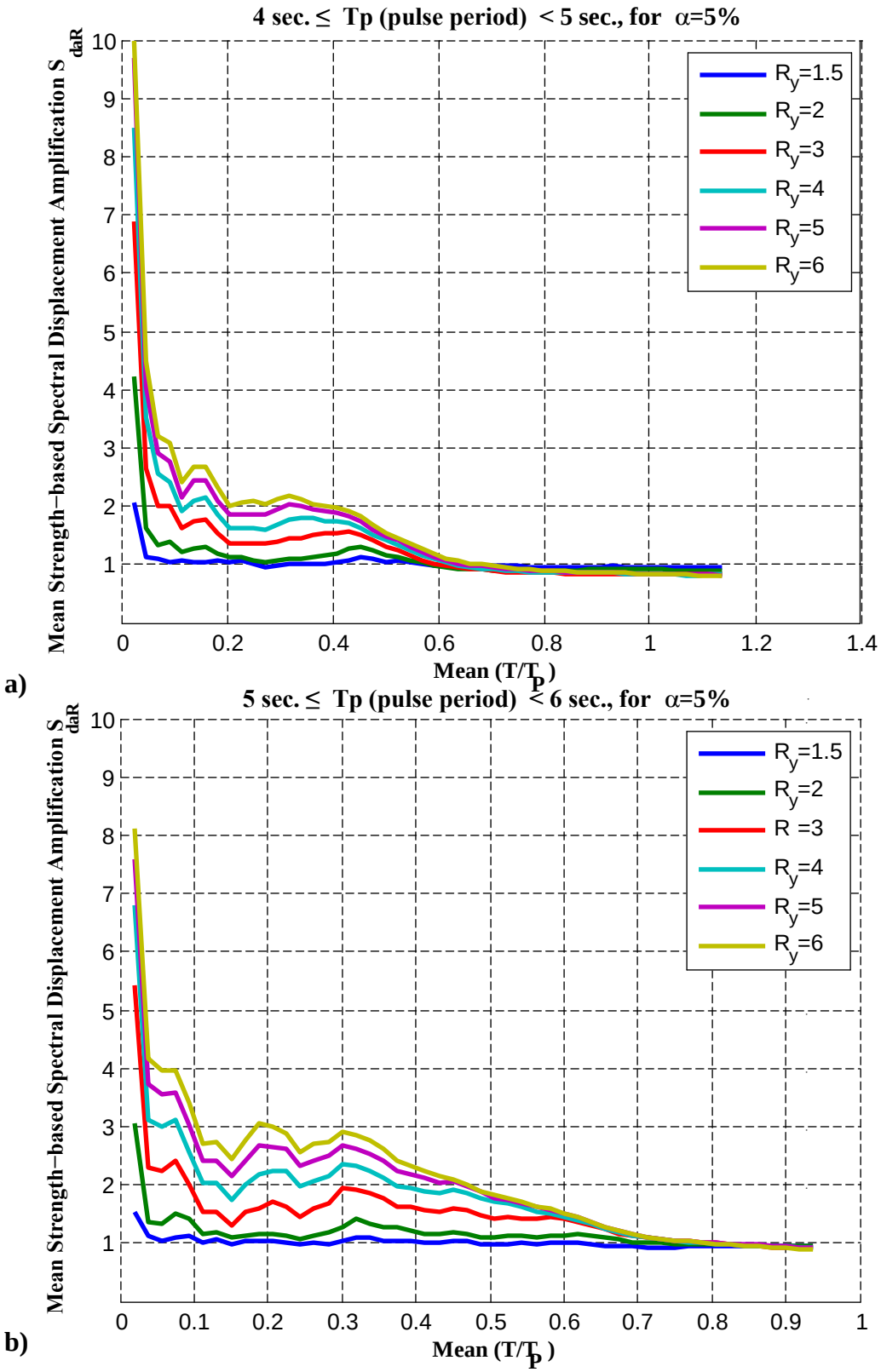

Figure 7.11. Mean strength-based spectral displacement amplification vs. mean T/T_p spectra of the near-field records have pulse periods range from **a)** 4 sec. to 5 sec. **b)** 5 sec. to 6 sec., and designed for post-yield stiffness ratio, α=5 percent, and R_y =1.5, 2, 3, 4, 5, and 6

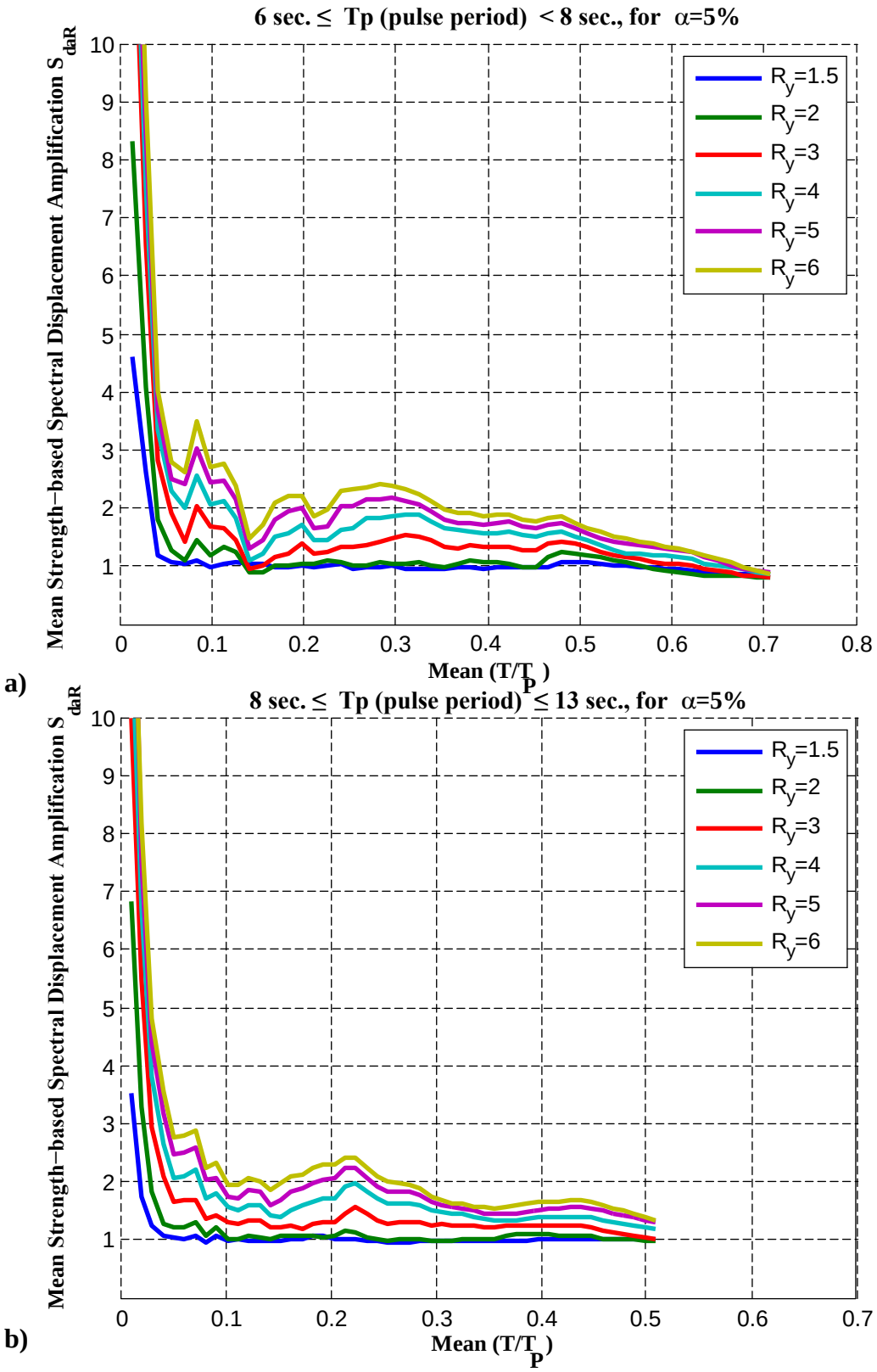

Figure 7.12. Mean strength-based spectral displacement amplification vs. mean T/T_p spectra of the near-field records have pulse periods range from **a)** 6 sec. to 8 sec. **b)** 8 sec. to 13 sec., and designed for post-yield stiffness ratio, α=5 percent, and R_y=1.5, 2, 3, 4, 5, and 6

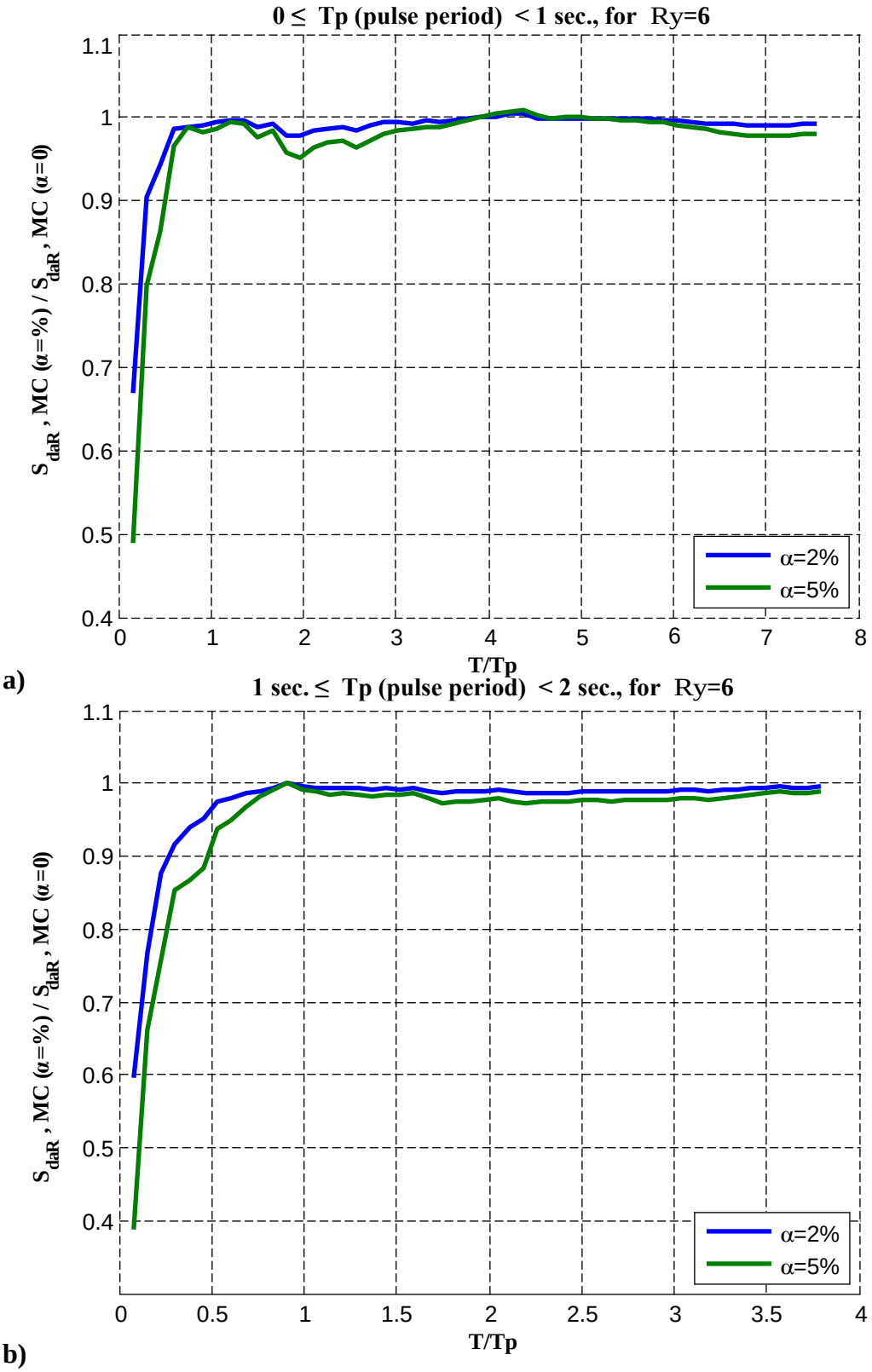

Figure 7.13. Effect of post-yield stiffness ratio on the strength-based spectral displacement amplification ratio for R_y =6 and mean of the **a)** 8 and **b)** 23 near-field records have pulse periods in the range of **a)** 0 to 1 sec., and **b)** 1 sec. to 2 sec.

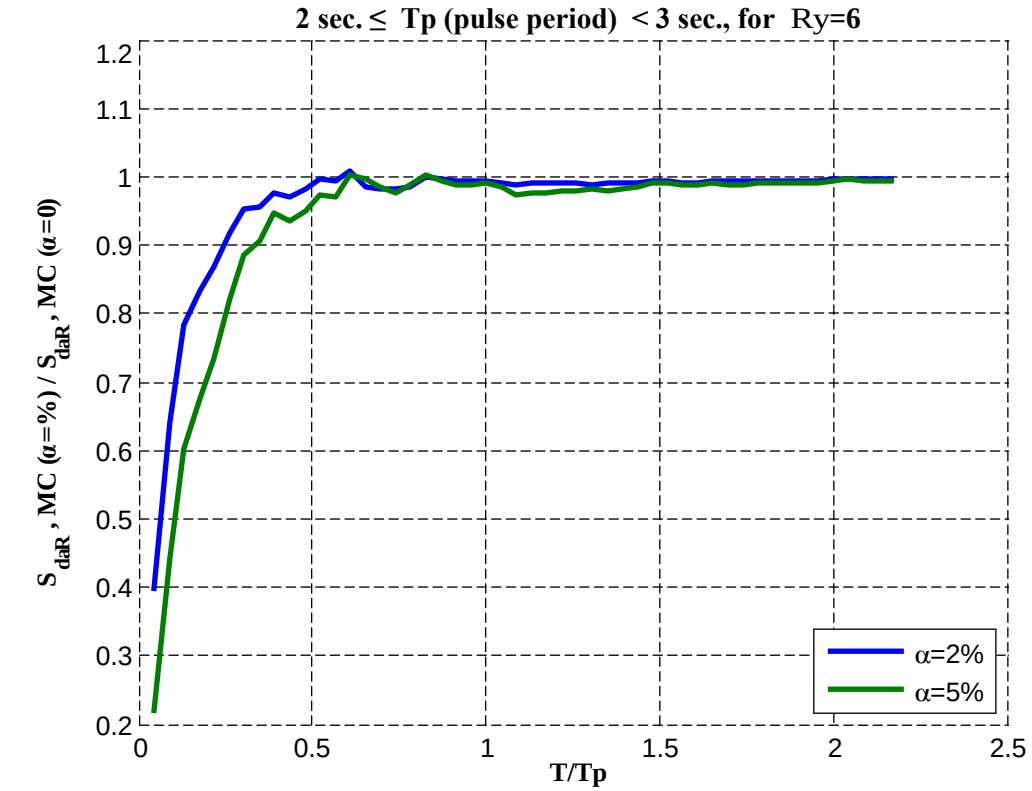

a)

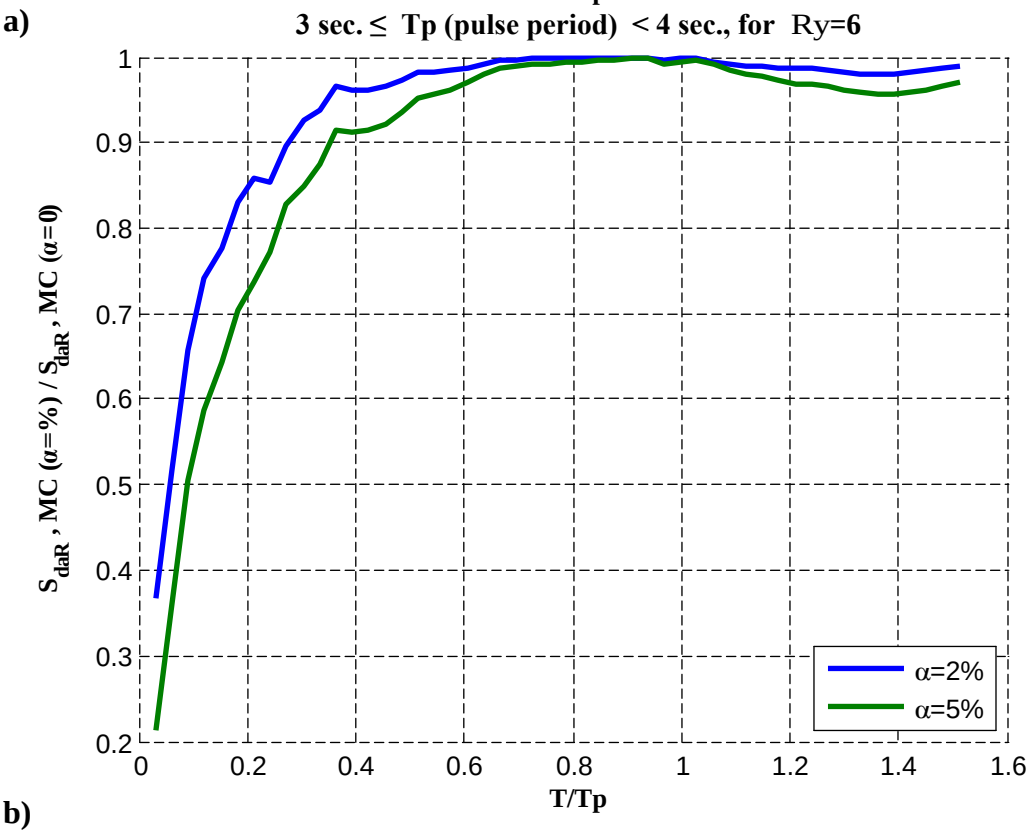

b)

Figure 7.14. Effect of post-yield stiffness ratio on the strength-based spectral displacement amplification ratio for R_y =6 and mean of the **a)** 13 and **b)** 12 near-field records have pulse periods in the range of **a)** 2 sec. to 3 sec., and **b)** 3 sec. to 4 sec.

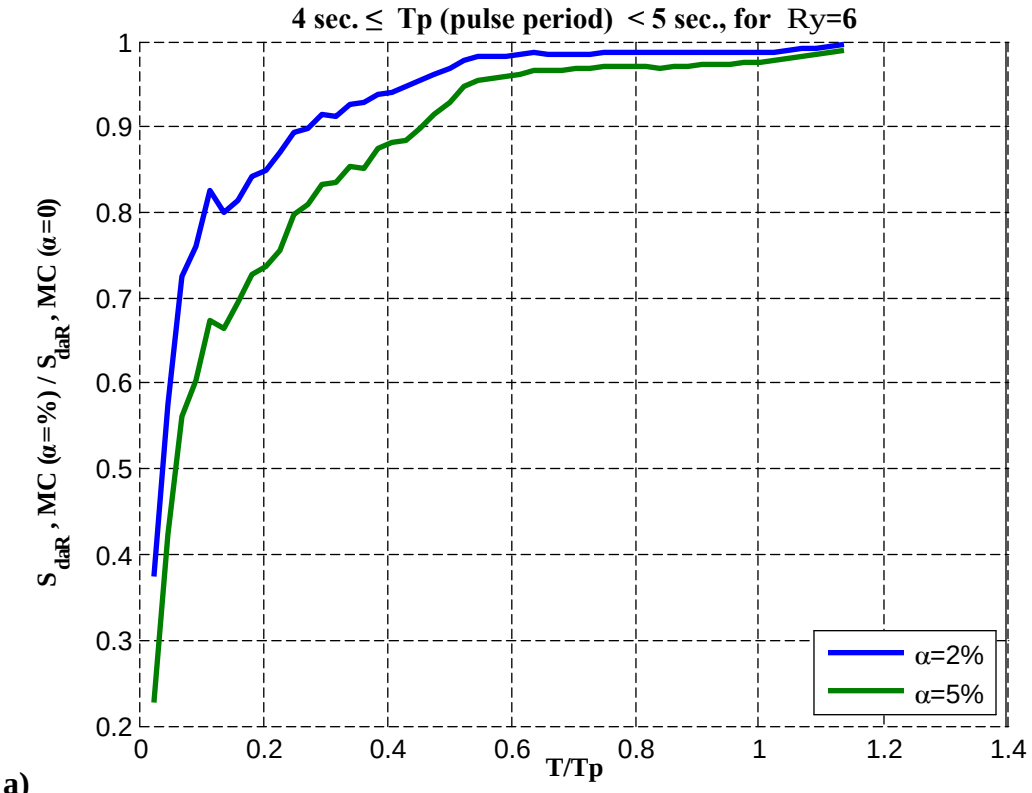

a)

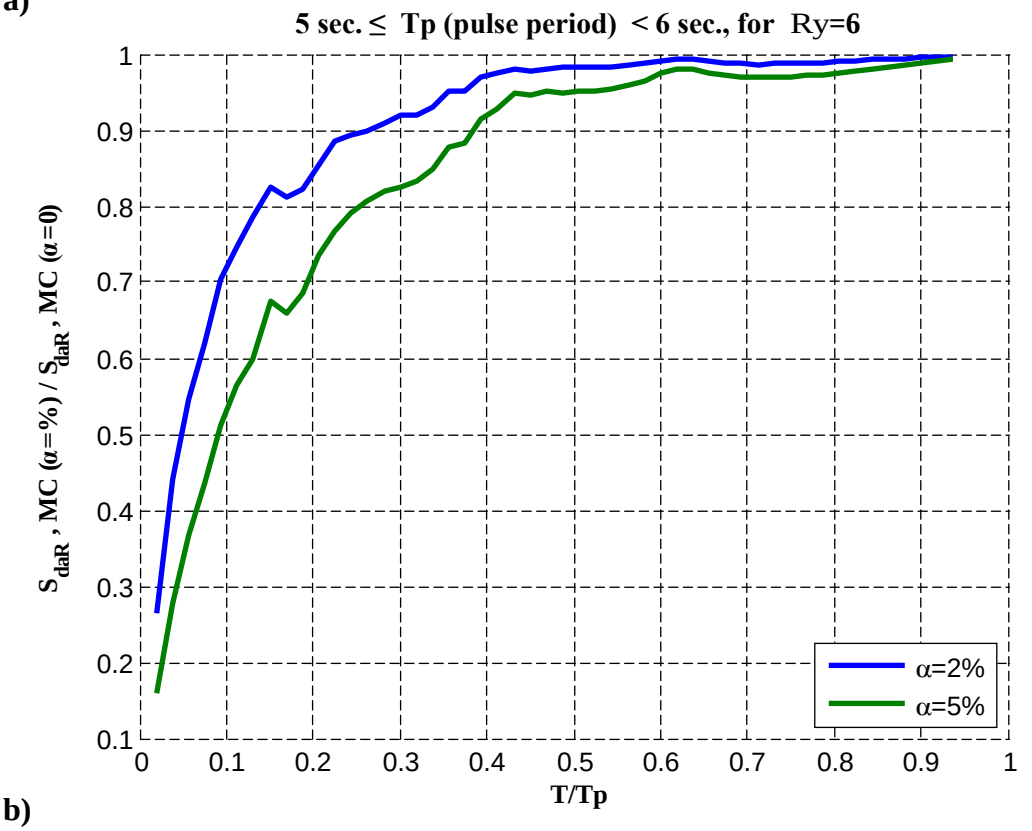

b)

Figure 7.15. Effect of post-yield stiffness ratio on the strength-based spectral displacement amplification ratio for R_y =6 and mean of the **a)** 16 and **b)** 10 near-field records have pulse periods in the range of **a)** 4 sec. to 5 sec., and **b)** 5 sec. to 6 sec.

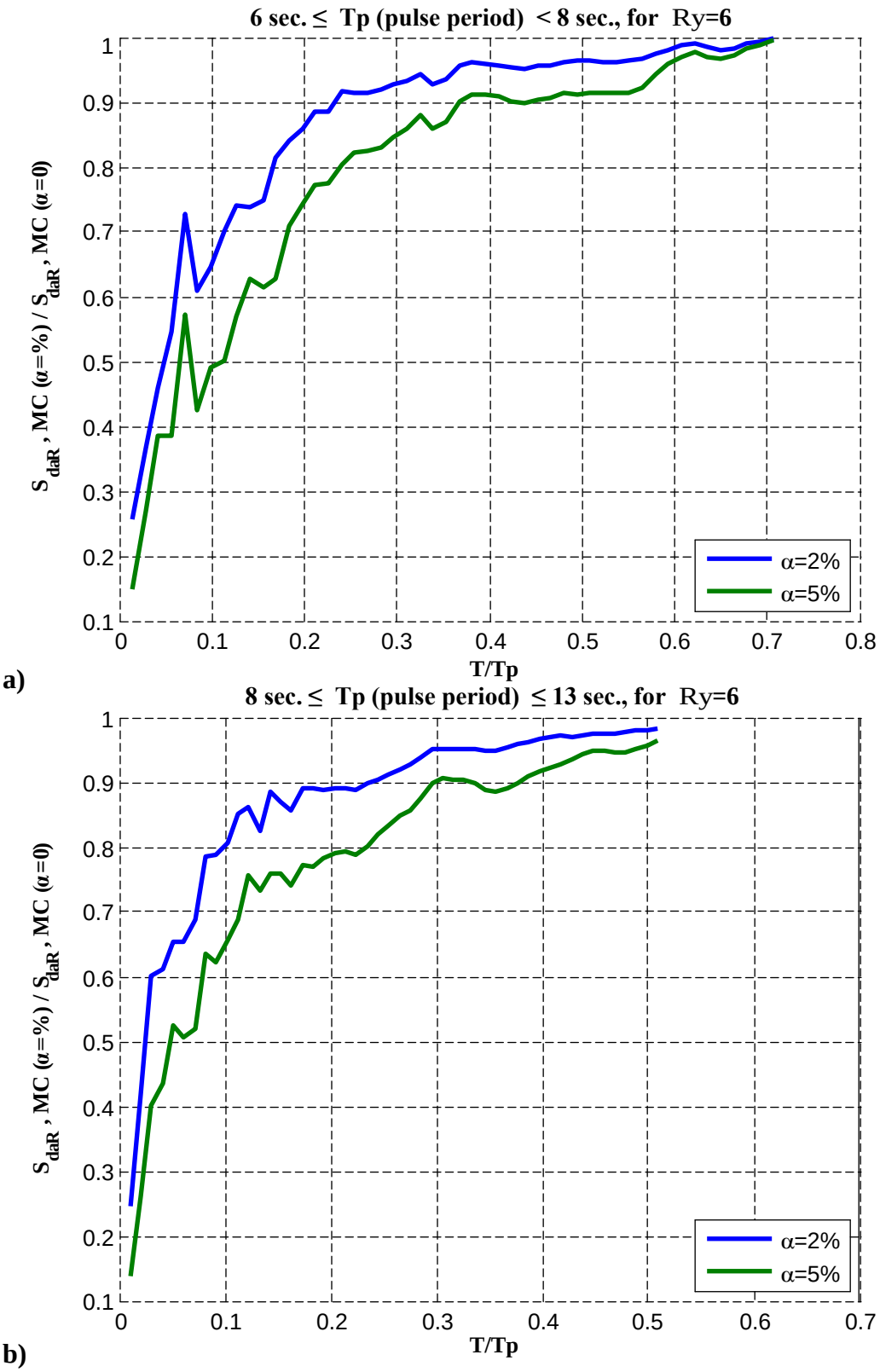

Figure 7.16. Effect of post-yield stiffness ratio on the strength-based spectral displacement amplification ratio for R_y =6 and mean of the **a)** 6 and **b)** 17 near-field records have pulse periods in the range of **a)** 6 sec. to 8 sec., and **b)** 8 sec. to 13 sec.

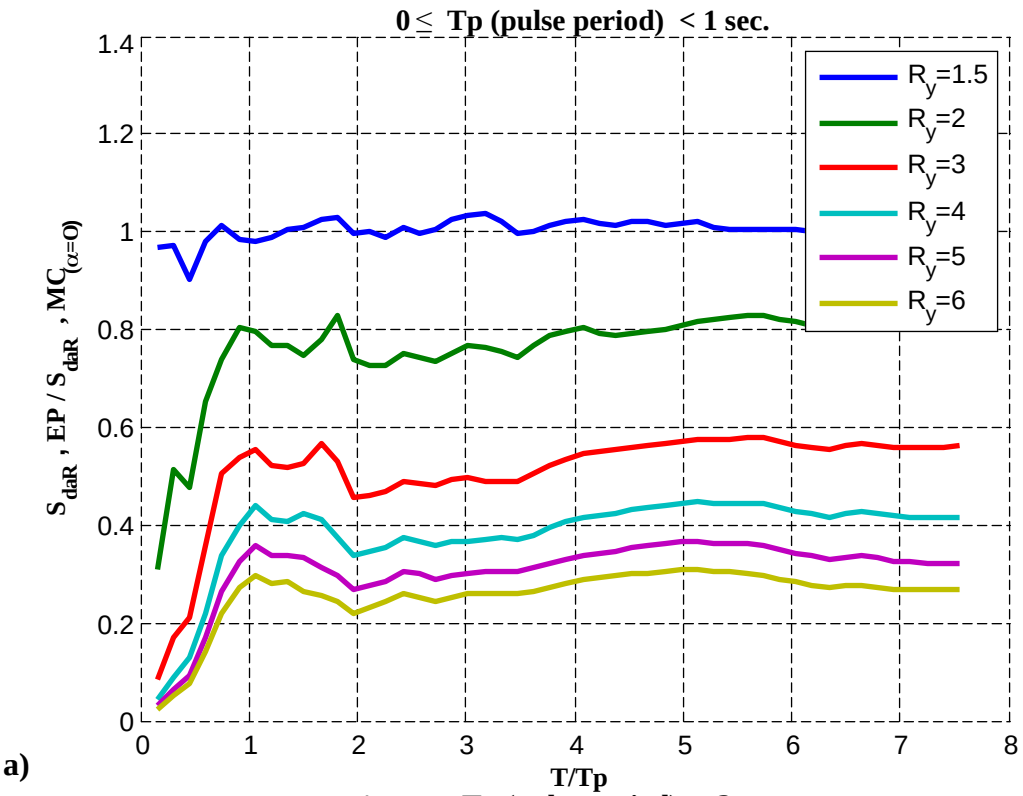

a)

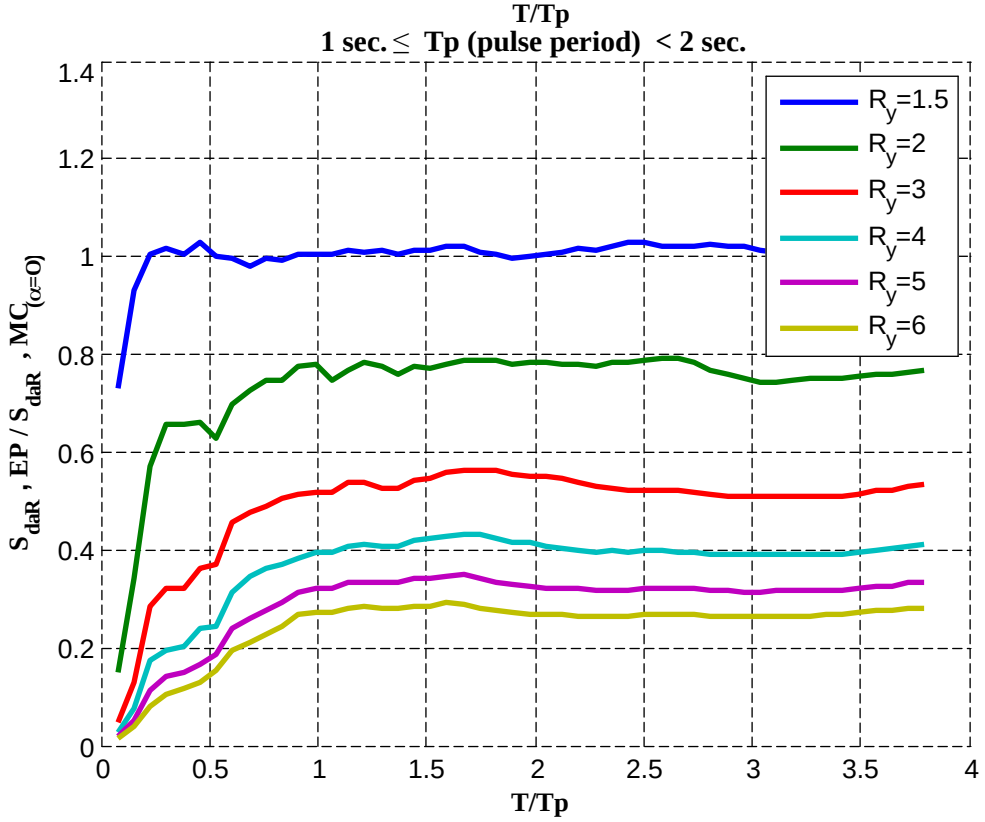

b)

Figure 7.17. Ratios of the strength-based spectral displacement amplification ratios of non-degrading (elasto-plastic) to stiffness degrading (modified-Clough) systems for different R_y levels obtained from **a)** 8 and **b)** 23 near-field records have pulse periods in the range of **a)** 0 to 1 sec., and **b)** 1 sec. to 2 sec.

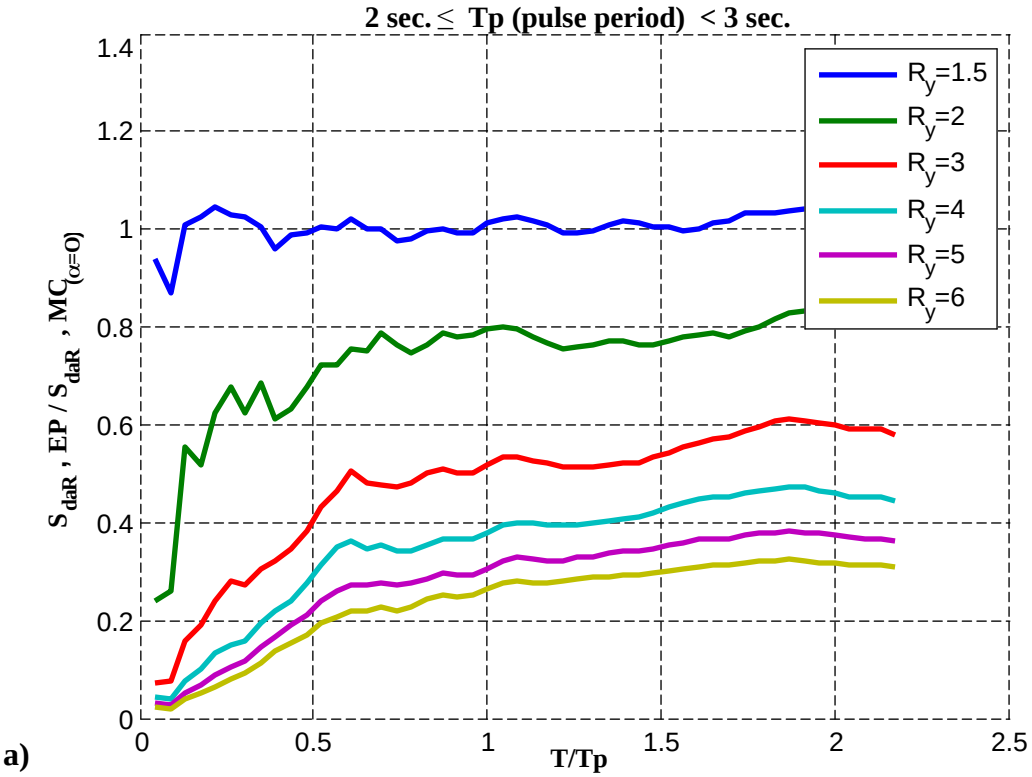

a)

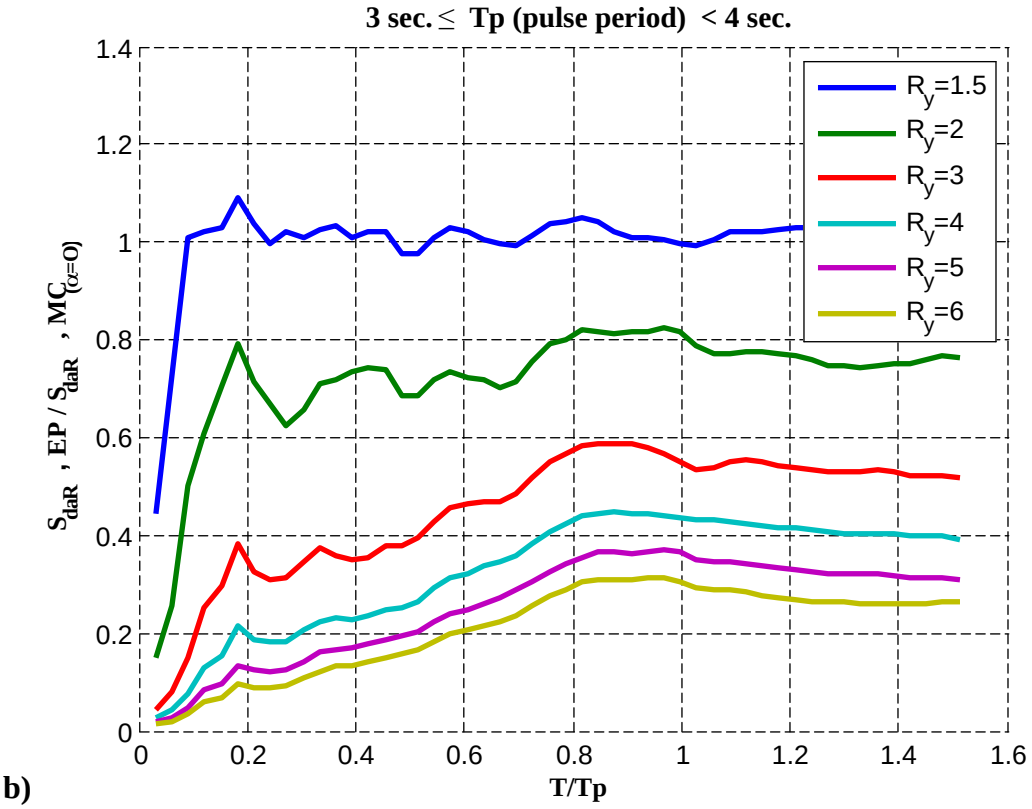

b)

Figure 7.18. Ratios of the strength-based spectral displacement amplification ratios of non-degrading (elasto-plastic) to stiffness degrading (modified-Clough) systems for different R_y levels obtained from **a)** 13 and **b)** 12 near-field records have pulse periods in the range of **a)** 2 sec. to 3 sec., and **b)** 3 sec. to 4 sec.

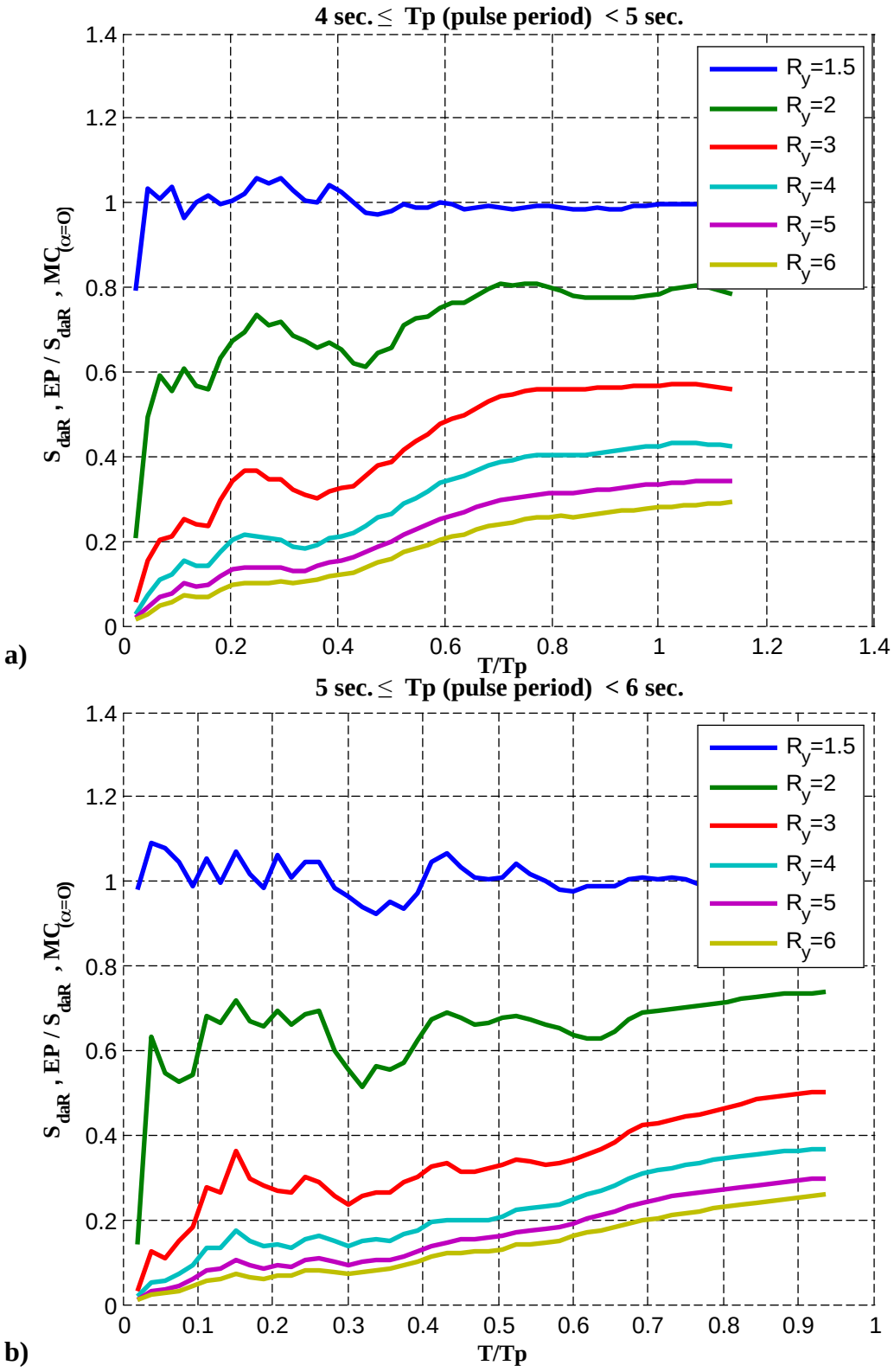

Figure 7.19. Ratios of the strength-based spectral displacement amplification ratios of non-degrading (elasto-plastic) to stiffness degrading (modified-Clough) systems for different R_y levels obtained from **a)** 16 and **b)** 10 near-field records have pulse periods in the range of **a)** 4 sec. to 5 sec., and **b)** 5 sec. to 6 sec.

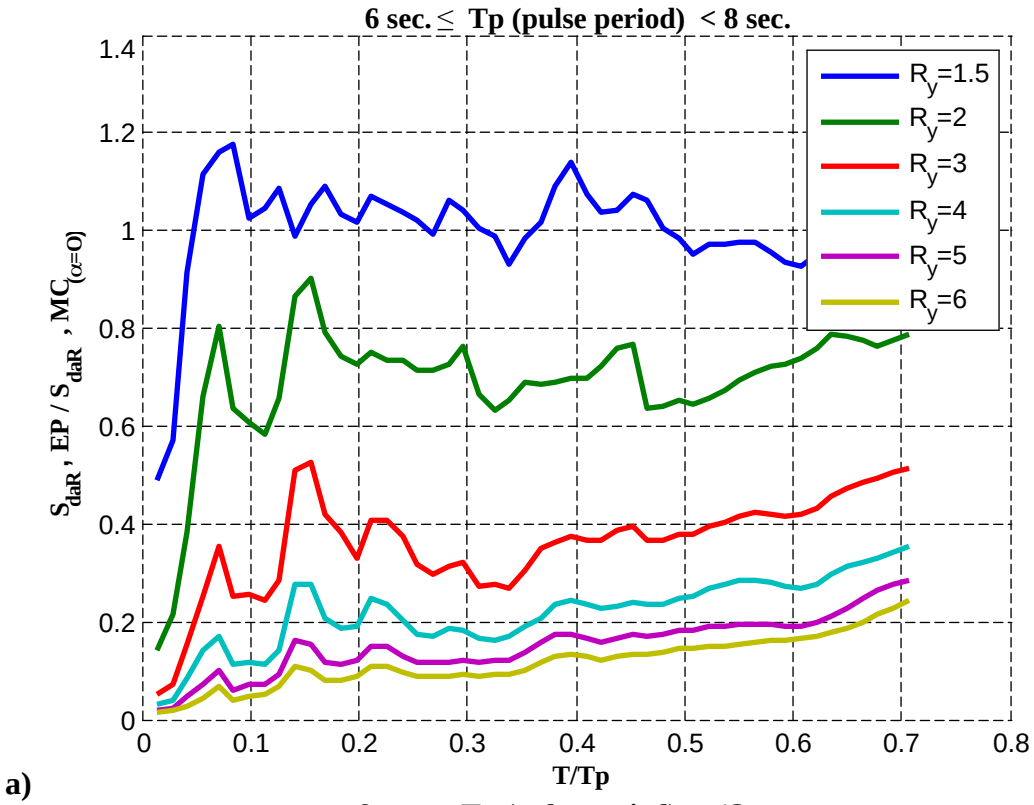

a)

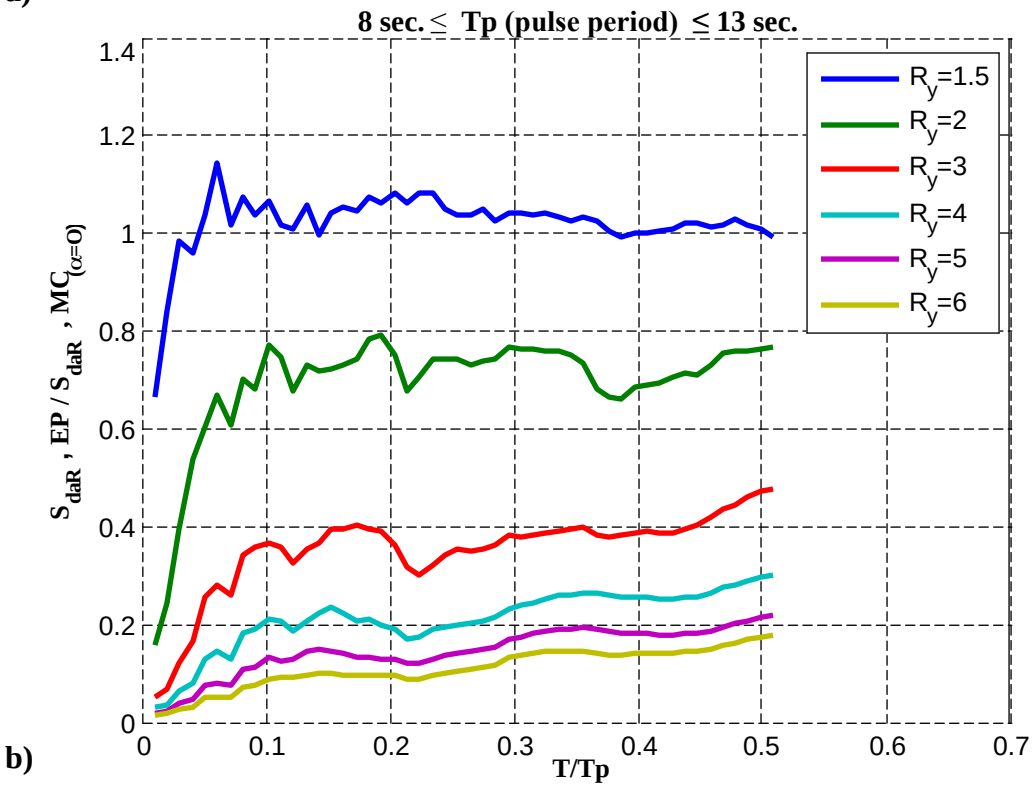

b)

Figure 7.20. Ratios of the strength-based spectral displacement amplification ratios of non-degrading (elasto-plastic) to stiffness degrading (modified-Clough) systems for different R_y levels obtained from **a)** 6 and **b)** 17 near-field records have pulse periods in the range of **a)** 6 sec. to 8 sec., and **b)** 8 sec. to 13 sec.

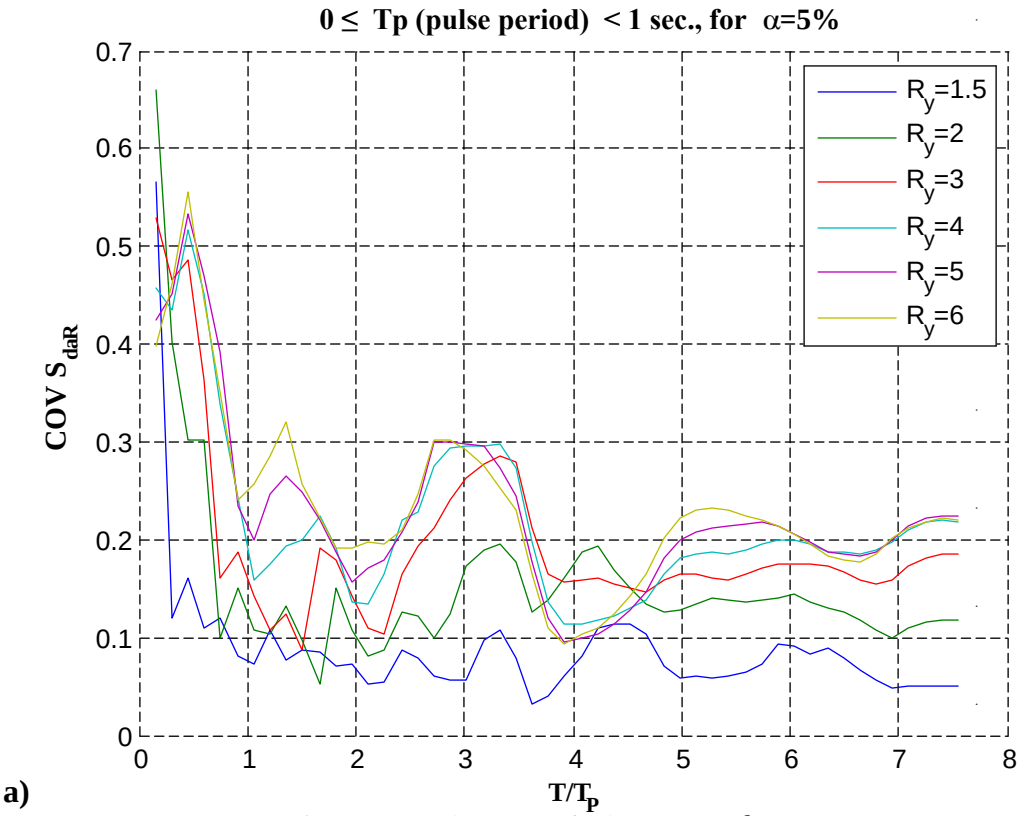

a)

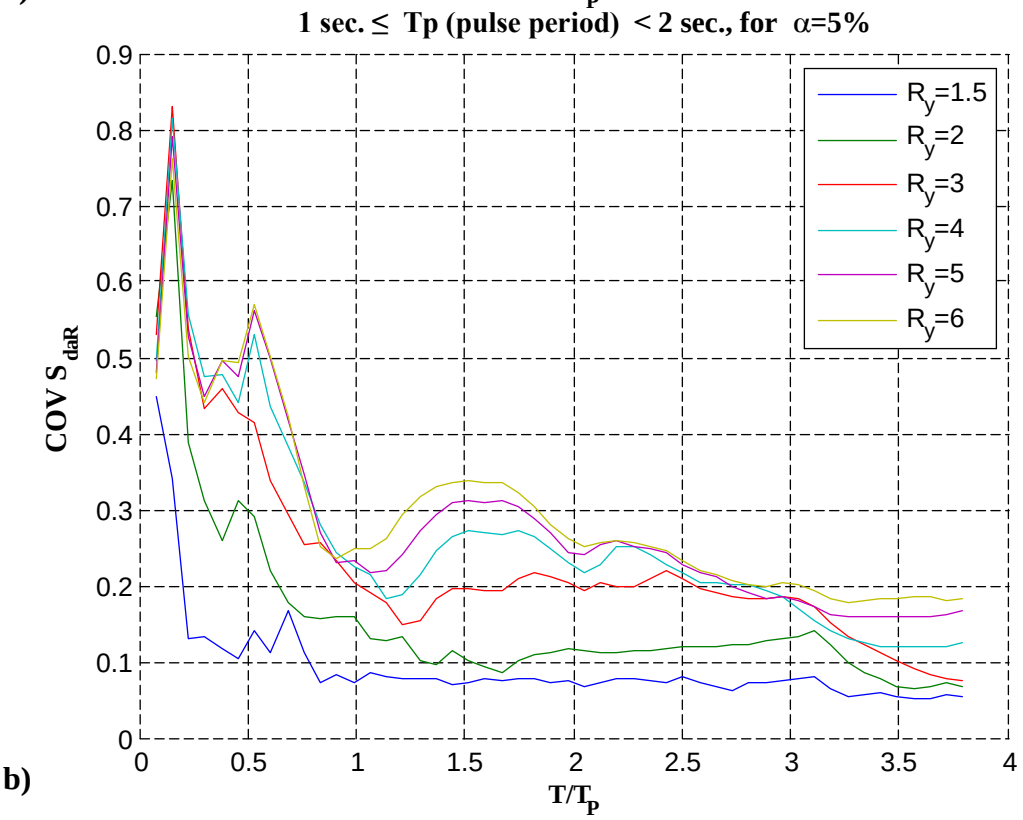

b)

Figure 7.21. Coefficient of variaton (COV) of the strength-based displacement amplication ratios of modified-Clough systems with 5 percent obtained from **a)** 8 and **b)** 23 near-field records have pulse periods in the range of **a)** 0 to 1 sec., and **b)** 1 sec. to 2 sec.

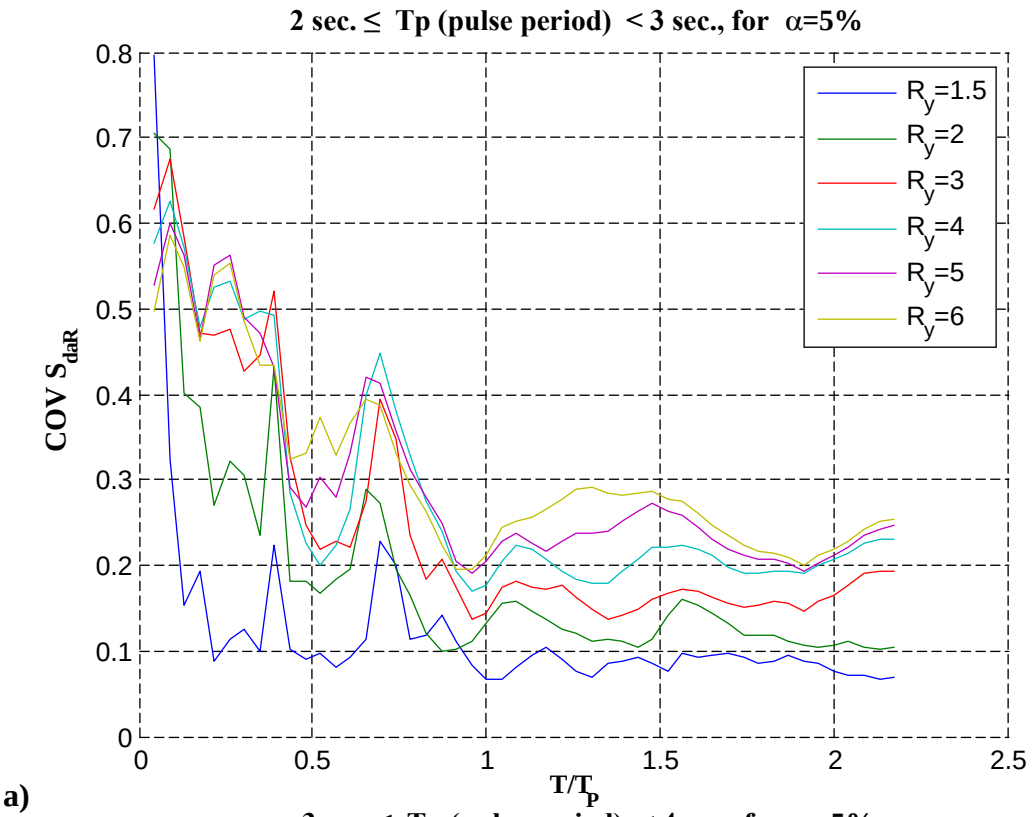

a)

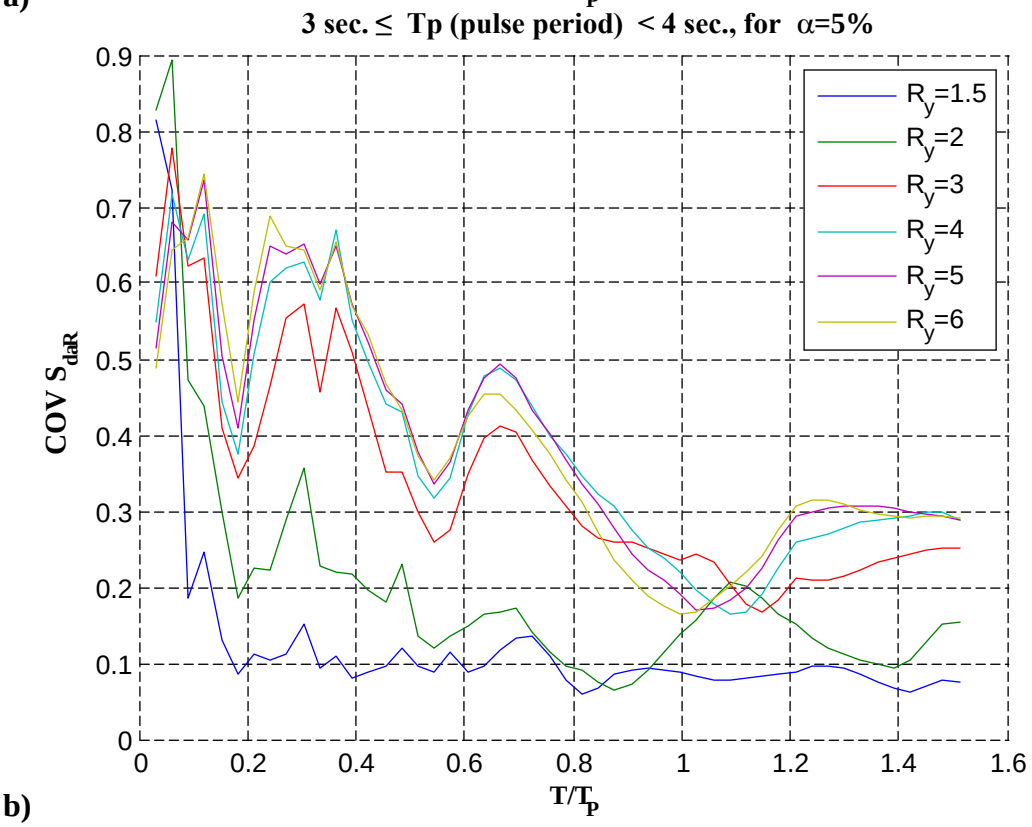

b)

Figure 7.22. Coefficient of variaton (COV) of the strength-based displacement amplication ratios of modified-Clough systems with 5 percent obtained from **a)** 13 and **b)** 12 near-field records have pulse periods in the range of **a)** 2 sec. to 3 sec., and **b)** 3 sec. to 4 sec.

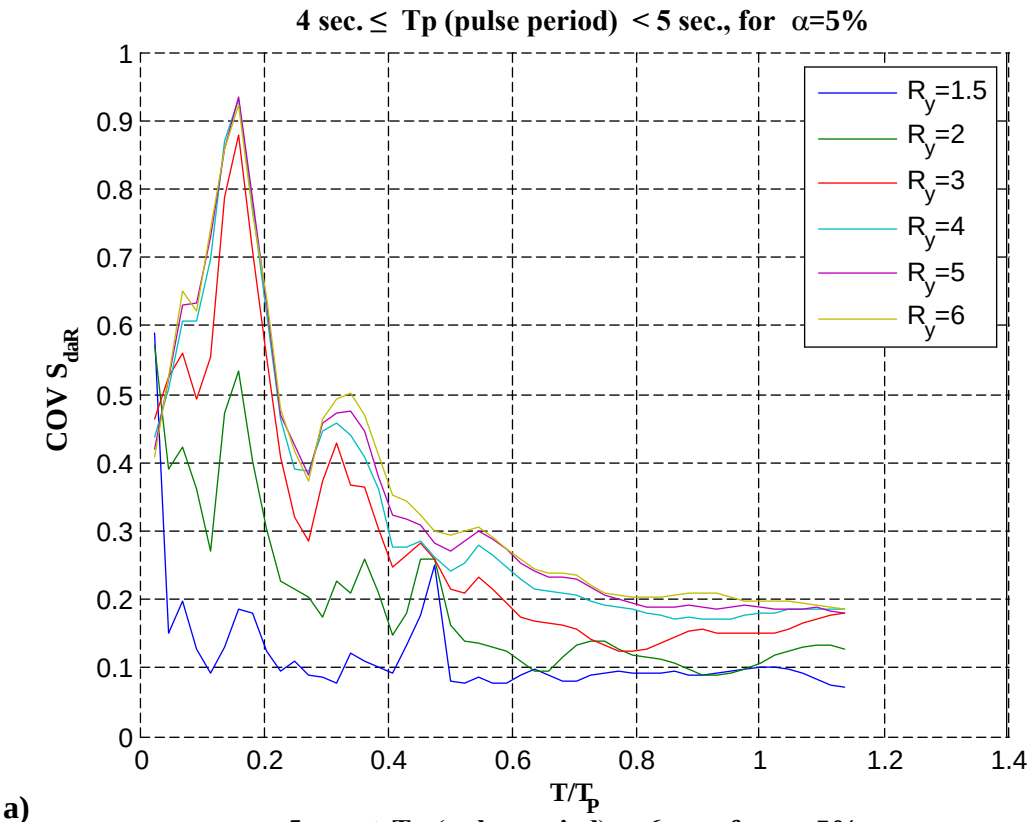

a)

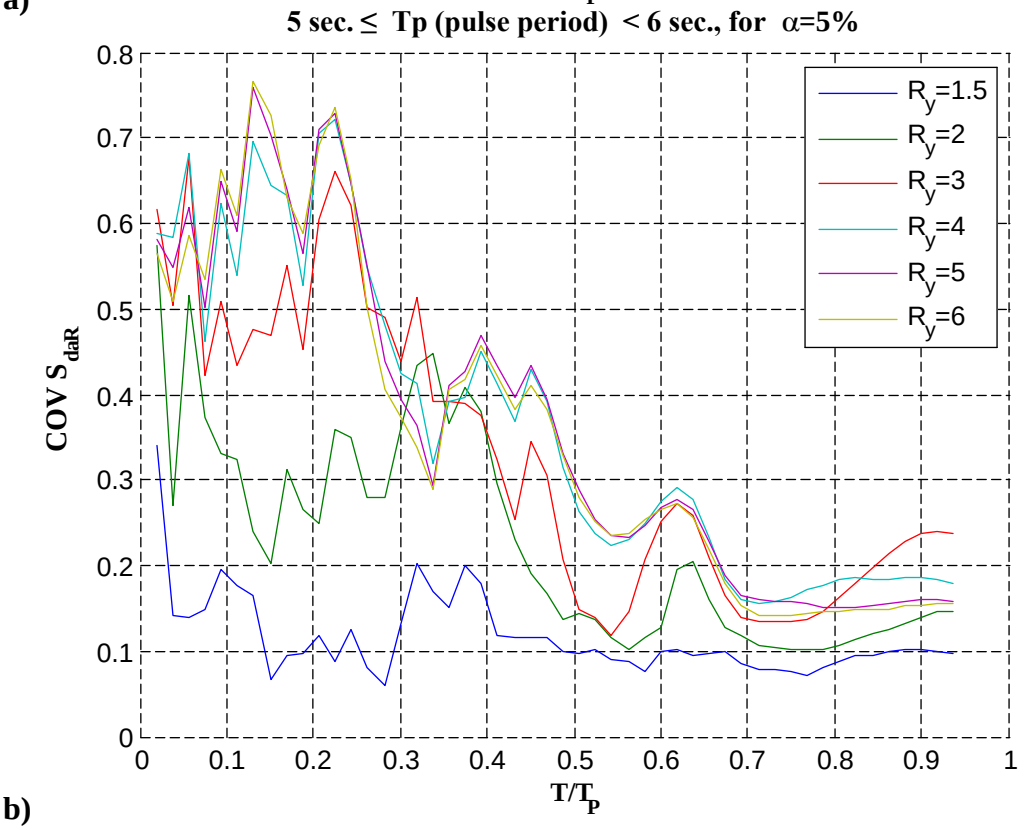

b)

Figure 7.23. Coefficient of variaton (COV) of the strength-based displacement amplication ratios of modified-Clough systems with 5 percent obtained from **a)** 16 and **b)** 10 near-field records have pulse periods in the range of **a)** 4 sec. to 5 sec., and **b)** 5 sec. to 6 sec.

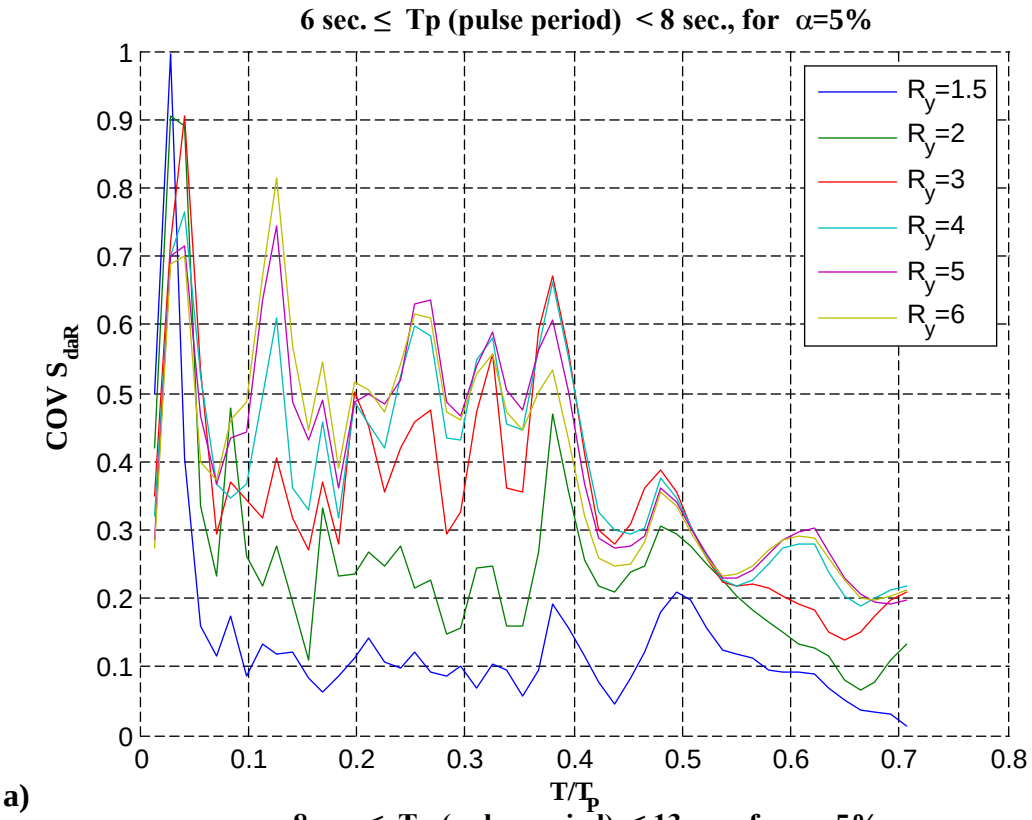

a)

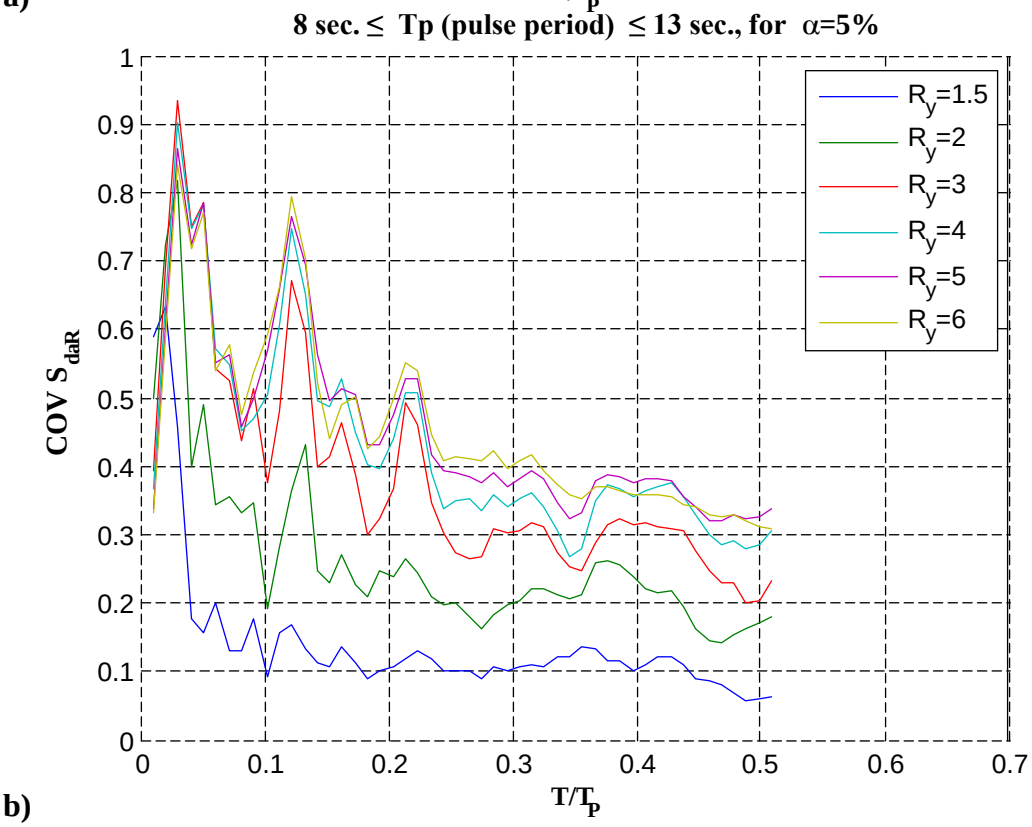

b)

Figure 7.24. Coefficient of variaton (COV) of the strength-based displacement amplication ratios of modified-Clough systems with 5 percent obtained from **a)** 6 and **b)** 17 near-field records have pulse periods in the range of **a)** 6 sec. to 8 sec., and **b)** 8 sec. to 13 sec.

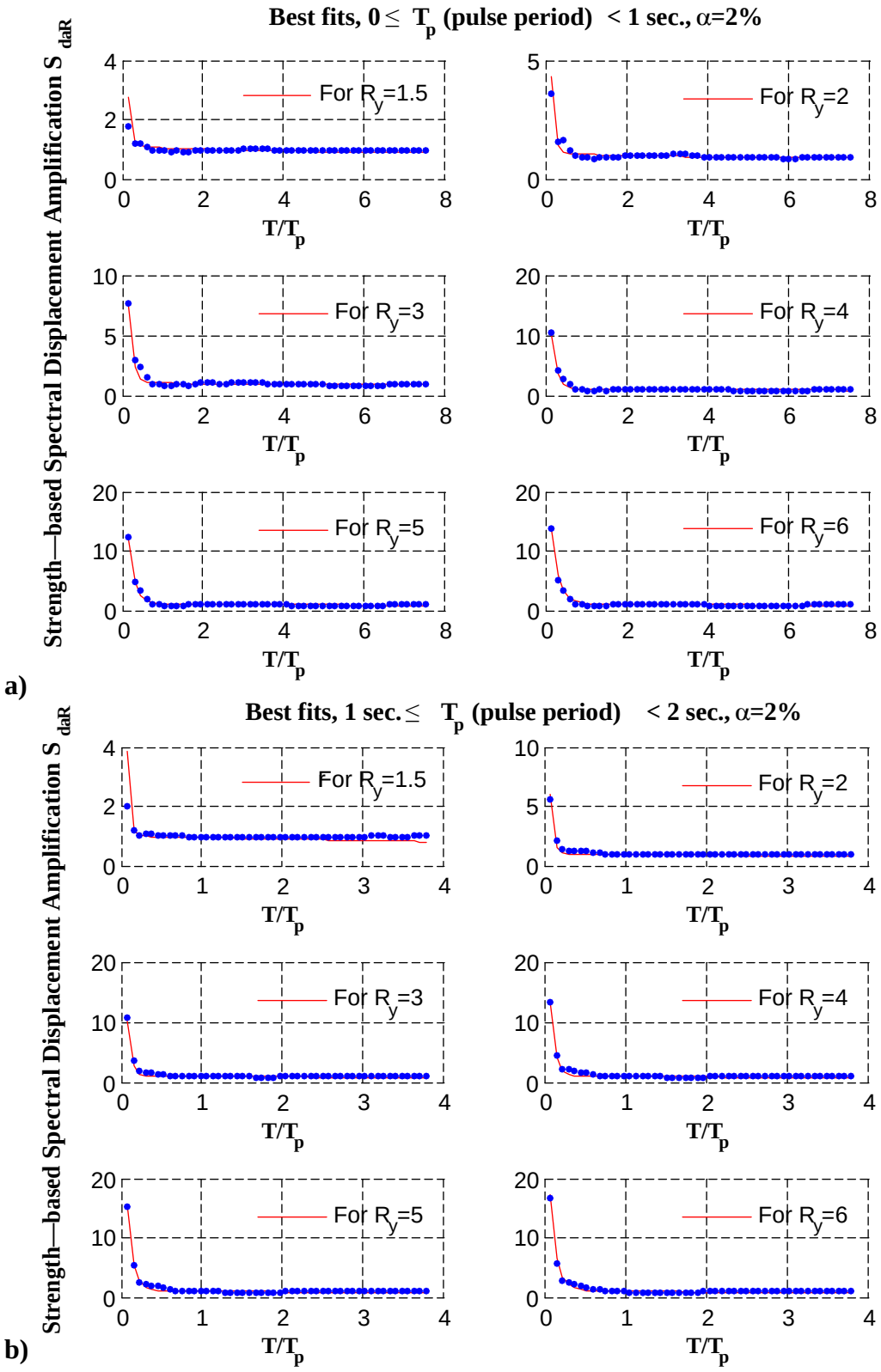

Figure 7.25. Proposed best fits for the mean strength-based spectral displacement amplification ratios of the near-field records have pulse periods **a)** between 0 and 1 sec., and **b)** between 1 sec. and 2 sec. and computed for different R_y values for each interval and post-yield stiffness ratio, α=2 percent

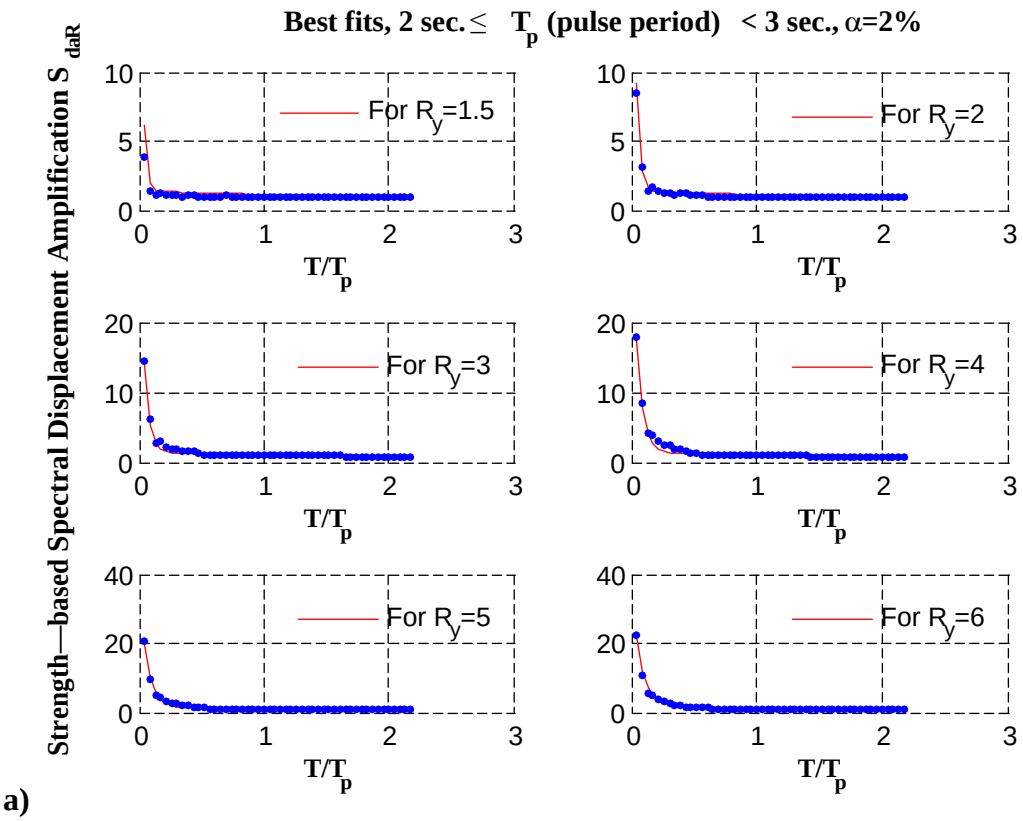

a)

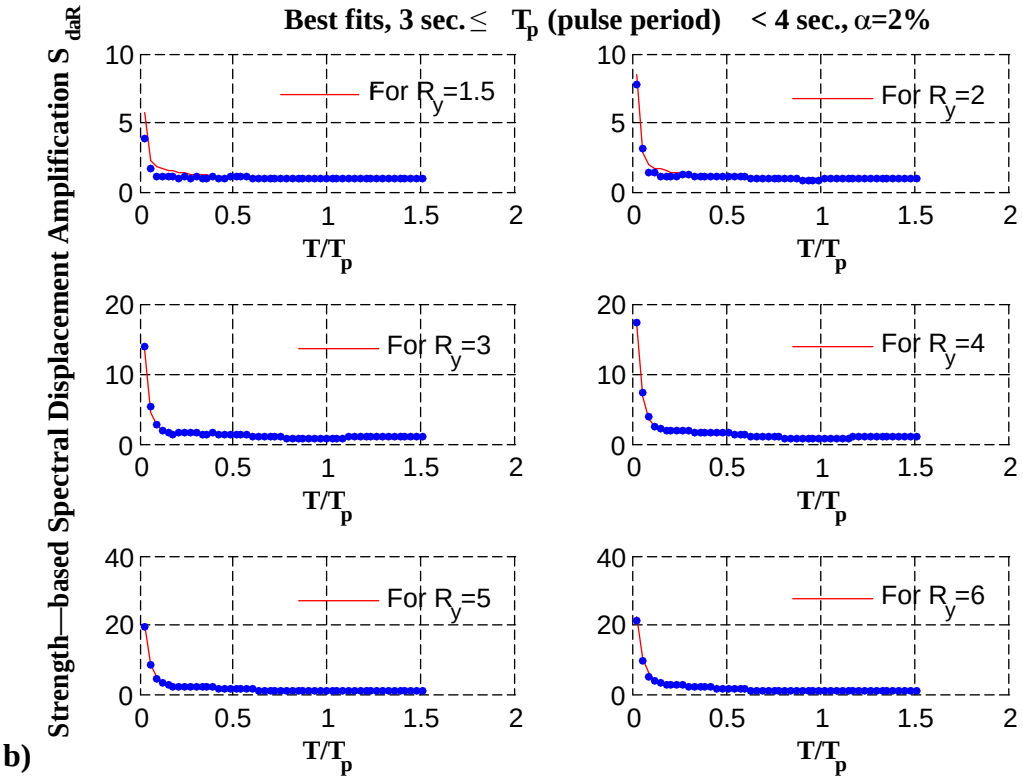

b)

Figure 7.26. Proposed best fits for the mean strength-based spectral displacement amplification ratios of the near-field records have pulse periods **a)** between 2 sec. and 3 sec., and **b)** between 3 sec. and 4 sec. and computed for different R_y values for each interval and post-yield stiffness ratio, α=2 percent

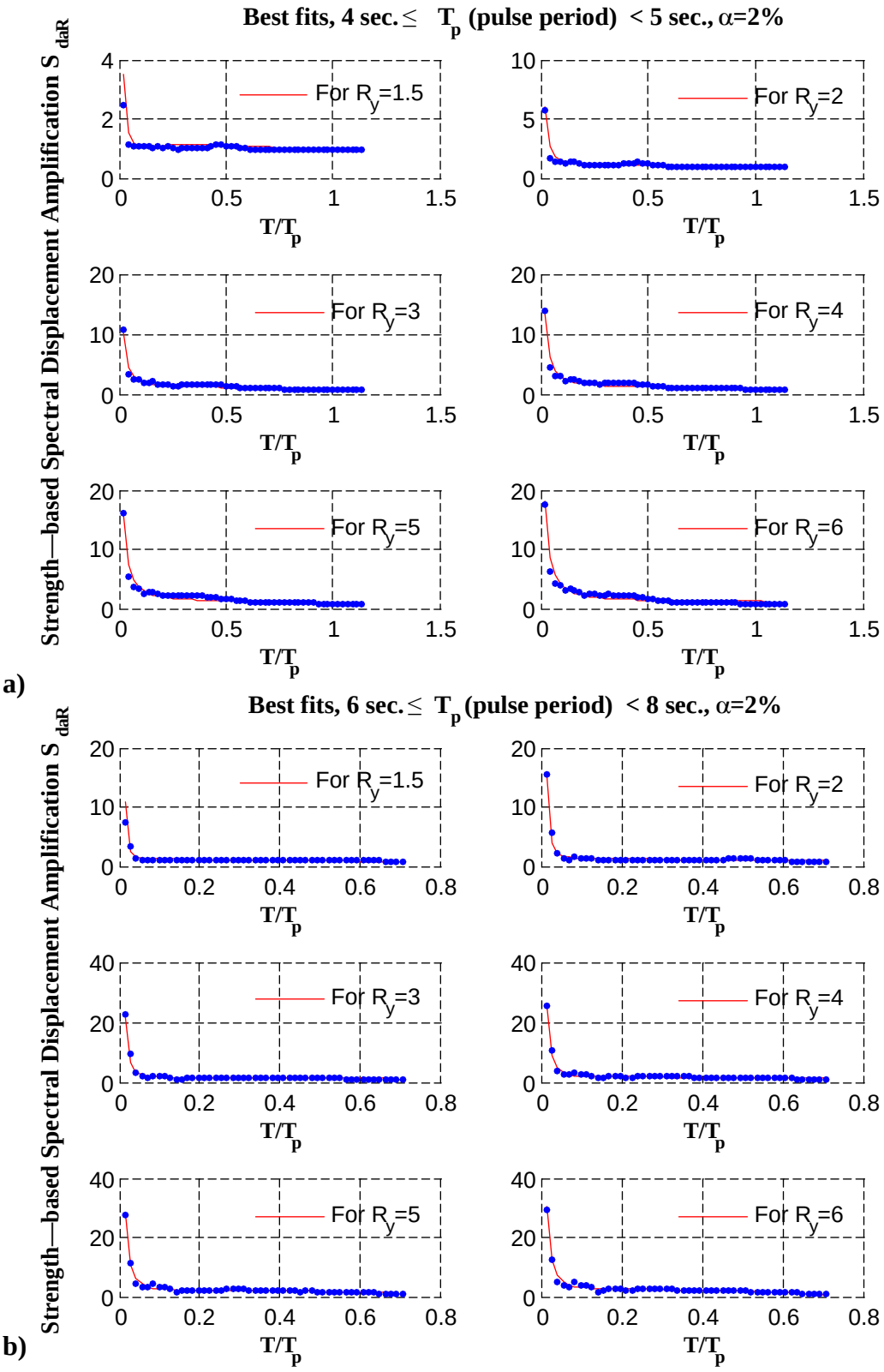

Figure 7.27. Proposed best fits for the mean strength-based spectral displacement amplification ratios of the near-field records have pulse periods **a)** between 4 sec. and 5 sec., and **b)** between 6 sec. and 8 sec. and computed for different R_y values for each interval and post-yield stiffness ratio, α=2 percent

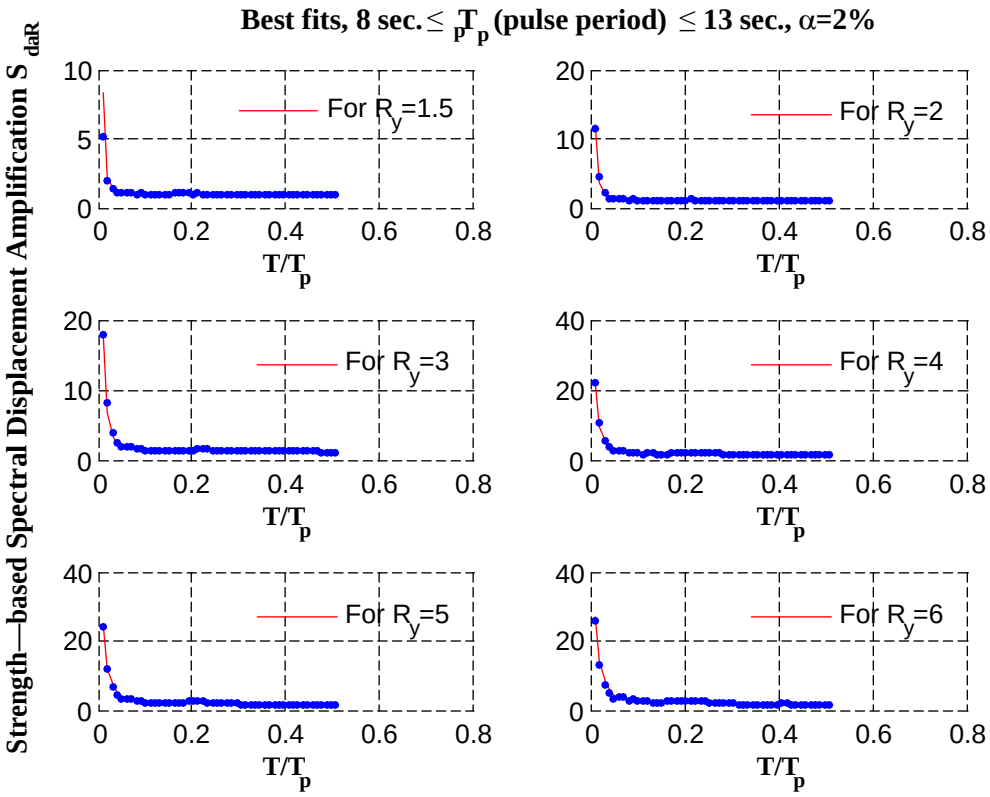

Figure 7.28. Proposed best fits for the mean strength-based spectral displacement amplification ratios of the near-field records have pulse periods between 8 sec. and 13 sec., and computed for different R_y values and post-yield stiffness ratio, α=2 percent

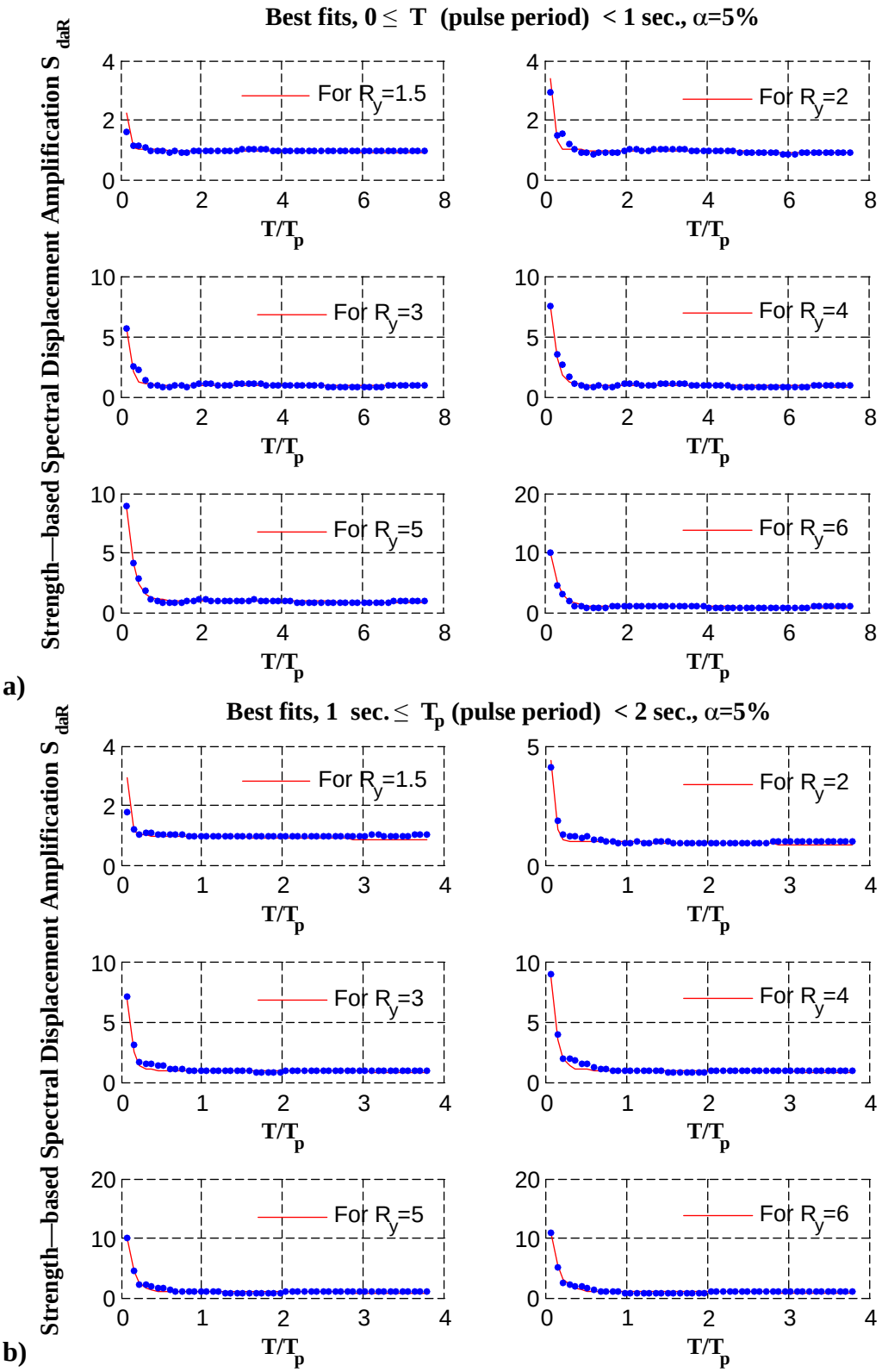

Figure 7.29. Proposed best fits for the mean strength-based spectral displacement amplification ratios of the near-field records have pulse periods **a)** between 0 and 1 sec., and **b)** between 1 sec. and 2 sec. and computed for different R_y values for each interval and post-yield stiffness ratio, α=5 percent

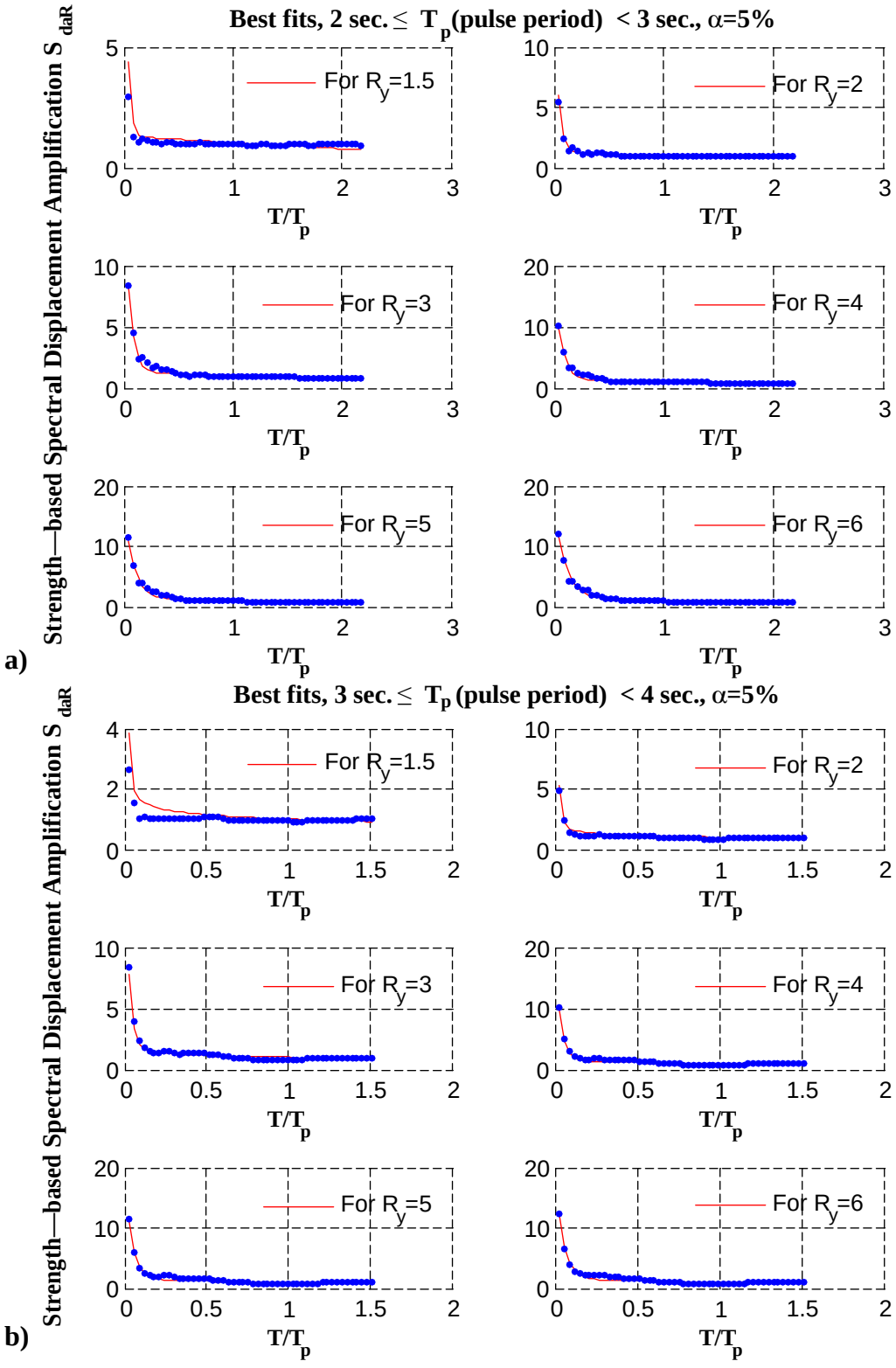

Figure 7.30. Proposed best fits for the mean strength-based spectral displacement amplification ratios of the near-field records have pulse periods **a)** between 2 sec. and 3 sec., and **b)** between 3 sec. and 4 sec. and computed for different R_y values for each interval and post-yield stiffness ratio, α=5 percent

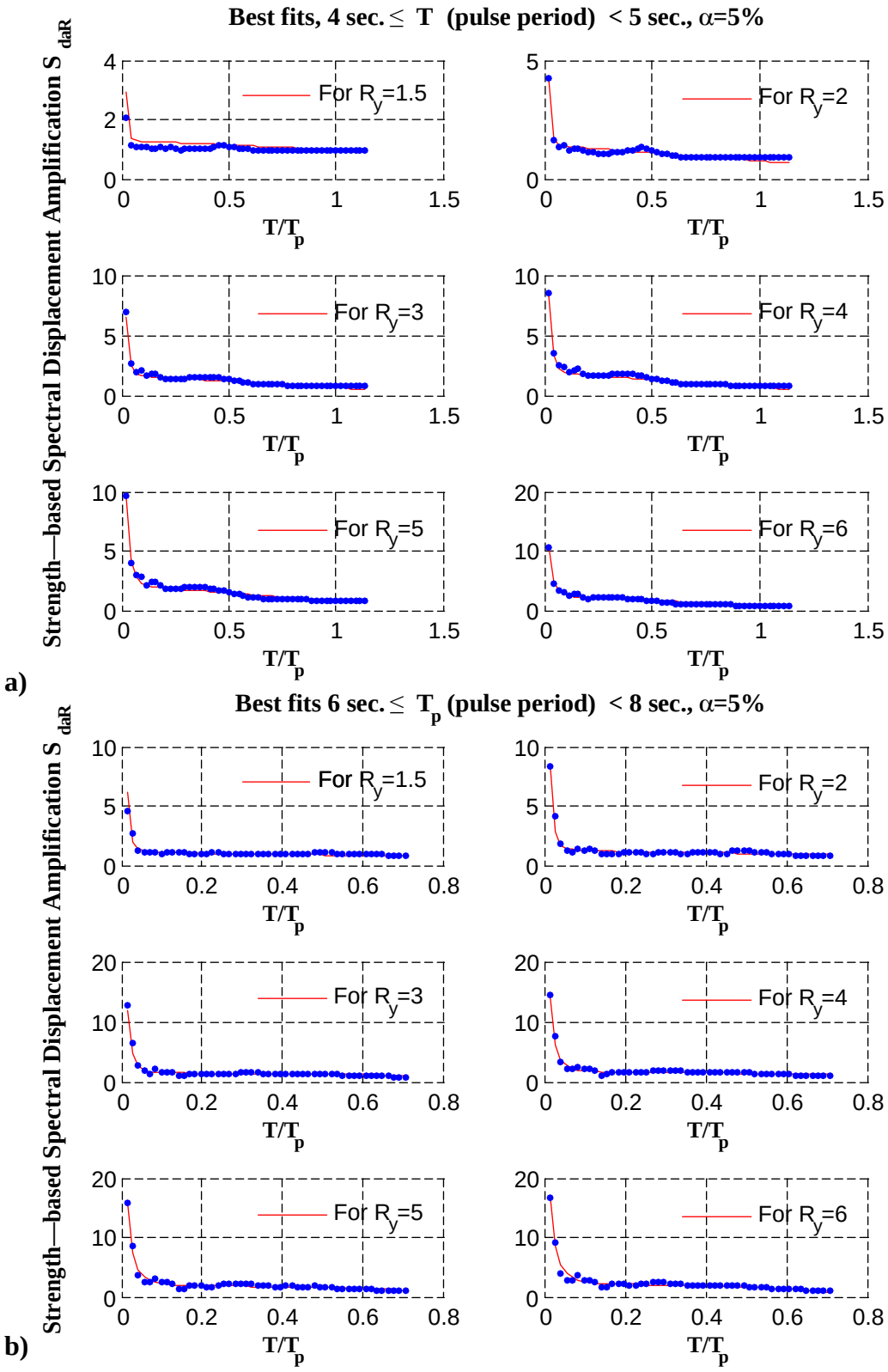

Figure 7.31. Proposed best fits for the mean strength-based spectral displacement amplification ratios of the near-field records have pulse periods **a)** between 4 sec. and 5 sec., and **b)** between 6 sec. and 8 sec. and computed for different R_y values for each interval and post-yield stiffness ratio, α=5 percent

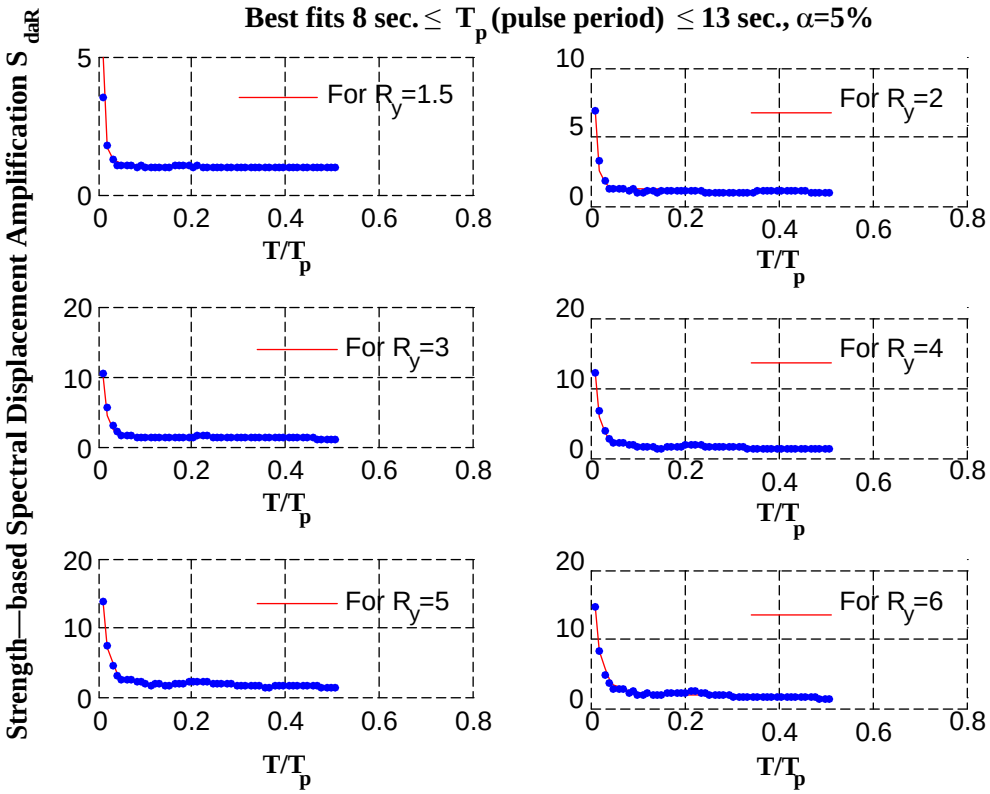

Figure 7.32. Proposed best fits for the mean strength-based spectral displacement amplification ratios of the near-field records have pulse periods between 8 sec. and 13 sec., and computed for different R_y values and post-yield stiffness ratio, α=5 percent

8. CONCLUSION

Performance-based seismic design and assessment is adopted in many codes such as FEMA 356, ASCE 41-06, Eurocode 8 (EN 1998-03, 2005) and new version of Turkish Seismic Code (TCS, 2007). One of the key parameters for performance-based design is the target displacement value of the structure and is utilized during the Nonlinear Static Procedure (Pushover Analysis) is a tool of the performance-based design.

In FEMA 356 and ASCE 41-06, displacement coefficient method is defined by different coefficients to characterize the overall target displacement. One of the coefficients in the proposed method is the C_1 coefficient. This is the modification factor and defines the relation between the maximum inelastic displacement and displacement calculated for the linear elastic response. C_1 coefficient is developed for the constant-μ factors and mainly using far-field strong ground motions. Yet, due to the characteristic properties of the near-field motions the ratio of inelastic displacement to elastic displacement needs to be investigated and modified. In addition, characteristic properties of near-field ground motions lead to be utilized constant-R_y spectrum instead of contant-μ spectrum.

In this study, by employing near-field ground motions, strength-based displacement amplification spectra are suggested. Near-field ground motions are determined by using a method proposed by Baker (2007). Near-field ground motions determined with respect to this pulse identification method exhibit forward-directivity effect. Totally 105 near-field ground motions include both fault-normal and fault-parallel are used to develop strength-based displacement amplification spectra. Near-field ground motions are classified by their site classes as defined in the NEHRP and earthquake magnitudes. Yet, it is observed that correlation between earthquakes fell into the same groups does not result in satisfactory results. Therefore, near-field ground motions are categorised according to their pulse periods and as a result of this categorisation, near-field ground motions are divided into 8 groups. The intervals of the groups vary due to the lack of the near-field records for different periods. Different soil types and earthquake magnitudes fell into these groups.

Initial period of vibration is normalized with respect to pulse periods of the near-field ground motions. By doing so, the distinct pulse effects of the near-field records at the long period range is eliminated from the strength-based spectral displacement amplification spectra (Mavroeidis *et al.*, 2004; Akkar *et al.*, 2004). For each T_p interval, regression formulae are developed to represent mean S_{daR} and mean T/T_p.

Effects of the hysteretic model, post-yield stiffness ratio, and stiffness degradation on the strength-based spectral displacement amplification spectra are examined. The following conclusions are drawn:

- For short mean T/T_p ranges, spectral displacement amplification ratio of systems with positive post-yield stiffness is smaller than that of systems with zero post-yield stiffness. It can be observed that when initial period, T, almost equals to mean of the pulse periods, T_p, of the records difference between systems with and without post-yield stiffness ratios is almost equal to 1. Moreover, for the very short T/T_p ratios ($\leq$0.2) the difference between systems with post-yield stiffness ratio and without post-yield stiffness ratio increases as the post-yield stiffness rises.

- At short T/T_p ratios, systems having stiffness degradation exhibit significantly greater strength demand (or inelastic displacement demand) than those having non-degrading. For R_y=1.5, ratio of $S_{daR,\ EP}$ / $S_{daR,\ MC\ (\alpha=0)}$ is equal to 1 with the exception of very short T/T_p range and records have pulse periods between 6 sec. and 8 sec., and 8 sec. and 13 sec.. Structures with high ductility levels and designed by using modified-Clough stiffness degrading hysteretic model experience higher inelastic displacement than systems having non-degrading hysteretic behavior. Therefore, when strength reduction factors obtained for the far-field ground motions are chosen for the structures that are at risk from the near-field ground motions should be utilized with care. In addition, there are significant differences between the results of the hysteretic models, and thus they should also be used with care.

- It can be observed from the tables given in Appendix an increase in moment magnitude results in increase in spectral displacement amplification ratio, S_{daR}.

Especially, as magnitude equals to 7.5 and R_y is taken 6, S_{daR} obtained from regression formulae is twice as large as the C_1 coefficient defined in ASCE 41-06. Numerical examples have revealed that for structures whose period larger than 1 sec., displacement amplification spectra take values between 1.1-2.6, where this value (modification factor, C_1, equation 3.14) is fixed to 1 in ASCE 41-06. S_{daR} values rise with the increase in R_y values. For magnitude 6.5 and systems with post-yield stiffness ratio equals to 5 percent, S_{daR} computed by suggested regression formulae are close to 1 with the increase in initial structural periods. This finding implies that C_1 value used in ASCE 41-06 standard results in underestimation of target displacement in pushover analysis, when structure is subjected to near field strong ground motion.

REFERENCES

Alavi, B., and Krawinkler, H., 2004, "Behavior of Moment-Resisting Frame Structures Subjected to Near-Fault Ground Motions", *Earthquake Engineering and Structural Dynamics*, Vol. 33, pp. 687-706.

Aydınoglu, M.N., and Kaçmaz, Ü., 2002, "*Strength-Based Displacement Amplification Spectra for Inelastic Seismic Performance Evaluation*", Kandilli Observatory and Earthquake Research Institute, Boğaziçi University, Istanbul.

Aydınoglu, M.N., and Önem, G., 2010 "*Evaluation of Practice-Oriented Nonlinear Analysis Methods for Seismic Performance Assessment*", Ph.D. Dissertation, Department of Earthquake Engineering, Boğaziçi University.

Baez, J. I. and Miranda, E., 2000, "Amplification Factors to Estimate Inelastic Displacement Demands for the Design of Structures in the Near Field", *12th World Conference on Earthquake Engineering*, New Zealand.

Bevington, P. R., and Robinson, D. K., 2003, "*Data Reduction and Error Analysis*", McGraw-Hill Companies, Inc., New York, NY, USA.

Baker, J. W., 2007, "Quantitative Classification of Near-Fault Ground Motions Using Wavelet Analysis", *Bulletin of the Seismological Society of America*, Vol. 97, No. 5, pp. 1486-1501, October.

Baker, J. W., 2008, "Identification of Near-Fault Velocity Pulses and Prediction of Resulting Response Spectra", *Geotechnical Earthquake Engineering and Soil Dynamics IV*, Sacremento, California, May 18-22.

Chopra, A. K. and Chintanapakdee, C., 2001, "Comparing Response of SDF Systems to Near-Fault and Far-Fault Earthquake Motions in the Context of Spectral Regions", *Earthquake Engineering and Structural Dynamics*, Vol. 30, pp. 1769-1789.

Chopra, A. K. and Chintanapakdee, C., 2004, "Inelastic Deformation Ratios for Design and Evaluation of Structures: Single-Degree-of-Freedom Bilinear Systems", *Journal of Structural Engineering, ASCE*, Vol. 130, No. 9, pp. 1309-1319.

Clough, R. W., and S. B. Johnston, 1966, "Effect of Stiffness Degradation on Earthquake Ductility Requirements", *Proceedings, 2nd Japan National Conference on Earthquake Engineering*, pp. 227-232.

Earthquake Solutions, 2010, *Bispec Professional* 2.03.0000.

Gillie, J. L., Rodriguez-Marek, A., McDaniel, C., 2010, "Strength Reduction Factors for Near-Fault Forward-Directivity Ground Motions", *Engineering Structures*, Vol. 32, pp. 273-285.

Loh, C-H., Wan, S., and Liao, W-I, 2002, "Effects of Hysteretic Model on Seismic Demands: Consideration of Near-Fault Ground Motions", *The Structural Design of Tall Buildings*, Vol. 11, pp. 155-169.

Mahin, S.A., and Bertero, V.V., 1975, "An Evaluation of Some Methods for Predicting Seismic Behavior of Reinforced Concrete Buildings", *Earthquake Engineering Research Center*, University of California at Berkeley, CA,.

Malhotra, P. K., 1999, "Response of Buildings to Near-Field Pulse-like Ground Motions", *Earthquake Engineering and Structural Dynamics*, Vol. 28, pp. 1309-1326.

MathWorks, *MATLAB*, 2010, Natick, MA: The MathWorks, Inc.

Mavroeidis, G. P., Dong, G. and Papageorgiou, A. S., 2004, "Near-Fault Ground Motions, and the Response of Elastic and Inelastic Single-Degree-of-Freedom (SDOF)

Systems", *Earthquake Engineering and Structural Dynamics*, Vol. 33, pp. 1023-1049.

Miles, J., and Shevlin M., 2001, "*Applying Regression & Correlation a Guide for Students and Researchers*", SAGE Publications Ltd, Great Britain.

Miranda, E., 1993, "Evaluation of Site-Dependent Inelastic Seismic Design Spectra", *Journal of Structural Engineering, ASCE*, Vol. 119, No. 5, pp. 1319-1338.

Miranda, E., 2000, "Inelastic Displacement Ratios for Structures on Firm Sites", *Journal of Structural Engineering, ASCE*, Vol. 126, No. 10, pp. 1150-1159.

Ruiz-García, J. and Miranda, E., 2003, "Inelastic Displacement Ratios for Evaluation of Existing Structures", *Earthquake Engineering and Structural Dynamics*, Vol. 32, pp. 1237–1258.

Ruiz-García, J. and Miranda, E., 2004, "Inelastic Displacement Ratios for Design of Structures on Soft Soils Sites", *Journal of Structural Engineering*, ASCE, Vol. 130, No. 12, pp. 2051-2061.

Ruiz-García, J. and Miranda, E., 2006, "Inelastic Displacement Ratios for Evaluation of Structures Built on Soft Soil Sites", *Earthquake Engineering and Structural Dynamics*, Vol. 35, pp. 679–694.

Ryan, T. P., 1997, "*Modern Regression Methods*", John Wiley & Sons Inc., New York, NY, USA.

Saiidi, M., Sozen, M. A., 1981, "Simple Nonlinear Seismic Analysis of R/C Structures", *Journal of Structural Engineering, ASCE*, Vol. 107, No. 5, pp. 937-953.

Veletsos, A. S., Newmark, N. M., 1960, "Effect of Inelastic Behaviour on the Response of Simple Systems to Earthquake Motions", *Proceedings of 2nd World Conference on Earthquake Engineering*, Vol. 2, pp. 895-912.

Veletsos A. S., Newmark N. M., Chepalati, C. V., 1965, “Deformation Spectra for Elastic and Elastoplastic Systems Subjected to Ground Shock and Earthquake Motion”, *Proceedings of 3rd World Conference on Earthquake Engineering*, Vol. 2, pp. 663-682.

APPENDIX: NUMERICAL EXAMPLES

Table A.1. For earthquake moment magnitude M_w=6.5 and systems with α=2 percent

M_w=6.5											
T_p=2.3396 sec.											
T=1 sec.		T=1.1 sec.	T=1.2 sec.	T=1.3 sec.	T=1.4 sec.	T=1.5 sec.	T=1.6 sec.	T=1.7 sec.	T=1.8 sec.	T=1.9 sec.	T=2 sec.
R_y	S_{daR}	S_{daR}	S_{daR}	S_{daR}	S_{daR}	S_{daR}	S_{daR}	S_{daR}	S_{daR}	S_{daR}	S_{daR}
1.5	1.2789	1.2668	1.2547	1.2426	1.2305	1.2184	1.2063	1.1941	1.1820	1.1699	1.1578
2	1.2752	1.2627	1.2502	1.2377	1.2252	1.2128	1.2003	1.1878	1.1753	1.1628	1.1503
3	1.2708	1.2569	1.2436	1.2304	1.2173	1.2043	1.1912	1.1782	1.1651	1.1521	1.1390
4	1.2791	1.2583	1.2414	1.2262	1.2120	1.1981	1.1845	1.1709	1.1574	1.1439	1.1304
5	1.3206	1.2801	1.2517	1.2299	1.2117	1.1954	1.1803	1.1657	1.1515	1.1374	1.1235
6	1.4130	1.3376	1.2866	1.2503	1.2227	1.2005	1.1814	1.1643	1.1484	1.1331	1.1183

Table A.2. For earthquake moment magnitude M_w=7.0 and systems with α=2 percent

M_w=7.0											
T_p=3.8962 sec.											
T=1 sec.		T=1.1 sec.	T=1.2 sec.	T=1.3 sec.	T=1.4 sec.	T=1.5 sec.	T=1.6 sec.	T=1.7 sec.	T=1.8 sec.	T=1.9 sec.	T=2 sec.
R_y	S_{daR}	S_{daR}	S_{daR}	S_{daR}	S_{daR}	S_{daR}	S_{daR}	S_{daR}	S_{daR}	S_{daR}	S_{daR}
1.5	1.3122	1.2730	1.2388	1.2087	1.1821	1.1585	1.1375	1.1189	1.1022	1.0875	1.0743
2	1.3381	1.2947	1.2562	1.2218	1.1909	1.1630	1.1378	1.1148	1.0939	1.0749	1.0574
3	1.4431	1.3951	1.3522	1.3135	1.2783	1.2461	1.2166	1.1894	1.1642	1.1409	1.1192
4	1.5921	1.5386	1.4920	1.4505	1.4128	1.3784	1.3467	1.3173	1.2900	1.2645	1.2406
5	1.7865	1.7212	1.6675	1.6215	1.5809	1.5442	1.5107	1.4798	1.4510	1.4242	1.3990
6	2.0352	1.9492	1.8824	1.8281	1.7821	1.7418	1.7057	1.6729	1.6427	1.6146	1.5883

Table A.3. For earthquake moment magnitude M_w=7.5 and systems with α=2 percent

M_w=7.5											
T_p=6.4883 sec.											
T=1 sec.		T=1.1 sec.	T=1.2 sec.	T=1.3 sec.	T=1.4 sec.	T=1.5 sec.	T=1.6 sec.	T=1.7 sec.	T=1.8 sec.	T=1.9 sec.	T=2 sec.
R_y	S_{daR}	S_{daR}	S_{daR}	S_{daR}	S_{daR}	S_{daR}	S_{daR}	S_{daR}	S_{daR}	S_{daR}	S_{daR}
1.5	1.1580	1.1387	1.1209	1.1045	1.0892	1.0750	1.0615	1.0488	1.0368	1.0253	1.0143
2	1.3000	1.2803	1.2622	1.2454	1.2298	1.2150	1.2012	1.1880	1.1755	1.1635	1.1521
3	1.5900	1.5686	1.5493	1.5314	1.5147	1.4988	1.4838	1.4694	1.4555	1.4421	1.4292
4	1.9010	1.8745	1.8518	1.8315	1.8128	1.7951	1.7782	1.7618	1.7459	1.7304	1.7150
5	2.2444	2.2074	2.1778	2.1526	2.1300	2.1090	2.0889	2.0695	2.0503	2.0313	2.0122
6	2.6252	2.5731	2.5327	2.4994	2.4703	2.4439	2.4188	2.3944	2.3702	2.3457	2.3207

Table A.4. For earthquake moment magnitude M_w=6.5 and systems with α=5 percent

M_w=6.5											
T_p=2.3396 sec.											
T=1 sec.		T=1.1 sec.	T=1.2 sec.	T=1.3 sec.	T=1.4 sec.	T=1.5 sec.	T=1.6 sec.	T=1.7 sec.	T=1.8 sec.	T=1.9 sec.	T=2 sec.
R_y	S_{daR}	S_{daR}	S_{daR}	S_{daR}	S_{daR}	S_{daR}	S_{daR}	S_{daR}	S_{daR}	S_{daR}	S_{daR}
1.5	1.1889	1.1778	1.1666	1.1555	1.1444	1.1333	1.1222	1.1111	1.1000	1.0889	1.0777
2	1.1890	1.1778	1.1667	1.1555	1.1444	1.1333	1.1222	1.1111	1.1000	1.0889	1.0777
3	1.1934	1.1798	1.1675	1.1559	1.1446	1.1334	1.1222	1.1111	1.1000	1.0889	1.0777
4	1.2221	1.1959	1.1765	1.1609	1.1474	1.1349	1.1231	1.1116	1.1002	1.0890	1.0778
5	1.2993	1.2456	1.2084	1.1812	1.1602	1.1430	1.1282	1.1148	1.1022	1.0903	1.0786
6	1.4349	1.3415	1.2757	1.2282	1.1929	1.1656	1.1437	1.1255	1.1096	1.0953	1.0820

Table A.5. For earthquake moment magnitude M_w=7.0 and systems with α=5 percent

M_w=7.0											
T_p=3.8962 sec.											
T=1 sec.		T=1.1 sec.	T=1.2 sec.	T=1.3 sec.	T=1.4 sec.	T=1.5 sec.	T=1.6 sec.	T=1.7 sec.	T=1.8 sec.	T=1.9 sec.	T=2 sec.
R_y	S_{daR}	S_{daR}	S_{daR}	S_{daR}	S_{daR}	S_{daR}	S_{daR}	S_{daR}	S_{daR}	S_{daR}	S_{daR}
1.5	1.3135	1.2887	1.2665	1.2464	1.2280	1.2112	1.1957	1.1813	1.1679	1.1553	1.1436
2	1.3140	1.2892	1.2670	1.2469	1.2286	1.2118	1.1962	1.1818	1.1684	1.1559	1.1441
3	1.3169	1.2917	1.2693	1.2492	1.2308	1.2140	1.1985	1.1841	1.1707	1.1581	1.1463
4	1.3301	1.3010	1.2767	1.2556	1.2369	1.2198	1.2042	1.1897	1.1763	1.1637	1.1520
5	1.3715	1.3307	1.2997	1.2748	1.2538	1.2356	1.2192	1.2044	1.1908	1.1781	1.1662
6	1.4655	1.4035	1.3588	1.3252	1.2987	1.2769	1.2584	1.2422	1.2277	1.2144	1.2022

Table A.6. For earthquake moment magnitude M_w=7.5 and systems with α=5 percent

M_w=7.5											
T_p=6.4883 sec.											
T=1 sec.		T=1.1 sec.	T=1.2 sec.	T=1.3 sec.	T=1.4 sec.	T=1.5 sec.	T=1.6 sec.	T=1.7 sec.	T=1.8 sec.	T=1.9 sec.	T=2 sec.
R_y	S_{daR}	S_{daR}	S_{daR}	S_{daR}	S_{daR}	S_{daR}	S_{daR}	S_{daR}	S_{daR}	S_{daR}	S_{daR}
1.5	1.0389	1.0259	1.0140	1.0031	0.9928	0.9832	0.9742	0.9657	0.9576	0.9499	0.9425
2	1.1813	1.1681	1.1559	1.1447	1.1341	1.1243	1.1149	1.1061	1.0976	1.0896	1.0818
3	1.4341	1.4197	1.4066	1.3945	1.3832	1.3725	1.3623	1.3525	1.3431	1.3340	1.3252
4	1.6720	1.6531	1.6372	1.6232	1.6103	1.5982	1.5866	1.5754	1.5645	1.5537	1.5432
5	1.9133	1.8849	1.8628	1.8444	1.8283	1.8135	1.7994	1.7859	1.7725	1.7592	1.7459
6	2.1664	2.1239	2.0918	2.0661	2.0443	2.0248	2.0066	1.9891	1.9719	1.9545	1.9368